Basic Mechanisms of TID and DDD Response in MOS and Bipolar Microelectronics

Timothy R. Oldham
DSFG, Inc, NASA Goddard, Radiation Effects and Analysis Group

Abstract

We review the basic physical mechanisms of the interactions of ionizing radiation with MOS materials and devices, and also bipolar devices, particularly the ELDRS problem. Displacement damage from non-ionizing radiation is also discussed.

1 Introduction

The development of military and space electronics technology has traditionally been heavily influenced by the commercial semiconductor industry. The development of microelectronic technology, both MOS (Metal-Oxide-Semiconductor) and bipolar technology, as dominant commercial technologies has occurred almost entirely within the lifetime of the NSREC. For this reason, it is not surprising that the study of radiation interactions with electronic materials, devices and circuits has been a major theme of this conference for most of its history. In this course, we will cover three main topics: (1) basic mechanisms of the interactions of ionizing radiation with MOS materials and devices; (2) interactions of ionizing radiation with bipolar materials and devices; and (3) displacement damage effects due to interactions with non-ionizing radiation.

2 Ionizing Radiation Effects In MOS Technology

The basic radiation problem in a MOS transistor is illustrated in Figure 1, where Figure 1a shows the normal operation of a MOSFET. The application of an appropriate gate voltage causes a conducting channel to form between the source and drain, so that current flows when the device is turned on. In Figure 1b, the effect of ionizing radiation is illustrated. Radiation-induced trapped charge has built up in the gate oxide, which causes a shift in the threshold voltage (that is, a change in the voltage which must be applied to turn the device on). If this shift is large enough, the device cannot be turned off, even at zero volts applied, and the device is said to have failed by going into depletion mode.

In practice, the radiation-induced charging of the oxide involves several different physical mechanisms, which take place on very different time scales, with different field dependences and different temperature dependences. For this reason, the overall radiation response of a device or circuit can be extremely complex, sometimes to the point of bewilderment. However, the overall response can be separated into its components, and the components can be studied individually. In fact, this has happened. Many different individual investigators have studied different parts of the radiation response over a period of many years, and a reasonable degree of understanding has now been achieved. Much of this understanding has been captured elsewhere already – Ma and Dressendorfer [1] edited a major review volume. In addition, Oldham [2] prepared another book, which was intended to update parts of the Ma and Dressendorfer book, to reflect later work. Both volumes discuss the same material to be presented here, and in far greater detail than is possible here.

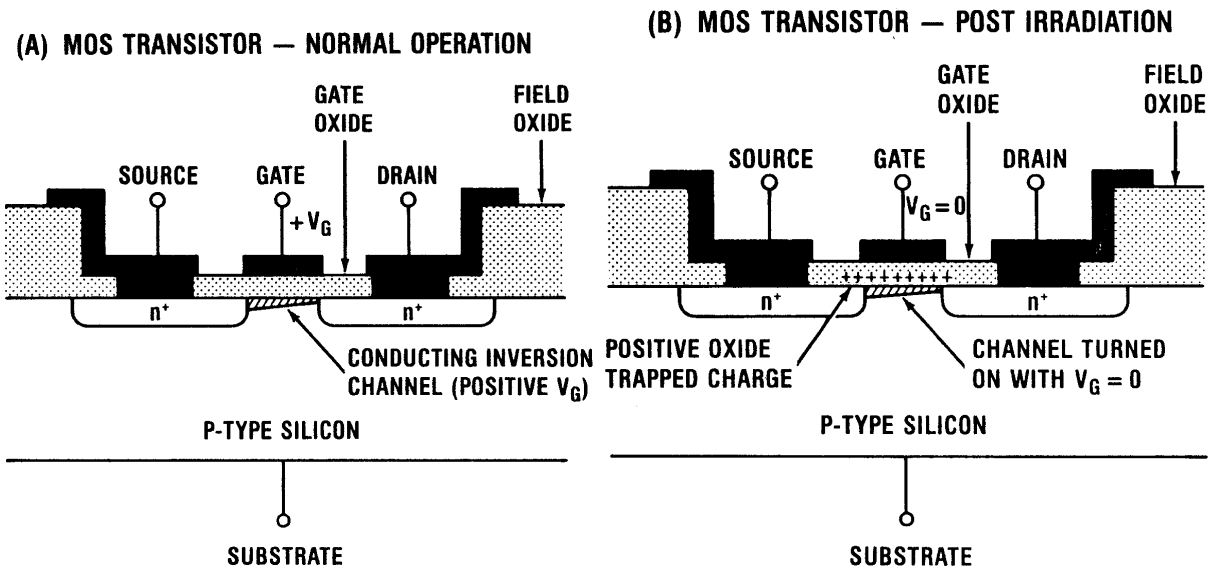

Figure 1. Schematic of n-channel MOSFET illustrating radiation-induced charging of the gate oxide: (a) normal operation and (b) post-irradiation.

2.1 Overview

We begin with an overview of the time-dependent radiation response of MOS systems, before discussing each of the major physical processes in greater detail. Then we will discuss the implications of the radiation response for testing, prediction, and hardness assurance. We will also discuss the implications of scaling (reducing the oxide thickness), and issues associated with oxide isolation structures and leakage currents.

In the history of the commercial semiconductor industry, few things have been more important than scaling, the regular shrinking of device feature sizes, so that larger and larger integrated circuits can be fabricated in a given chip area. Of course, the radiation effects community has been swept along, with a new generation of chips every few years, and similar hardening problems to be solved in each new generation. Oxide thinning has had a major impact on the TID response of CMOS technology.

The impact of oxide thinning is illustrated in Figure 2. Thirty years ago, oxides were pure SiO_2, typically about 100 nm thick, but now, commercially available oxides are only a few nm thick. McGarrity [5] worked out the gains in gate oxide hardening that could be achieved merely by thinning the oxide, without special processing. The point of his analysis is that $\Delta V_T = Q_{ox} / C_{ox}$, which leads to the prediction that the threshold voltage shift is proportional to oxide thickness squared. The total charge in the oxide is proportional to thickness, and the capacitance is inversely proportional to thickness. (We note that other dependences have occasionally been reported, and oxide processing varies so much there is no reason not to believe data showing a different thickness dependence for a particular oxide. But other dependences have not been shown to be reproducible, in general.) The most important deviation from the t_{ox}^2 dependence occurs in very thin oxides, where tunnel annealing eliminates, or at least neutralizes, trapped charge near the interface. The point is that for thin oxides, this annealing process occurs at both interfaces, and accounts for all or nearly all of the trapped oxide charge. For thin enough oxides, the two tunneling fronts meet in the center of the oxide, leaving no net positive oxide

charge. Data illustrating this effect are shown in Figure 2 [3,4]. Even several years ago, leading edge commercial oxides were approaching 1nm, but leakage current and power consumption issues were forcing the industry to abandon pure SiO_2 oxides. For this reason, gate oxides in advanced technology are now high κ materials, which are physically thicker, and which we will discuss later. But a key point is that even the thicker oxides are still extremely thin—off the bottom of the chart, or close to it, in Figure 2. Since mainstream commercial oxides are now thin enough that radiation-induced ΔV_T has essentially vanished, the problem of hardening gate oxides is basically solved. This leaves field oxide isolation structures as the main total dose radiation problem. The models for charge generation, recombination, transport and trapping, and interface trap build-up were all developed originally to explain effects in CMOS gate oxides. Although effects in gate oxides have diminished in importance, the same models today are widely used because they also apply to isolation structures, including bipolar isolation structures. Therefore, we will now discuss these mechanisms in more detail.

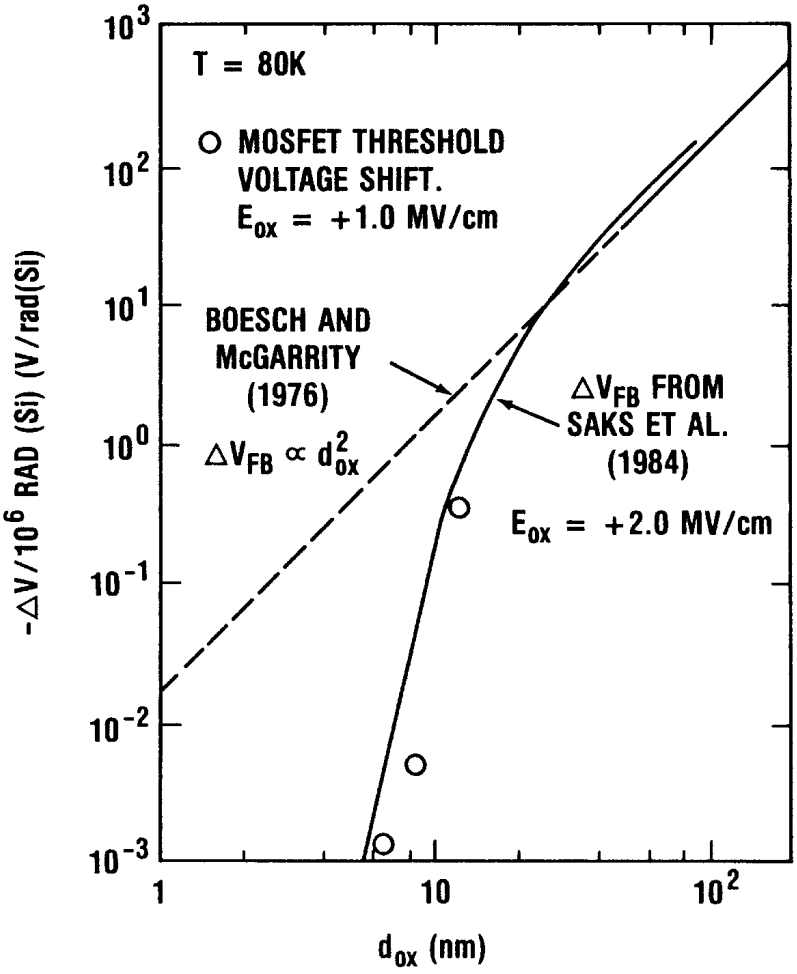

Figure 2. Threshold and flatband voltage shifts per unit dose as a function of oxide thickness at 80K. Dashed line is thickness squared, solid line and points are experimental results. [3, 4]

Figure 3 shows a schematic energy band diagram of a MOS structure, where positive bias is applied to the gate, so that electrons flow toward the gate and holes move to the Si substrate. Four major physical processes, which contribute to the radiation response of a MOS device, are also indicated. The most sensitive parts of a MOS system to radiation are the oxide insulators. When radiation passes through a gate oxide, electron/hole pairs are created by the deposited energy. In SiO_2, the electrons are much more mobile than the holes [6], and they are swept out of the oxide, typically in a picosecond or less. However, in that first picosecond, some fraction of the electrons and holes will recombine. That fraction will depend greatly on the energy and type of the incident particle. The holes, which escape initial recombination, are relatively immobile, and remain near their point of generation, where they cause a negative threshold voltage shift in a MOS transistor. These processes, electron/hole pair generation and recombination, together are the first process depicted in Figure 3. In Figure 4, this process determines the (maximum) initial threshold voltage shift.

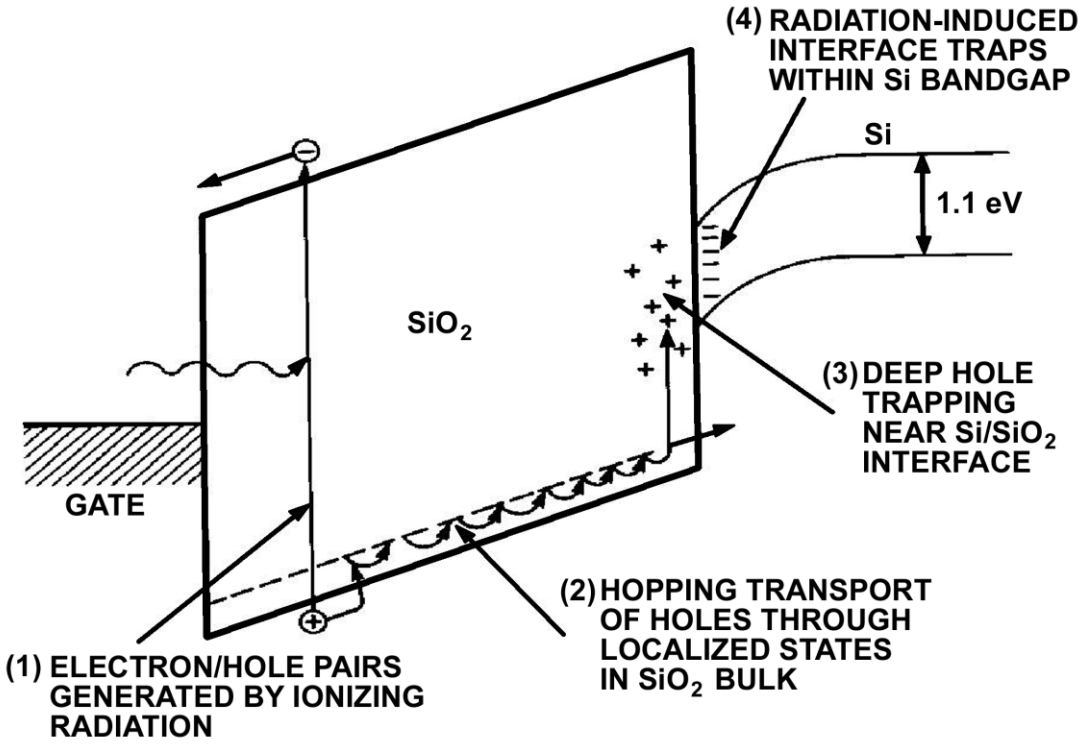

Figure 3. Schematic energy band diagram for MOS structure, indicating major physical processes underlying radiation response

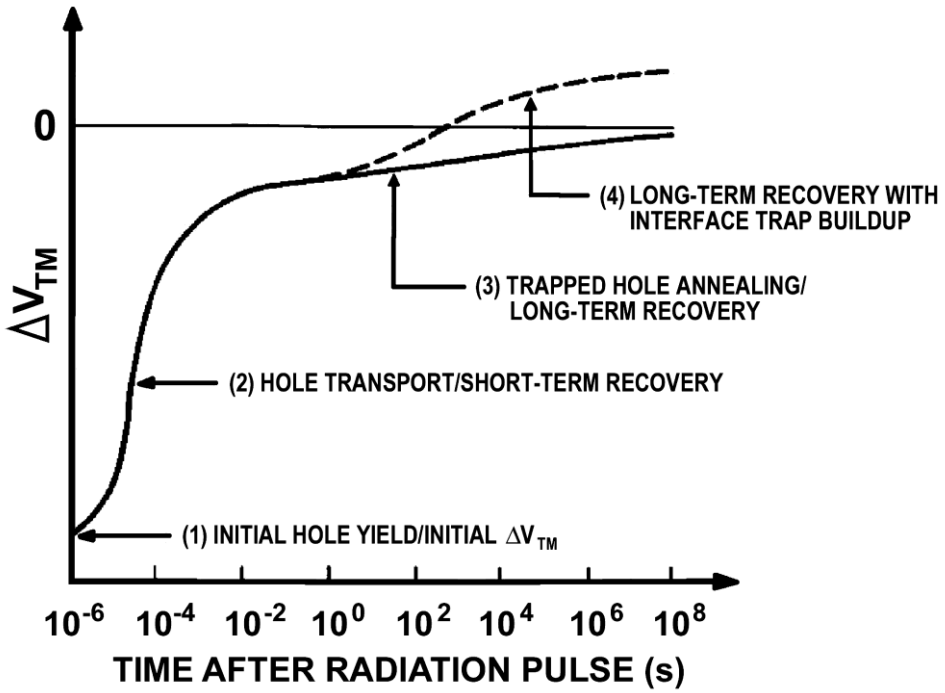

Figure 4. Schematic time-dependent post-irradiation threshold voltage recovery of n-channel MOSFET, relating major features of the response to underlying physical processes.

The second process in Figure 3 is the transport of the holes to the Si/SiO_2 interface, which causes the short-term recovery of the threshold voltage in Figure 4. This process is dispersive, meaning that it takes place over many decades in time, and it is very sensitive to the applied field, temperature, oxide thickness, and (to a lesser extent) oxide processing history. This process is normally over in much less than a second at room temperature, but it can be many orders of magnitude slower at low temperature.

The third process in Figure 3 and Figure 4 is that when they reach the Si interface, some fraction of the transporting holes fall into relatively deep, long-lived trap states. These trapped holes cause a remnant negative voltage shift, which can persist for hours or even for years. But even these stable trapped holes undergo a gradual annealing, which is illustrated in Figure 4.

The fourth major component of MOS radiation response is the radiation-induced buildup of interface traps right at the Si/SiO_2 interface. These traps are localized states with energy levels in the Si band-gap. Their occupancy is determined by the Fermi level (or by the applied voltage), giving rise to a voltage-dependent threshold shift. Interface traps are highly dependent on oxide processing, and other variables (applied field and temperature).

Figure 4 is schematic in that it does not show real data, but it reasonably represents the main features of the radiation response of a hardened n-channel MOS transistor. The range of data, from 10^{-6} s to 10^{8} s, is enormous, as it has to be to include qualitatively the four main processes we have discussed. For the oxide illustrated in Figure 4, a relatively small fraction of the holes reaching the interface are trapped, which is why we say it is realistic for a hardened oxide. Many oxides would trap more charge than is shown here. In addition, the final threshold

shift, including interface traps, is positive (the so-called rebound or super-recovery effect) here because the number of negatively charged interface traps finally exceeds the number of trapped holes. Not all oxides really have this behavior, but it is one of the results which can be considered "typical."

2.2 Description of Basic Physical Processes Underlying the Radiation Response of MOS Devices.

Next, we consider these basic physical mechanisms in more detail, and provide critical references. But for a complete review, the readers should consult the references.

2.2.1 Electron-Hole Pair Generation Energy

The electron/hole pair creation energy, E_p, was determined to be 18 ± 3 eV in SiO_2 by Ausman and McLean [7], based on experimental data obtained by Curtis et al. [8]. This result has been confirmed independently by others [9], [10], including a more accurate set of measurements and analysis by Benedetto and Boesch [11], which established $E_p = 17 \pm 1$ eV. From this value of E_p, one can calculate the charge pair volume density per rad, $g_0 = 8.1 \times 10^{12}$ pairs/cm^3-rad. But this initial density is quickly reduced by the initial recombination process, which we discuss next. For Si, E_p is 3.6 eV, and 4.8 eV for GaAs.

2.2.2 Initial Hole Yield

The electrons are swept out of the oxide very rapidly, in a time on the order of a picosecond, but in that time some fraction of them recombine with the holes. The fraction of holes escaping recombination, $f_y(E_{ox})$, is determined mainly by two factors: the magnitude of the electric field, which acts to separate the pairs; and the initial line density of charge pairs created by the incident radiation. The pair line density is determined by the linear energy transfer (LET), and is, therefore, a function of the incident particle type and energy. The line density is also inversely proportional to the average separation distance between electron/hole pairs –obviously, the closer the average spacing of the pairs, the more recombination will occur at a given field, and the less the final yield of holes will be.

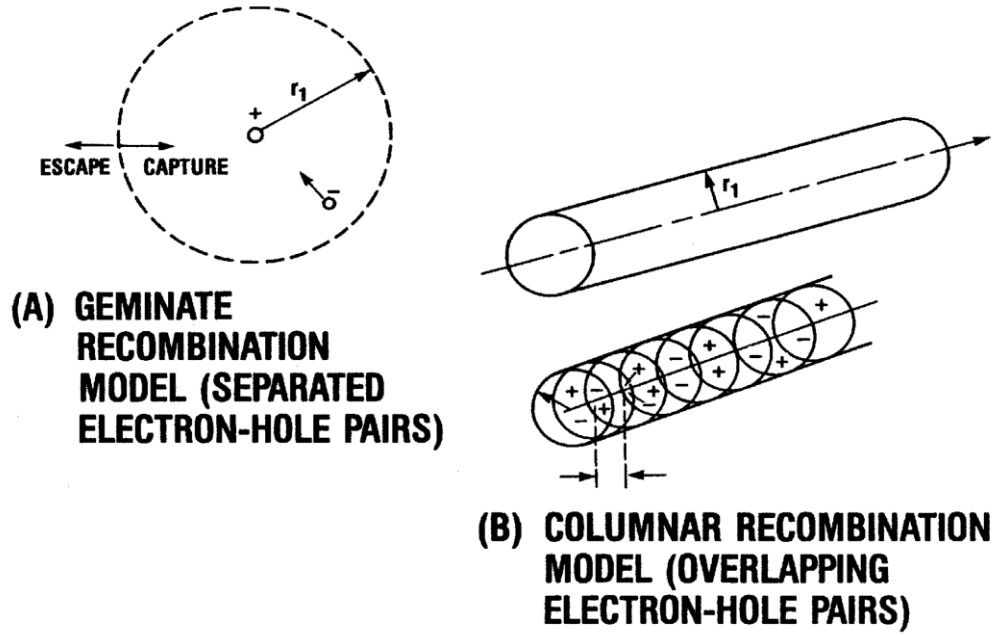

Figure 5. Schematic diagrams indicating pair separation distances for two recombination models: (a) geminate (separate electron/hole pairs) and (b) columnar (overlapping electron/hole pairs).

The recombination problem cannot be solved analytically for arbitrary line density, but analytic solutions do exist for the limiting cases, where the pairs are either far apart, or very close together. These cases are illustrated in Figure 5. Figure 5a shows the so-called geminate recombination model, where the average separation between pairs is much greater than the thermalization distance, the distance between the hole and the electron. One can treat the interaction between the charges of an isolated pair, which have a mutual coulomb attraction, which undergo drift motion in opposite directions under the influence of the applied field, and which have a random diffusion motion driven by the thermal fluctuations of the system. But interactions with other pairs can be neglected. The geminate recombination model was first formulated by Smoluchowski [12], and later solved by Onsager [13], originally for the recombination of electrons and positive ions in gases. Experimental and theoretical results for the geminate process are shown in Figure 6, where the theoretical curve was obtained by Ausman [14], assuming the average thermalization radius, r_t, to be 5 nm.

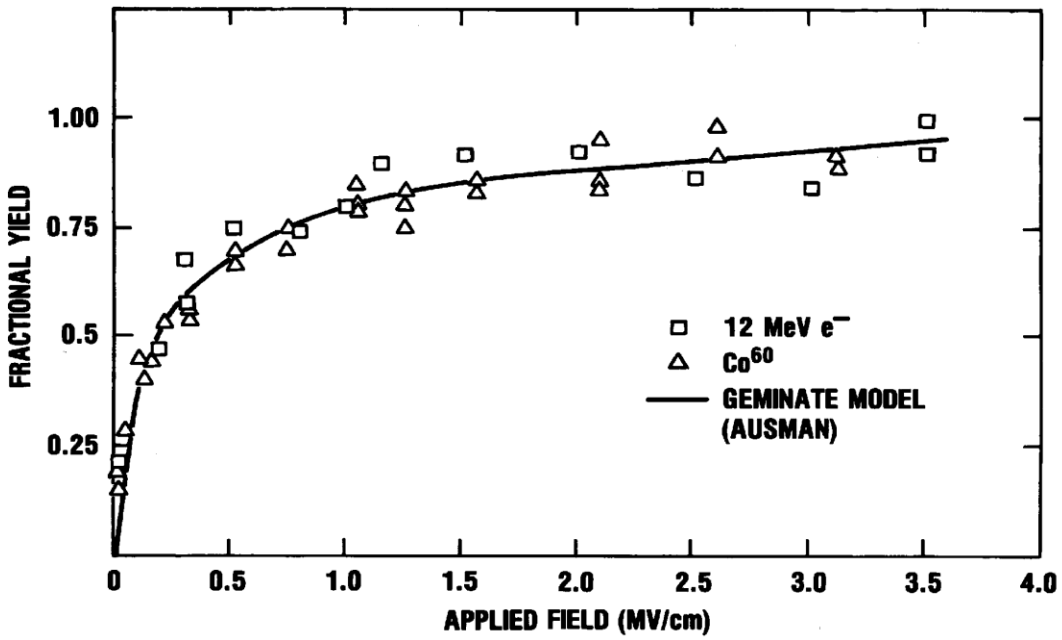

Figure 6. Fractional yield as a function of applied field for Co60 gamma rays, 12-MeV electrons, and geminate model calculations. [10], [14], [21]

The other case, called columnar recombination, is illustrated in Figure 5b, where the separation between pairs is much less than r_t. There are several electrons closer to any given hole than the electron which was its original partner, so the probability of recombination is obviously much greater than in the geminate case. The columnar model was originally solved analytically by Jaffe [15], extending earlier work by Langevin [16]. More recently, Oldham [17]-[19] has presented a more accurate numerical solution of the Jaffe equation, which extends the range of applicability of the model. Representative experimental data, for 2 MeV alpha particles, are presented in Figure 7 [17], along with theoretical curves. The parameter, b, is the half-diameter assumed for the initial Gaussian charge distribution. Recombination results for a variety of incident particles are summarized in Figure 8 [21]. At a field of 1 MV/cm, there is a difference of more than an order of magnitude in the yields shown for different particles. Clearly, recombination is an important effect, which must be accounted for, when comparing the effect of different radiation sources. One case of considerable practical importance is the comparison of yield between Co^{60} gamma rays and 10 keV X-rays, which has been studied extensively by several different groups [11], [21-23].

We note that many cases of practical interest are intermediate between these two limiting cases, meaning the separation between electron hole pairs is roughly comparable to the separation between an electron and its original hole partner. This point is illustrated in Figure 9 [20], LET is given as a function of energy for electrons and protons. For secondary electrons produced in a Co-60 source, the separation between charge pairs is such that the geminate model clearly applies. Most heavy ions have LETs off the top of the chart, so the columnar model applies to them. But many proton energies of practical interest fall in the middle transition

region. Here we have discussed simple models as the best way to convey physical insight, but there are complex Monte Carlo codes that are better for making quantitative predictions [24, 25].

In Figure 10, we show model results calculating the fractional yield columnar recombination for heavy ions. N_0 is the line density for charge pairs, which is proportional to LET. The electric field that is given is not the total field, but just the component normal to the particle track. For very high LETs, especially with low normal field components, the calculated yield is less than 0.01, and as little as 0.001. However, experimental results are usually not less than 0.01. The significance of this difference depends on how one looks at it, though. The ratio of two small numbers can vary widely, but the difference between two small numbers is always a small number. Plotted in Figure 8, the difference between 0.01 and 0.001 would be almost imperceptible.

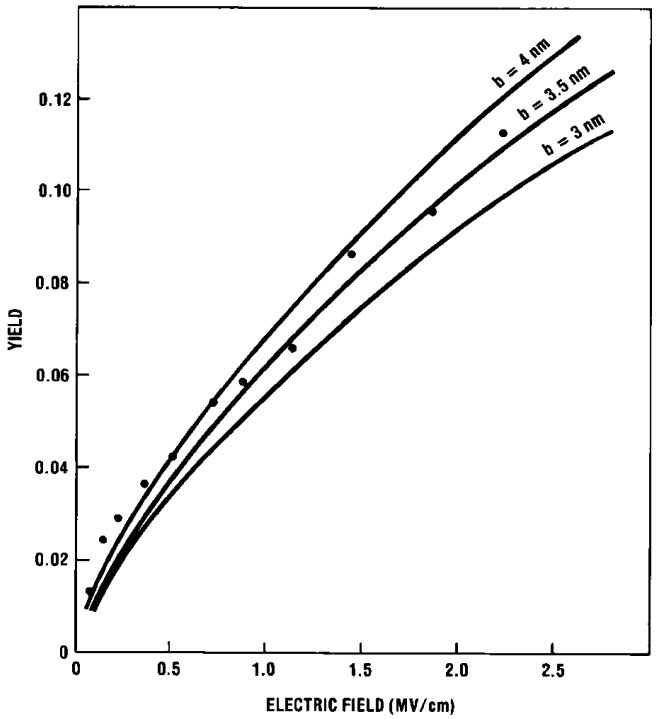

Figure 7. Fractional yield as a function of applied field for alpha particles incident on SiO_2. Solid lines indicate columnar model results for different initial column radii [17-18].

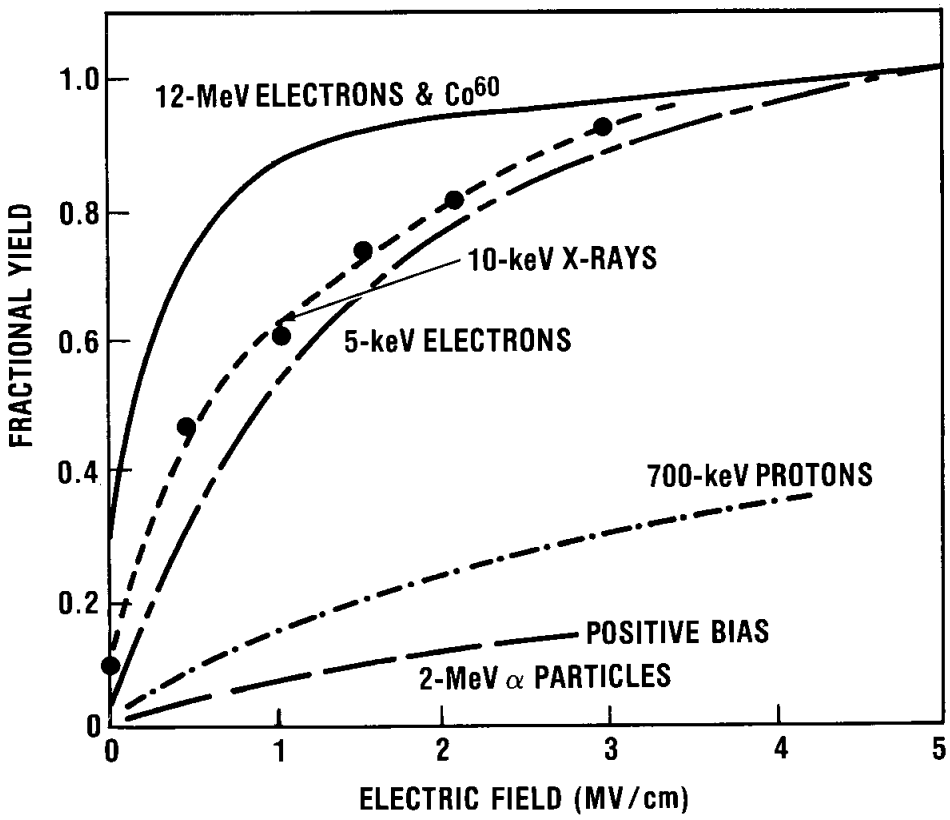

Figure 8. Experimentally measured fractional hole yield as a function of applied field, for a number of incident particles [21].

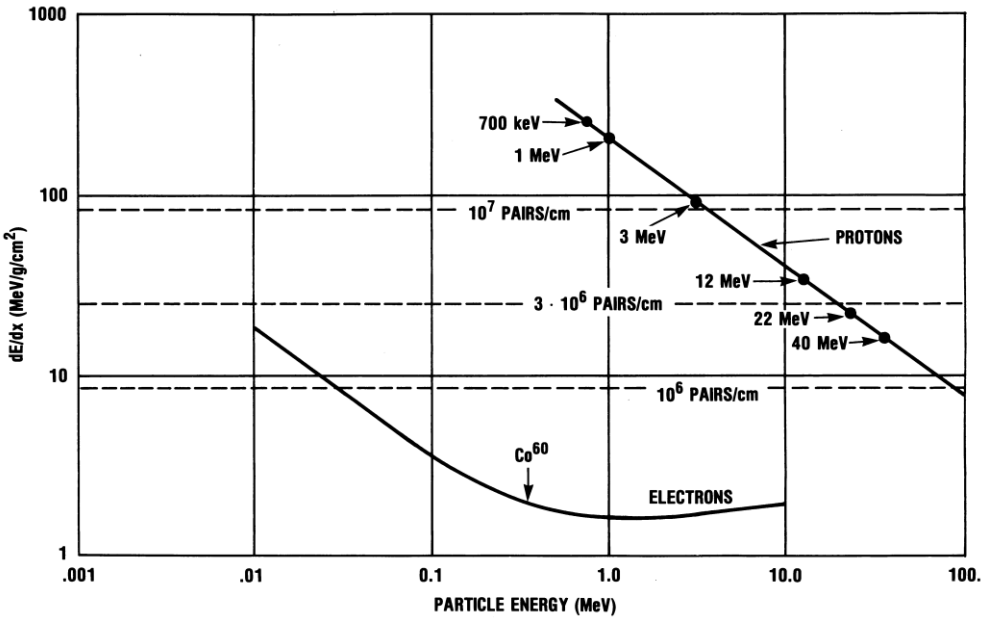

Figure 9. LET as a function of energy for protons and electrons [20].

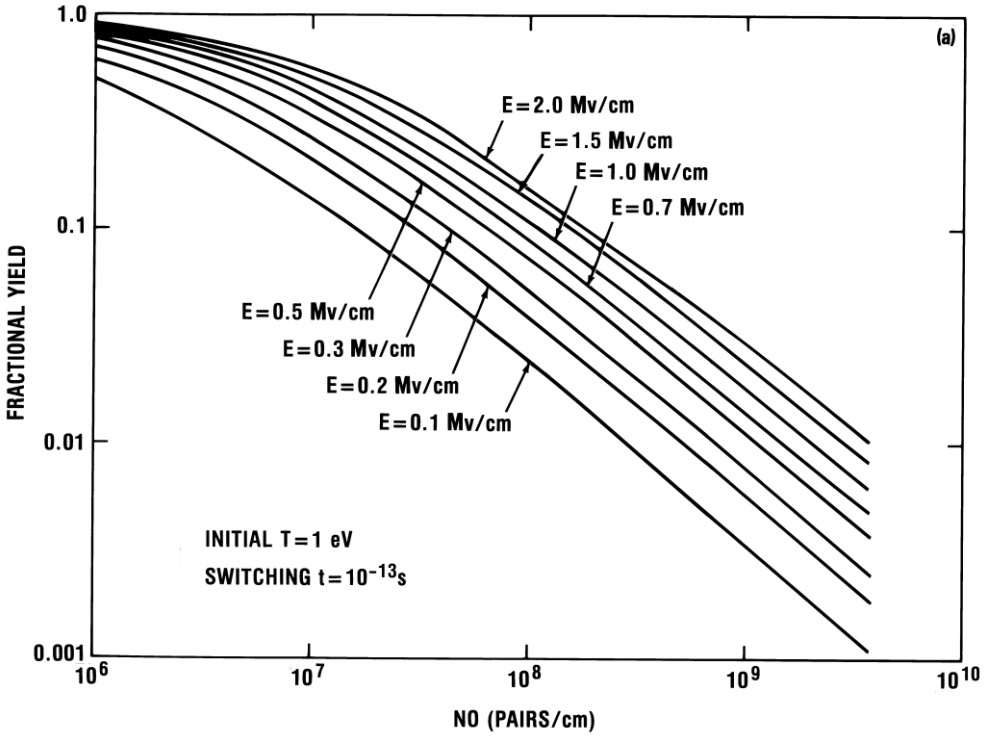

Figure 10. Calculated fractional yield for heavy ions as a function of charge line density (N_0) and normal field component [19].

As one might expect, there are also a number of intermediate cases of practical interest, where neither model is strictly applicable, as illustrated in Figure 11. The original version of this figure was published by Oldham [20] in 1984, based on experimental data by Stassinopoulos et al. [26-28] and Brucker et al. [29, 30]. But additional data points have been added from time-to-time, as other experiments were reported [31-33]. These later experiments have generally reported lower yield (that is, more recombination) than the earlier experiments. The different experiments have all been done at different fields, so the geminate model limit is different in each case, which is not indicated in Figure 11. Strictly speaking, the theoretical curves in Figure 11 apply only to the Stassinopoulos and Brucker measurements. The other key point is that the LET for a proton and an electron is not really the same until their energy is about 1000 MeV, well above the energy of any incident particle in any of these experiments. In the original version of Figure 11, the geminate model was indicated schematically to apply from 1000 MeV down to about 150 MeV because it appeared to fit the data available at that time. But the more recent data indicates that the recombination process is not purely geminate until the proton energy is well above 100-200 MeV.

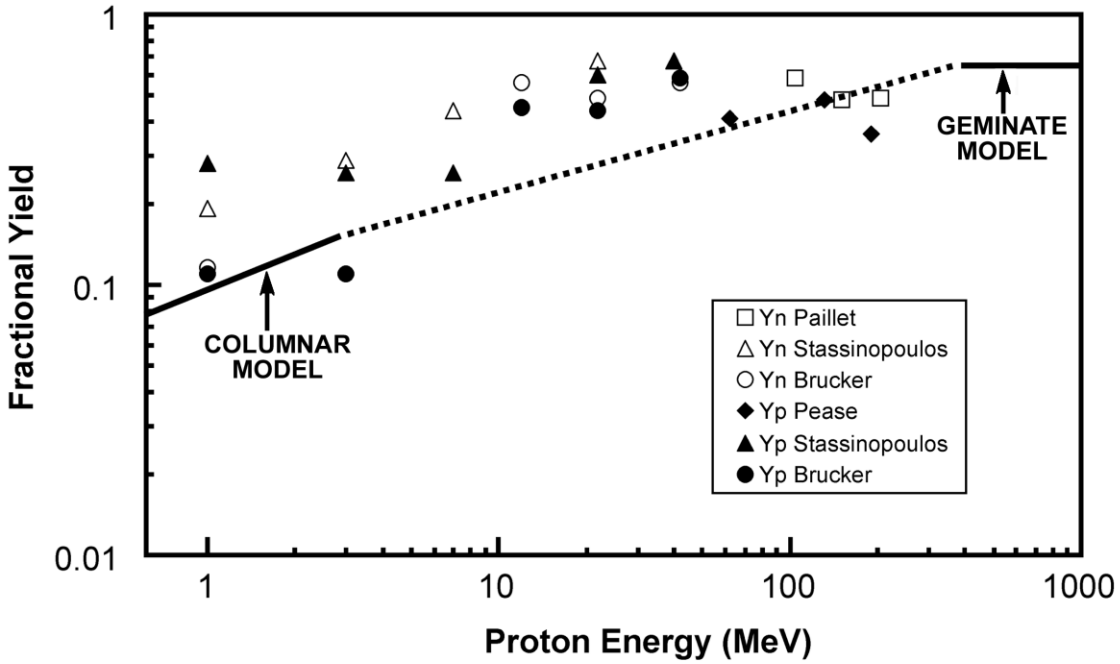

Figure 11. Recombination measurements and calculations for protons incident on SiO_2. N and p refer to n-and p-channel transistors, respectively.

2.2.3 Hole Transport

The transport of holes through the oxide layer has been studied extensively by several groups [34-45], and it has the following properties: (1) transport is highly dispersive, taking place over many decades in time following a radiation pulse. (2) It is universal in nature, meaning that changes in temperature, field and thickness do not change the shape or dispersion of the recovery curves on a log-time plot. Changes in these variables affect only the time-scale of the recovery. (3) The transport is field activated. (4) At temperatures above about 140K, the transport is strongly temperature activated, but it is not temperature activated below about 140K. (5) The hole transport time, or recovery time, has a strong super-linear power law dependence on oxide thickness.

The best overall description of the experimental hole transport data seems to be provided by the CTRW (continuous-time-random-walk) hopping transport formalism, which was originally developed by Montroll, Weiss, Scher and others [46-49]. This formalism has been applied to hole transport in silicon dioxide by McLean [34], [37-38], [42-45] and by Hughes [35], [36], [41]. (However, the multiple trapping model [39-40] also accounts for many of the features of the experimental data.) The specific transfer mechanism seems most likely to be small polaron hopping of the holes between localized, shallow trap states having a random spatial distribution, but having an average separation of about 1 nm. This process is illustrated in Figure 12. The term polaron refers to the situation where the carrier interacts strongly with the surrounding medium, creating a lattice distortion in its immediate vicinity (also referred to as self-trapping, line b of Figure 12). When random thermal agitation brings the energy level of the trapped hole in line with that of the next trap, tunneling can occur (line c). As the hole hops through the material, it carries the lattice distortion with it (line d). The strongest evidence for

the polaron hopping mechanism is the transition from thermally activated transport above about 140K, to non-activated transport at lower temperatures. This transition is a classic signature of polaron hopping [50-52]. Many other features of the hole transport, such as dispersion, universality, and superlinear thickness dependence, can be attributed to a wide distribution of hopping times for the individual holes.

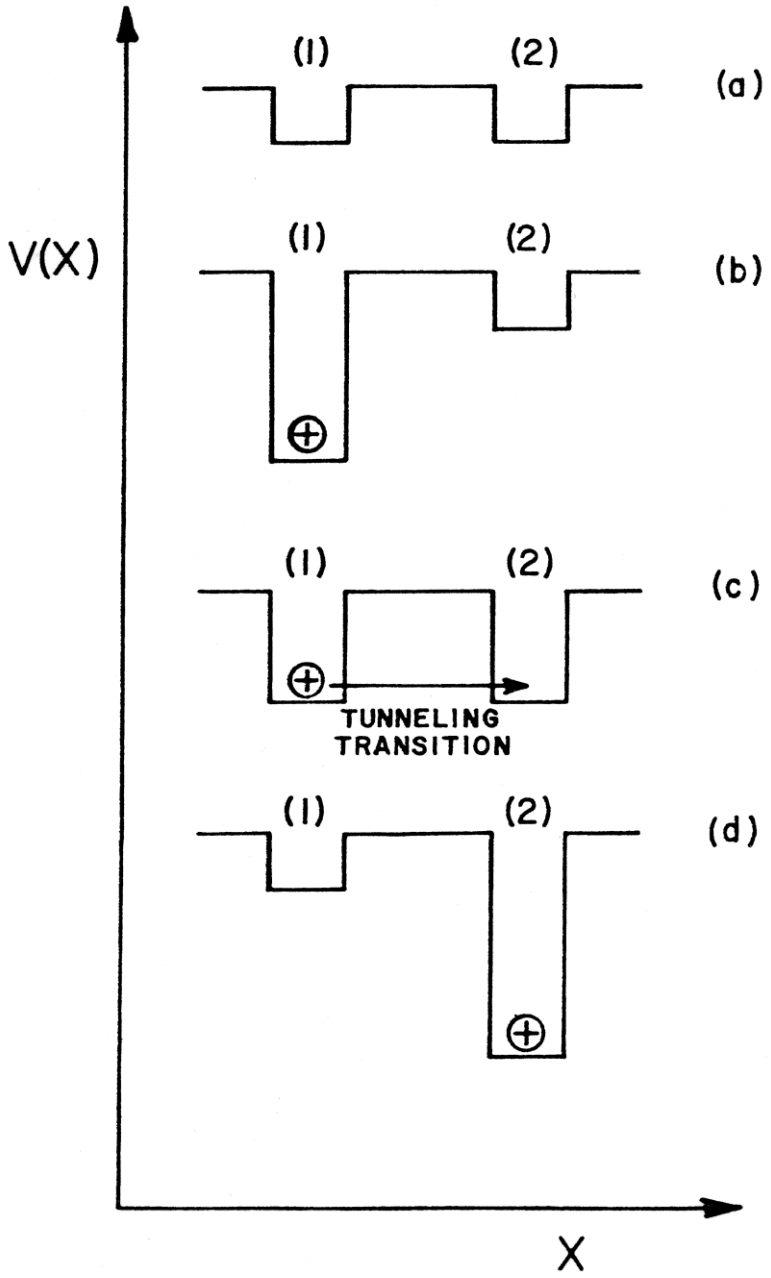

Figure 12. Illustration of polaron hopping transport.

Representative experimental data are presented in Figures 13-16. Figure 13 shows the effect of temperature variation, and Figure 15 shows the effect of varying the electric field. In both Figures, the results cover seven decades in log-time, following a short radiation pulse. In both Figure 13 and 15, the flatband voltage shift is plotted as a function of log-time, normalized

to the calculated shift before any transport occurs. In Figure 13, the field is 1 MV/cm, and the strong temperature activation above 140K is apparent. In Figure 15, all the curves are taken at T=79K. The universality and dispersion of the transport is better illustrated in Figure 14, where all the curves from Figure 13 are replotted for scaled time. The entire transport process covers 14 decades in time (!), and all the curves have the same "S" shape. The time, $t_{1/2}$, at which the flat-band voltage reaches 50% recovery, has been used as the scaling parameter. The solid line is an analytical fit of the CTRW model, where the shape parameter, α, has the value 0.25. Finally, Figure 16 shows how the hole transit time varies with oxide thickness, as $t_{ox}^{1/\alpha}$, or about t_{ox}^{4}. This oxide thickness dependence arises because the farther the holes transport, the greater the probability that some of them will be in states where the next hop is a difficult one, one that takes a long time to happen. Then, the farther the holes go, the slower they move.

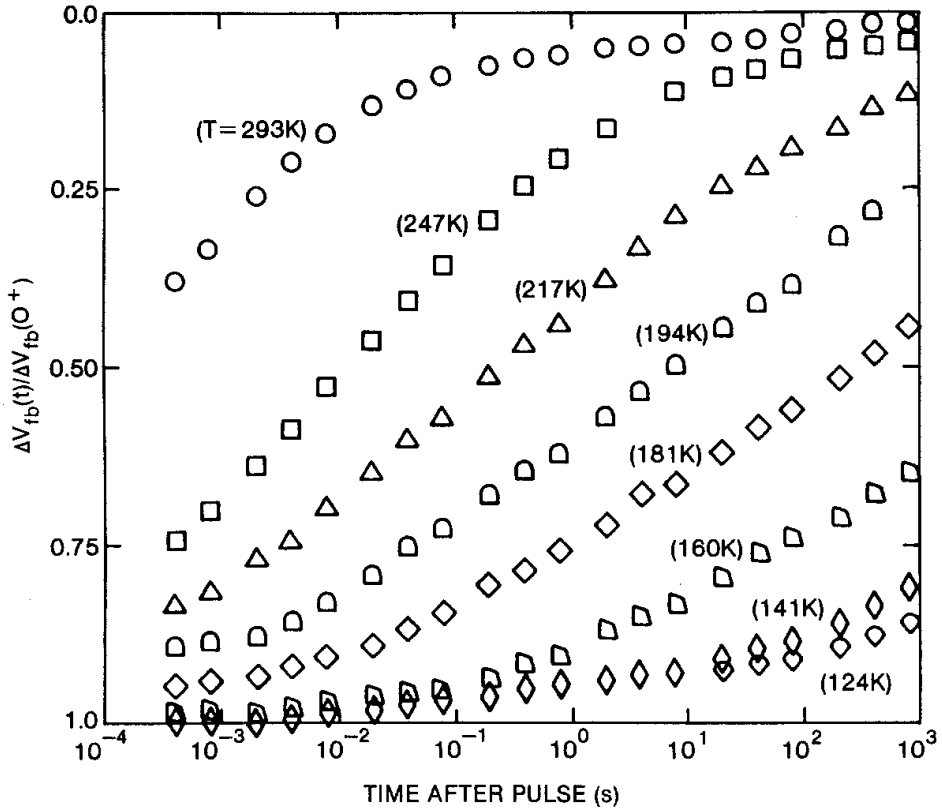

Figure 13. Normalized flatband voltage recovery following pulsed Linac 12-MeV electron irradiation of 96.5 nm oxide at different temperatures [38].

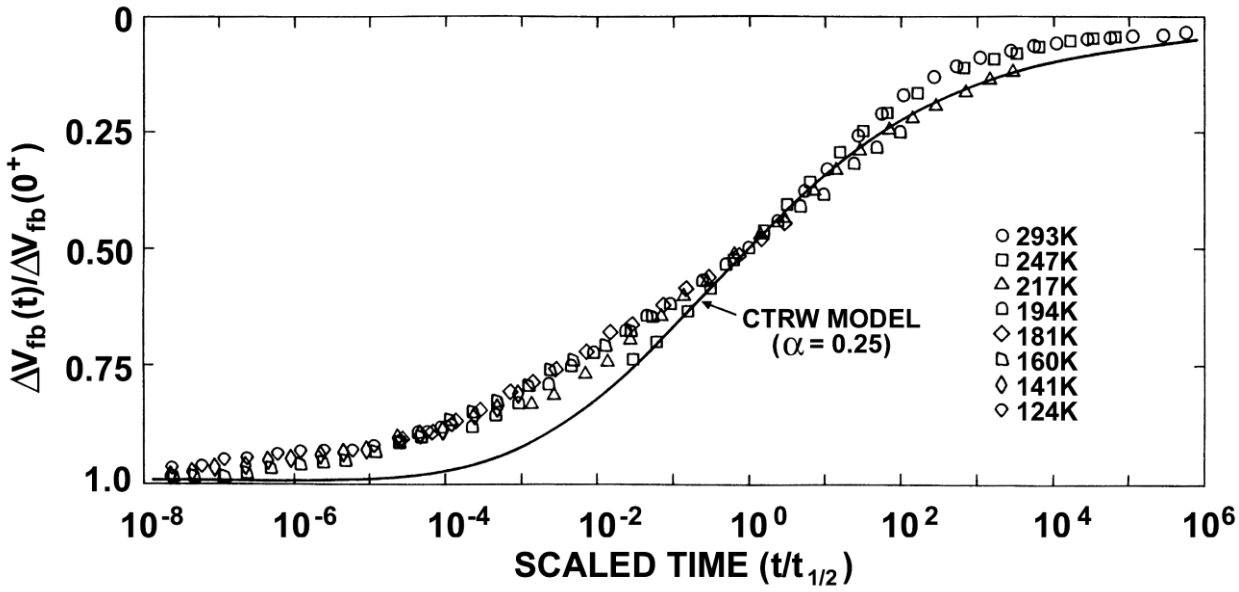

Figure 14. Normalized flatband recovery data of Figure 9 replotted with time scaled to half recovery time, showing universal response with respect to temperature (E_{0X} = 1 MV/cm). Solid curve is CTRW model result for α =0.25 [38].

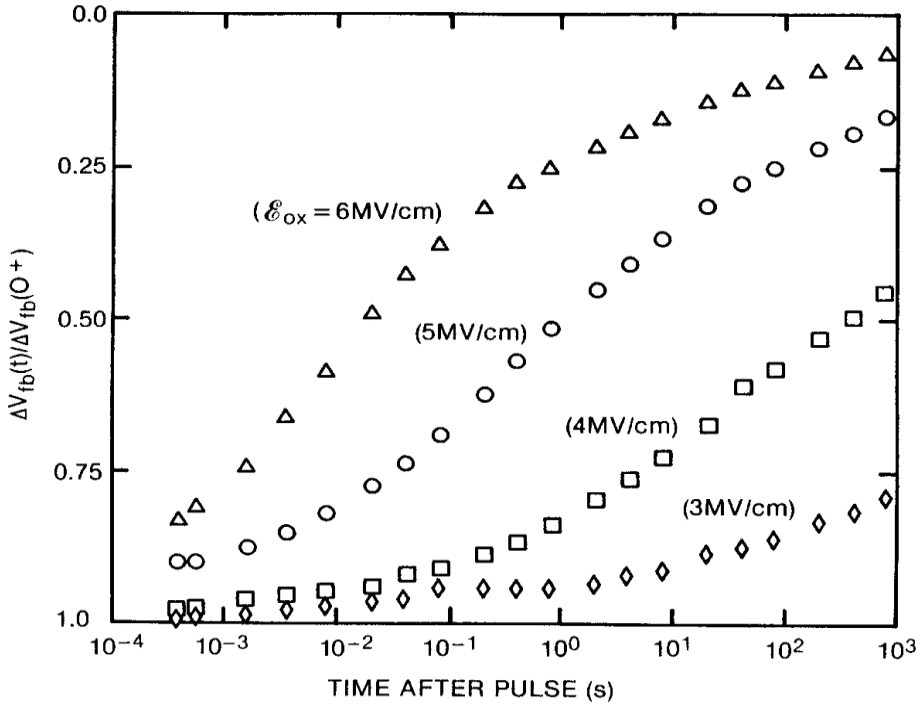

Figure 15. Normalized flatband voltage recovery data following pulsed Linac electron beam exposure of 96.5 nm oxide capacitor at 80K for different fields [43].

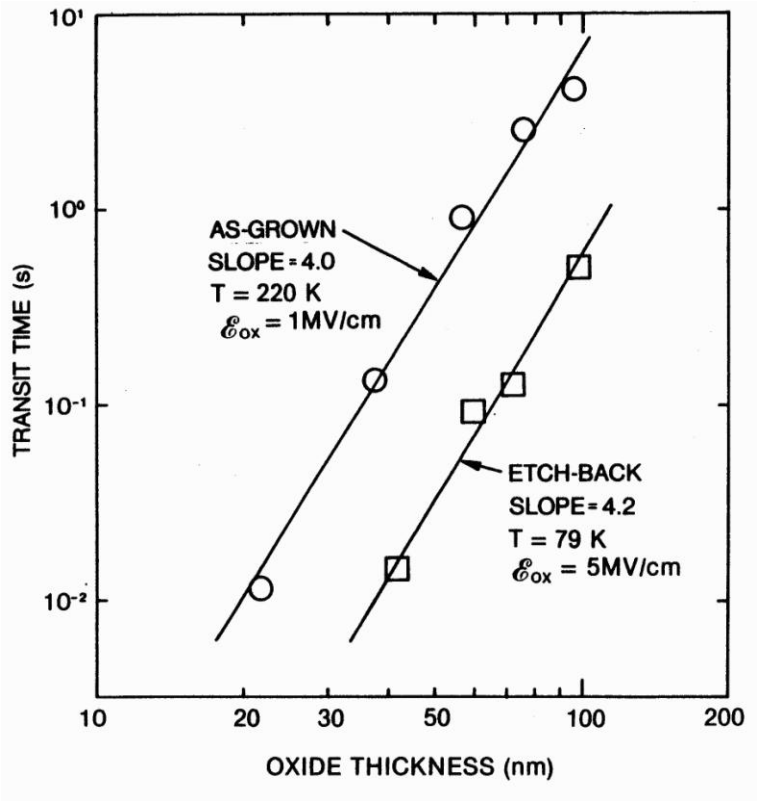

Figure 16. Recovery time as a function of oxide thickness for etched-back and as-grown oxides [43].

2.2.4 Deep Hole Trapping and Annealing

The most complete discussion of hole trapping and annealing is by Oldham [2]. Deep hole traps near the Si/SiO_2 interface arise because there is a transition region where oxidation is not complete. This region contains excess Si, or oxygen vacancies, depending on how one looks at it. The oxidation process was described by Deal et al. [53] in an early review article, which was based on original work done even earlier. Eventually, Feigl et al. [54] presented a convincing model for the single oxygen vacancy. Basically, there is one oxygen atom missing from the usual lattice configuration, leaving a weak Si-Si bond, where each Si atom is back-bonded to three oxygen atoms. When a positive charge is trapped, the Si-Si bond is broken, and the lattice relaxes. The key point that Feigl et al. added to earlier discussions was that the relaxation is asymmetric—one atom relaxes into a planar configuration, and the other remains in a tetrahedral configuration. The oxygen vacancy was also eventually connected to the E' center, originally detected by Weeks [55] in α-quartz, but also later detected in bulk glasses and thermally grown SiO_2. The correlation of E' centers, and oxygen vacancies, with radiation-induced trapped holes was first established by Lenahan and Dressendorfer [56]. Their results are shown in Figure 17.

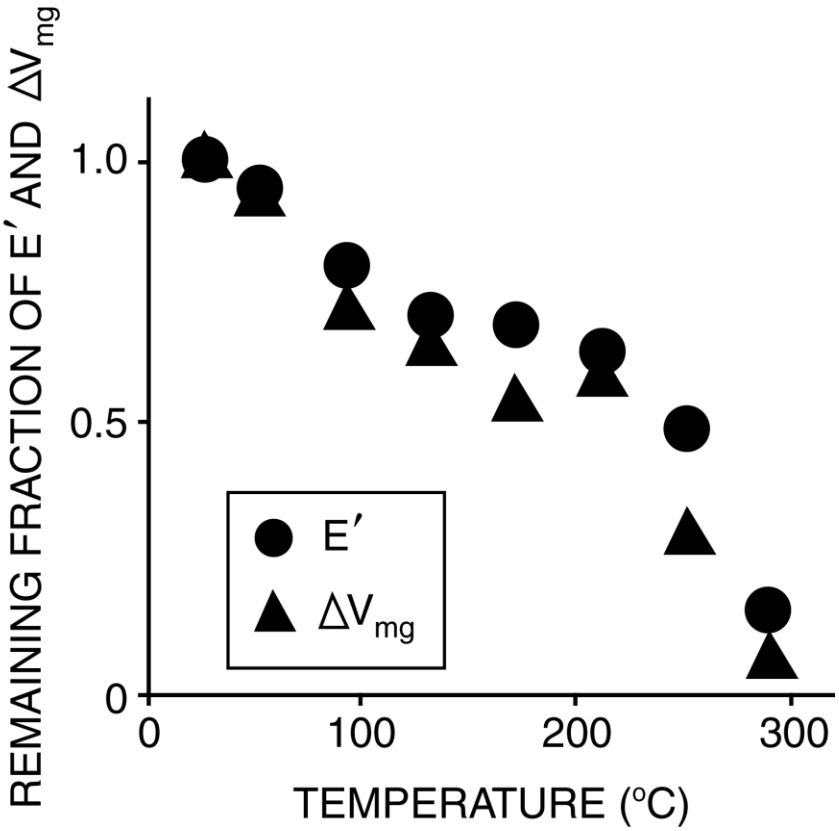

Figure 17. E' signal and ΔVMG , trapped positive charge, are removed at the same rate by isochronal annealing treatments [56]. (Copyright American institute of Physics, reprinted by permission.)

Oxide trapped holes are relatively stable, but they do undergo a long-term annealing process which can extend for hours or even years, with a complex dependence on time, temperature, and applied field. Generally, trapped hole annealing can proceed by either of two processes, tunneling or thermal excitation. At or near room temperature, tunneling is the dominant mechanism, but if the temperature is raised enough, the thermal process will eventually dominate. Tunneling has been analyzed by several authors [57-63], as has the thermal process [64-76]. Both processes can give rise to the linear-with-log t dependence that has been observed empirically [58-60], but one has to make different assumptions about the trap energy level distribution for the two processes.

The tunneling process is illustrated in Figure 18. The tunneling probability is a strong exponential function of distance. For this reason, traps near the interface will be neutralized very quickly, but traps farther from the interface will take much longer. As a result, there is an apparent tunneling front, where traps to the right of the front in Figure 18 have been neutralized, while those to the left have not. For the energy level shown in Figure 18, the front is about 0.2 nm wide, and moves into the oxide about 0.2 nm/decade in time. If the traps have a uniform spatial density, the recovery of V_t will be linear-with-log t. If the spatial density of traps is decreasing with distance into the oxide, the slope of the annealing curve will decrease with time. If thermal annealing is included, with the trap energy level distribution shown in Figure 19, the thermal process will also give an annealing curve linear-with- log t, because equal numbers of

traps will be removed each decade in time. But for the trap distribution shown in Figure 18, the thermal process will give a backward "S" curve—flat on top until the thermal annealing front reaches the band with the traps, then an abrupt change when the traps are neutralized in a short period, then flat again on the bottom.

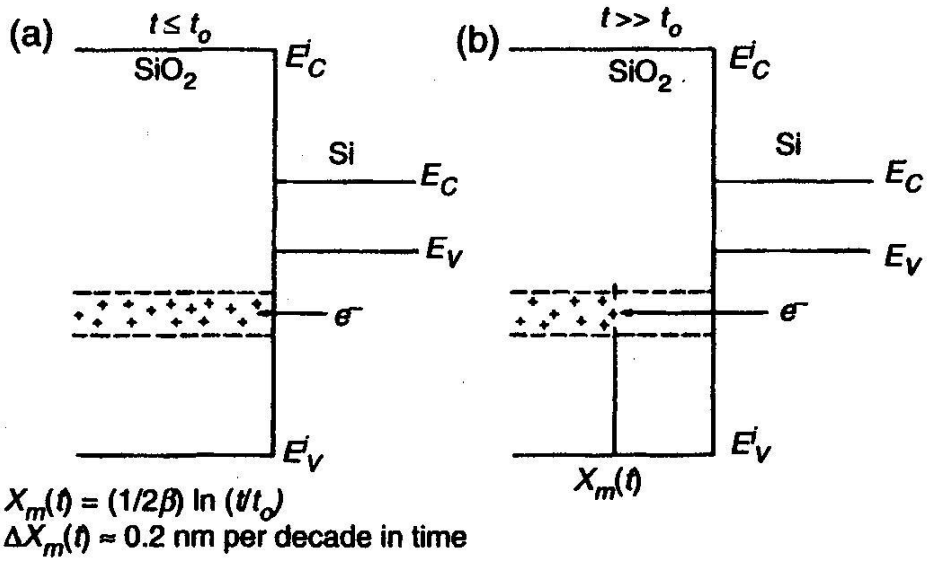

Figure 18. Tunneling front moves into the oxide about 0.2 nm/decade in time [62]

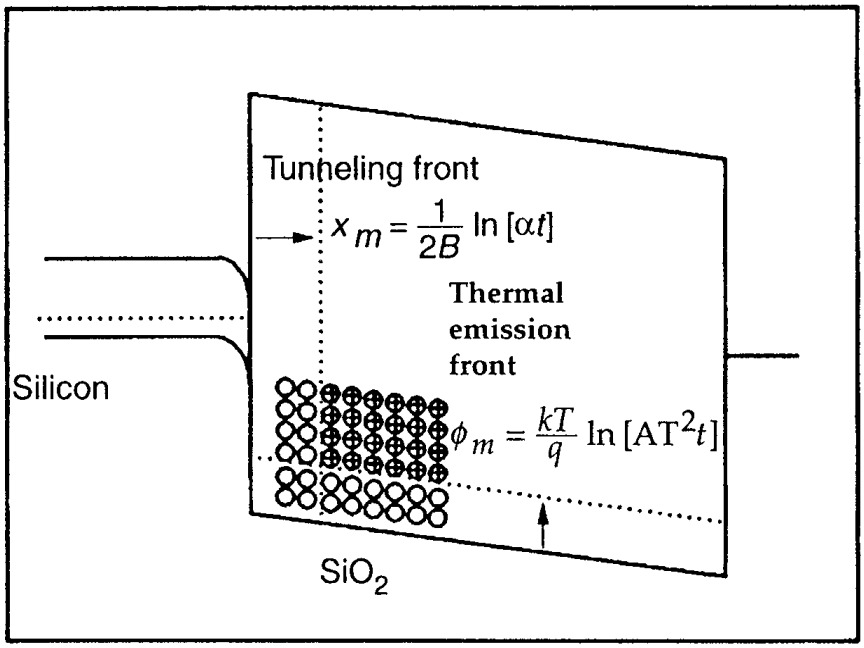

Figure 19. Annealing due to combined tunneling and thermal annealing [75].

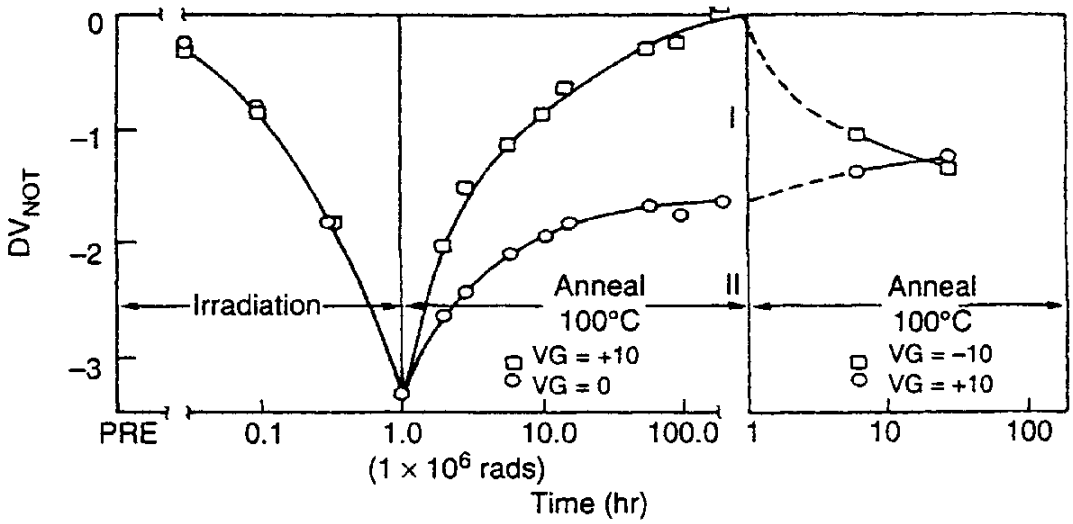

Figure 20. Trapped hole annealing; negative bias curve shows that "annealed" holes are not really removed [77].

The study of radiation-induced trapped hole annealing has led to new insights about the atomic structure of the oxide trap, which in turn has led to new insights into the structure of neutral electron traps, which play a critical role in breakdown studies and in other reliability problems. (For a full discussion, see reference 2.) One of the key results is illustrated in Figure 20, originally reported by Schwank et al. [77]. An irradiated sample was annealed under positive bias at 100 C for about one week, and all the trapped positive charge appeared to be removed. But then they applied a negative bias, and about half the neutralized positive charge was restored within a day. This result led to the idea that annealing of radiation damage involved a compensation process. That is, defects were neutralized without being removed. Although other groups quickly confirmed the basic result [62], [78], several years passed before Lelis et al. did a thorough study [79-81]. One of their key results is shown in Figure 21, where a hardened oxide is exposed to a short Linac radiation pulse, and then subject to a series of alternating positive and negative bias annealing steps. Under negative bias, a significant amount of neutralized positive charge reappears, but there is also a significant amount of "true" annealing, where the trapped charge really appears to be removed. Lelis et al. proposed a model, illustrated in Figure 22, to account for their results and results of others. Generally, it had been assumed that annealing proceeded by an electron tunneling to the positively charged Si, neutralizing it, and reforming the Si-Si bond. Instead, Lelis et al. proposed the electron tunnels to the neutral Si, forming a dipole structure, where the extra electron can then tunnel back and forth to the substrate in response to bias changes. This model is consistent with the ESR work of Lenahan et al. [56] and with the electrical results of Schwank and others, explaining a variety of complex results in terms of a single defect, which was already well-known. The transition from Figure 22a to 22b was described by Feigl et al. The transition from Figure 22b to 22c and back describes the switching reported by Schwank et al. and by Lelis et al. And the transition from Figure 22c back to 22a indicates the true annealing, which is also observed.

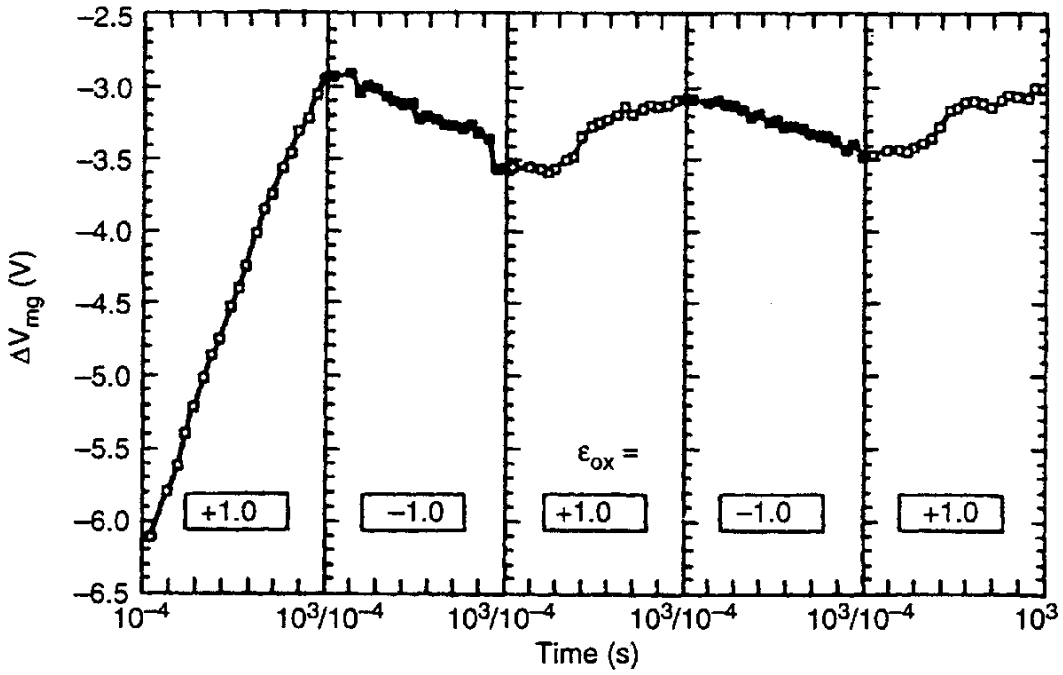

Figure 21. Alternate positive and negative bias annealing for capacitor exposed to 4-μs Linac pulse.

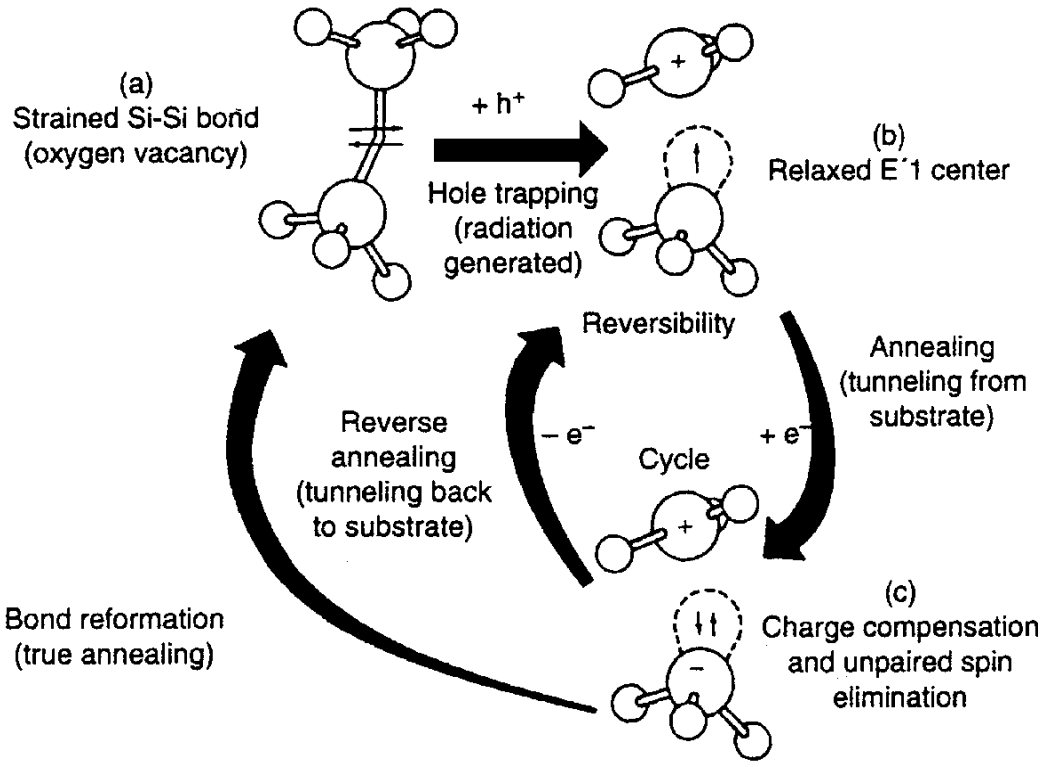

Figure 22. Model of hole trapping, permanent annealing, and compensation processes.

The dipole hypothesis by Lelis et al. was attractive, because it explained many things very simply, but at first, it was also controversial. It was criticized by three different groups, [82-85], for different reasons. The biggest problem was that putting an extra electron on a neutral Si atom instead of a positive Si required overcoming an electron-electron repulsion. Lelis et al. pointed out that adding the extra electron to the positive Si would require changing a planar configuration of atoms into a tetrahedral configuration, moving around atoms in the lattice to change bond angles, which would require adding energy. The energy to rearrange the lattice might be greater than the electron-electron energy, which would mean stable dipoles would be energetically favored. But, initially, they lacked the means to quantify this argument, so debate continued for several years.

Several other, independent, experiments produced results, which seemed to support the dipole hypothesis. These included TSC (thermally stimulated current) measurements, first by Shanfield et al. [67-69], and later by Fleetwood et al. [70-74]. In addition Walters et al. [86] concluded that the dipole proposed by Lelis et al. acted as a neutral electron trap in their injection experiments. This result is shown in Figure 23. Basically, the number of positively charged hole traps saturates after a certain dose, because all the newly generated electrons are captured to form the dipole state. That is, positive centers are being consumed almost as fast as they are created. Once there is a high density of the dipoles, they see large amounts of electron trapping when they inject just electrons. This work was an important independent confirmation of the dipole hypothesis, but it was also a significant extension of it. Basically, they argued that the positive end of the dipole acted as an electron trap, so that a second electron could be trapped, making the whole complex net negative. The reason this result was important was that there is an enormous body of literature on neutral electron traps and the critical role they play in non-radiation-induced reliability problems, and also on efforts to passivate these centers with hydrogen annealing treatments. (This literature is too extensive to review here—see [2]). The Lelis et al. hypothesis became an important piece of the puzzle for explaining all this other work. Conley et al. [87, 88], conducted ESR experiments, where they cycled charge back and forth by alternating bias, while monitoring the E' signal. Their main result is shown in Figure 24. The dipole model was the only one consistent with this result, so it settled the debate, at least on the experimental side. Even more recently, two theoretical groups have done quantum mechanical calculations, using different mathematical approaches, which have also indicated that dipoles should be energetically favored under certain conditions [89, 90]. In addition, Fleetwood et al. have recently extended this model to argue that it also accounts for 1/f noise results, which they reported [91]. We note an interesting recent result by Ryan et al. [92] which seems to indicate that the hole trap, and this model, will play a key role in the ongoing discussion of NBTI (negative bias temperature instability). The experimental result is shown in Figure 25. If either negative bias or high temperature is applied alone, there is no change in the ESR signature from the pre-stress condition. But if both are applied together, a very strong E' signal appears, indicating a high concentration of hole traps. When the NBT stress is removed, the E' signal disappears, and a smaller, residual P_{b1} interface trap signal remains. (Interface traps will be discussed in the next section.) Neither the structure of the P_{b1} center, nor the other details of this process is fully understood, but it seems clear the hole trap plays a significant role.

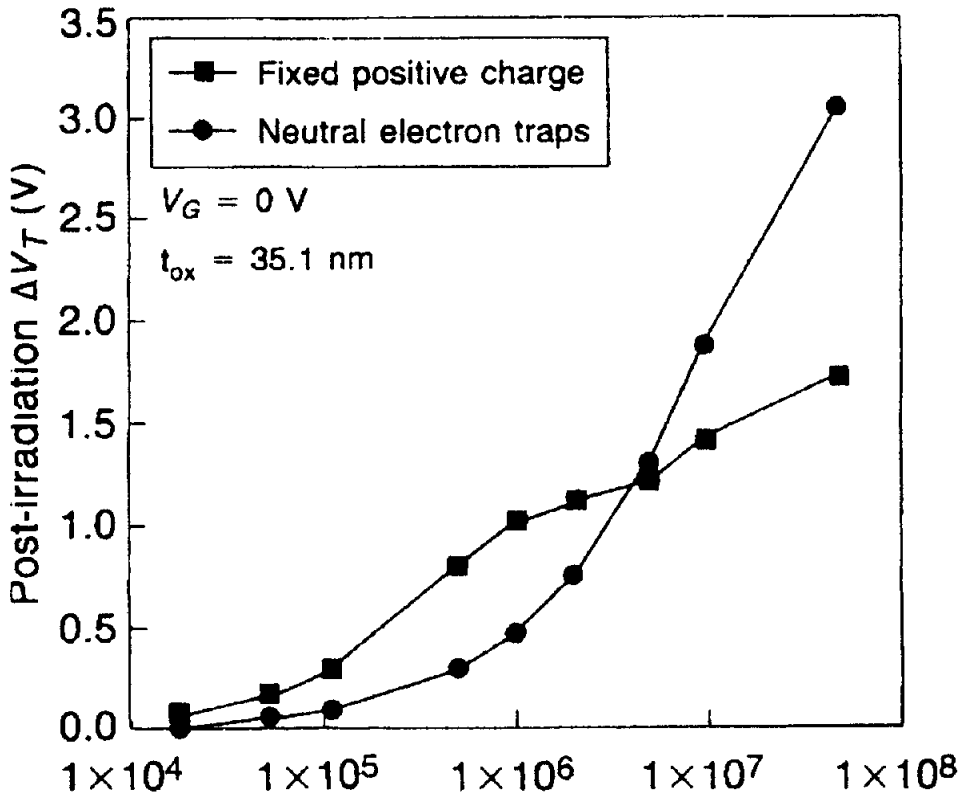

Figure 23. Density of positive centers saturates above about 10^6 rads (SiO_2), because they are consumed almost as quickly as they are created, forming a high density of the dipole state. When electrons are injected, dipoles act as electron traps, and large numbers of electrons are trapped, after [86]. (Copyright Electrochemical Society [86], reprinted by permission.)

One reliability problem where the hole trap clearly plays a role is TID-induced soft breakdown (SBD). This is also referred to as radiation-induced leakage current (RILC), and has been addressed in several papers by Paccagnella and co-workers [93-95]. For thin enough oxides, electrons can tunnel directly from the substrate to the gate contact, and the level of such current that can be tolerated is an important constraint on the design of a circuit. RILC is a variation on this idea, in that a radiation-induced defect increases the substrate-to-gate tunnel leakage current. The basic idea is that electrons tunnel from the substrate to a trap state in the oxide, which is induced by radiation, and then the electron also tunnels from the trap to another trap, or to the gate contact. Of course, one candidate for this defect is the hole trap described above. This effect is a consequence of oxide thinning, or scaling, and it is a gate oxide total dose effect. The impact is that the effects of the excess leakage current may have circuit implications, even though the threshold voltage shift is insignificant. RILC may also be related to breakdown in the oxide, because it has been argued that leakage currents contribute to oxide wearout, which in turn leads to breakdown. But a full discussion of breakdown is beyond the scope of this paper.

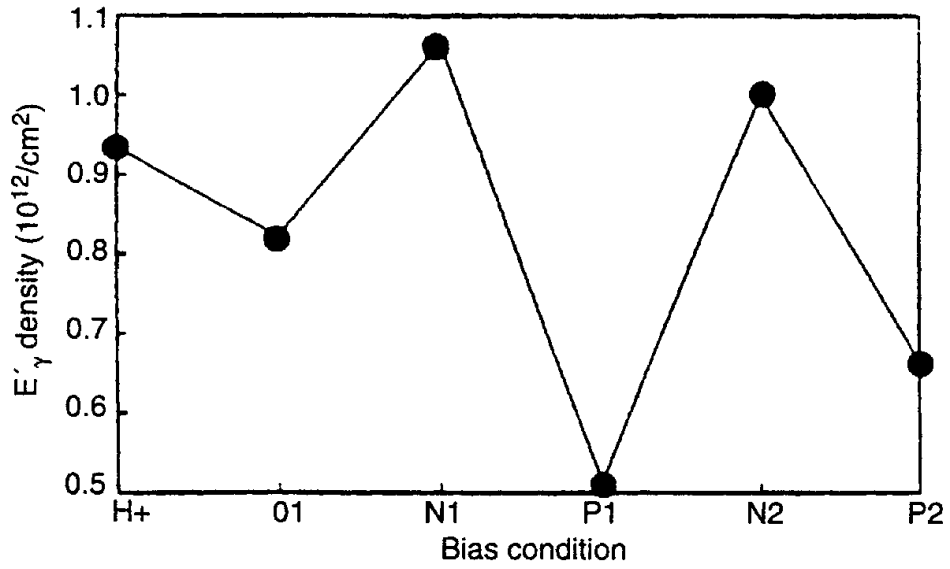

Figure 24. E' density during alternate positive and negative bias annealing.

We note that, in recent years, there has been much discussion of the role of border traps, oxide traps that exchange charge with the Si substrate. The proposal to call these traps border traps was made by Fleetwood [96] in 1992. At that time, the dipole model by Lelis et al. had been in the literature for four years, and was already well known. Now, more than ten additional years have passed, and the defect described by Lelis et al. is still the only confirmed border trap, at least in the Si/SiO_2 system. Other border trap structures have occasionally been proposed [97], but they have not done well in experimental tests [87, 88].

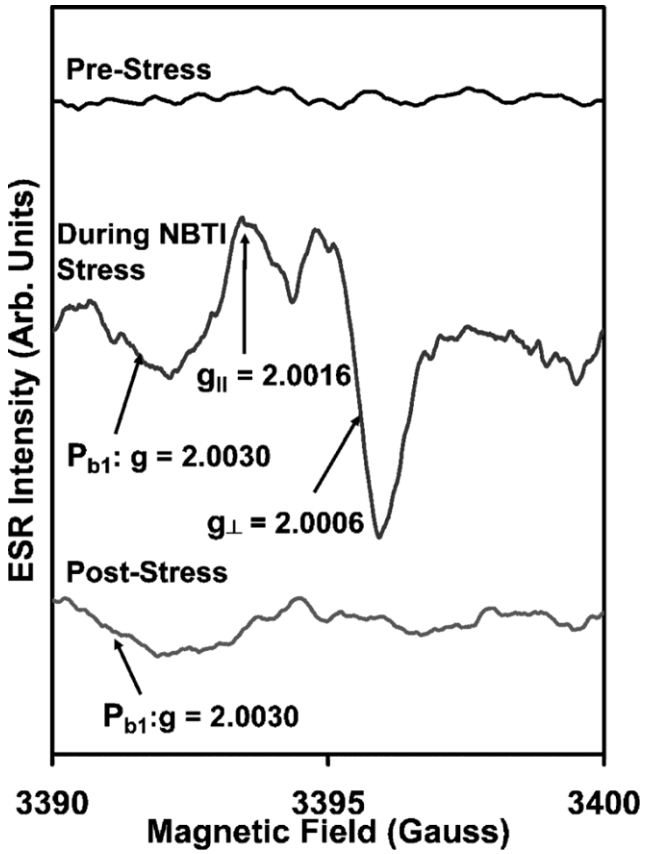

Figure 25. Strong E' signal during NBT stress indicates activation of hole traps. Residual P_{b1} signal indicates presence of interface traps after stress is removed [92]. (Copyright American Institute of Physics, reprinted by permission.)

2.2.5 Radiation-Induced Interface Traps

Radiation-induced interface states have been identified with the so-called P_{b0} resonance in ESR studies, by Lenahan and Dressendorfer [98], which is illustrated in Figure 26. This center is a tri-valent Si atom, back bonded to three other Si atoms, with a dangling bond extending into the oxide. This defect is amphoteric, negatively charged above mid-gap, neutral near mid-gap, and positively charged below mid-gap. Lenahan and Dressendorfer showed a very strong correlation between the build-up of the P_{b0} resonance and the buildup of interface traps, as determined by electrical measurements. There is also an extensive literature suggesting that this same defect is also present as a process-induced interface trap. We cannot review all this literature here, but other reviews have already been published [1], [2]. [99, 100]. (In particular, see the references in Chapter 3 of reference 2.) The basic picture, however, is that when the oxide is grown, there are still about $10^{13}/cm^2$ unpassivated tri-valent Si centers. In subsequent processing, almost all these centers are passivated by reacting with hydrogen. However, they can also be depassivated, either by radiation interactions or by other environmental stresses.

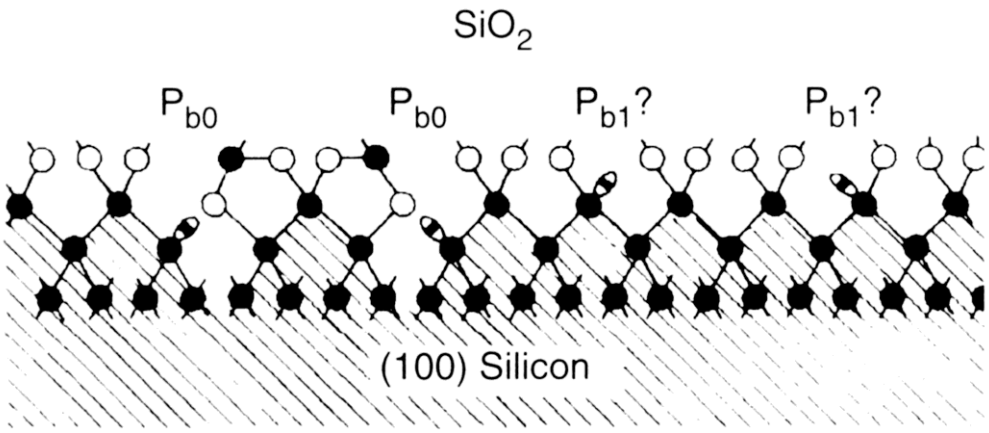

Figure 26. Structure of the P_{b0} interface trap, illustrated.

There have been many conflicting models proposed to describe the process(es) by which radiation produces interface traps, and much controversy about them. However, a reasonable degree of consensus has finally emerged. All the models are consistent with the idea that the precursor of the radiation-induced interface trap is a Si atom bonded to three other Si atoms and a hydrogen atom. When the Si-H bond is broken, the Si is left with an unpassivated dangling bond, as an electrically active defect. The process by which the Si atom is depassivated is where the models differ. Now it has become clear that the dominant process is a two stage process involving hopping transport of protons, originally described by McLean [101], which was based on a series of experimental studies by his coworkers [102-110]. This work was confirmed and extended in a series of additional studies by Saks and his coworkers [111-117]. In the first stage of this process, radiation-induced holes transport through the oxide and free hydrogen in the form of protons. In the second stage, the protons undergo hopping transport (following the CTRW formalism described above). When the protons reach the interface, they react, breaking the SiH bonds already there, forming H_2 and a trivalent Si defect. One of the critical experimental results is shown in Figure 27 [99, 110], which shows the results of bias switching experiments. For curve A, the sample was irradiated under positive bias, which was maintained throughout the experiment, and a large interface trap density eventually resulted. For curve B, the bias was negative during irradiation and hole transport, so the holes were pushed away from the interface, but the bias was switched positive after 1 sec, during the proton transport. The final number of interface states for curves A and B is almost the same, however. For curve E, the bias is maintained negative throughout both stages, and interface trap production is suppressed completely. For curves C and D, the bias is negative during irradiation and hole transport, but switched positive later than for curve B. In all cases, bias polarity during the hole generation and transport made no difference, but positive bias during the proton transport was necessary to move the protons to the Si/SiO_2 interface. The time scale of the interface trap build-up was determined by the transport time of the protons. (For curves B, C, and D, the protons were initially pushed away from the interface, so it took them longer to get there after the proper bias was applied.) McLean also worked out the average hopping distance for protons to be 0.26 nm, which is the average distance between oxygen atoms. And he determined the

activation energy for the interface trap buildup to be 0.82 eV, which is consistent with proton transport [118].

Saks et al. eventually succeeded in monitoring the motion of the protons directly [115], as shown in Figure 28. They annealed their samples in a hydrogen ambient to maximize the hydrogen content of the oxide, before irradiation. The bump on the V_T curve after irradiation occurs because positively charged hydrogen ions are approaching the interface. But they do not build up because when they reach the interface, they are consumed in a chemical reaction, producing unpassivated trivalent Si interface traps and molecular hydrogen. As the protons are consumed in this reaction, the number of interface traps increases dramatically. This was an elegant confirmation of the two stage model, with proton transport as the second stage.

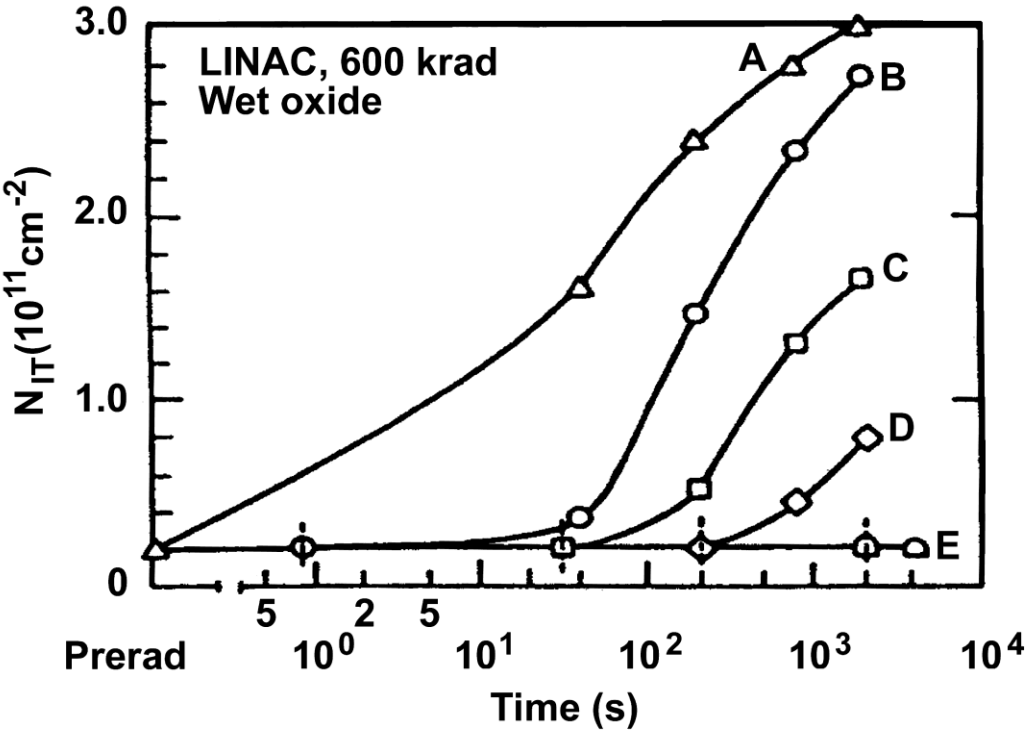

Figure 27. Experimental results from field switching experiments that support H+ transport model.

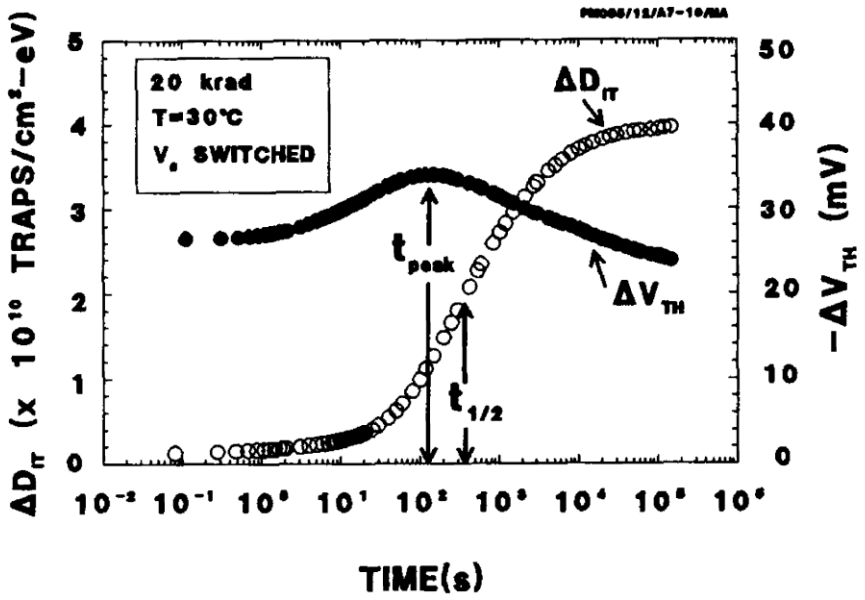

Figure 28. Proton transport followed by the reaction consuming protons and leaving interface traps [115].

The two-stage, proton transport model is a robust model at this point. It has been confirmed by different groups (McLean and coworkers, and Saks and coworkers), using different test structures (capacitors and transistors, respectively), different gate technologies (Al active metal and poly-Si, respectively), and different measurement techniques (C-V analysis and charge pumping, respectively). Despite all these variations, this process has always been the main effect. However, it does not explain everything. Boesch [119] and Saks [112] have identified a second order effect, where a small part of the interface trap build-up seems to correlate with the arrival of transporting holes at the interface. Presumably, the holes break the Si-H bonds instead of protons. Boesch's result is shown in Figure 29, where the temperature is lowered to 200 K to slow down the hole transport. The left axis shows the N_{IT} buildup at room temperature, where a few percent of the total buildup is already present at the first data point, occurring too quickly to be resolved. When the temperature is lowered to slow down the hole transport, this buildup is resolved, and is plotted against the right axis. It amounts to about 7-8% of the total buildup.

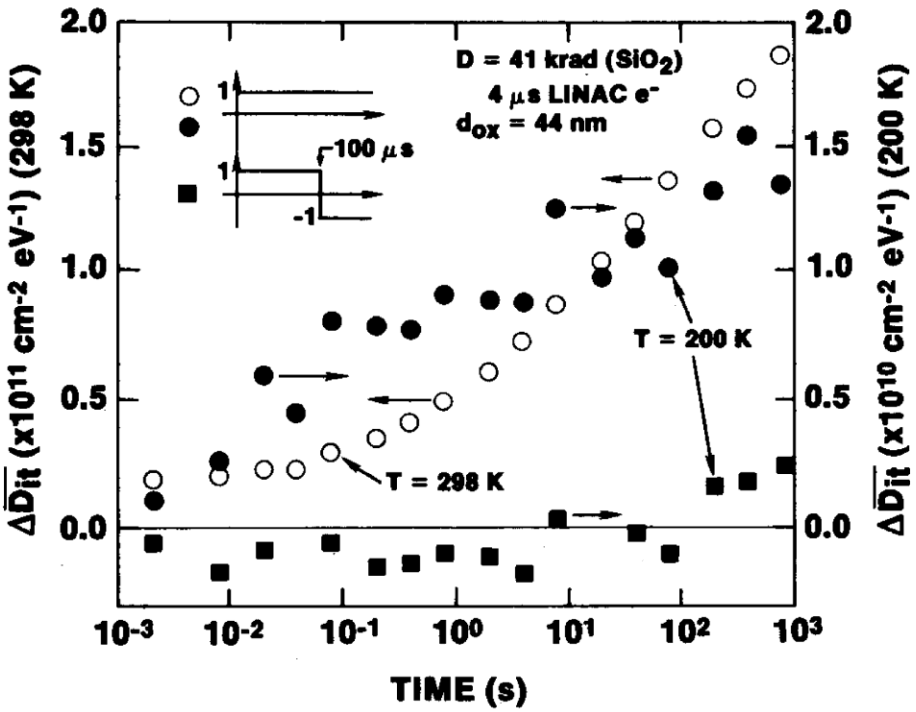

Figure 29. Interface trap formation correlated with hole transport, resolved at low temperature [119].

Also, Griscom [120] and Brown [121] had proposed originally that diffusion of neutral hydrogen, rather than drift transport of protons, was the main mechanism for interface trap production. But, Saks et al. [113] were able to isolate the neutral hydrogen effect, and showed that it was also small. The key result is shown in Figure 30, where the interface trap build-up between 120K and 150K is due to neutral hydrogen, and the build-up above 200K is due to proton transport. The vertical scale is a log scale here, so the neutral hydrogen process accounts for only a few percent of the total build-up. Griscom and Brown both eventually endorsed the McLean model [122] and extended the analysis, as is shown in Figure 31 [123]. They carried the CTRW analysis beyond what McLean had done, and obtained the results shown below. They show that proton transport obeys the same CTRW formalism that was used previously to model hole transport, except that the shape parameter, α, has a different value, 0.38 for protons.

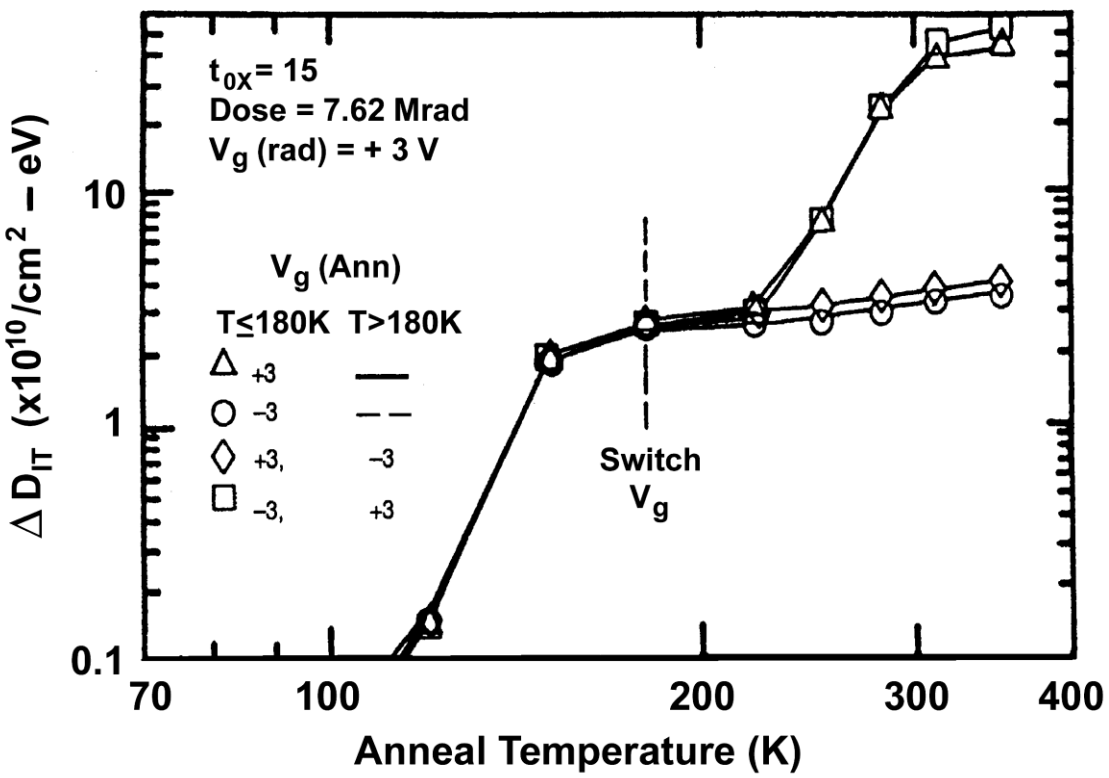

Figure 30. Isochronal annealing results showing small neutral hydrogen diffusion process and larger H+ transport process for interface trap formation [113].

There have also been several models proposed where trapped holes are somehow converted to interface traps – usually the details of the conversion process are not specified [124-128]. These models are not well regarded today. For example, in Figure 27, curves B and E have the same hole trapping. For this reason, one might expect these models to predict similar interface trap build-ups, contrary to what is shown in the figure. If one studies hole trap removal and interface trap build-up carefully, the two processes have different time dependences, different temperature dependences, and different bias dependences. They have the same dose dependence, but otherwise seem to be completely independent. Here, we cannot discuss these things in detail, but full discussions appear in Chapter 3 of [2], and in [99]. However, Oldham et al. [99] provided a reasonable explanation for experimental results purporting to show trapped hole conversions. They pointed out that trapped holes that do *not* undergo a defect transformation can account for most of these results—that is, trapped holes can exchange charge with the substrate by tunneling, and can, therefore, look like interface traps in some experiments. (The model for these holes is discussed in the previous section.) The exchange of charge between trapped holes and the Si substrate has been extensively studied since then (usually under the name border traps) [96], [129], and the idea that such charge exchange takes place is no longer considered unusual.

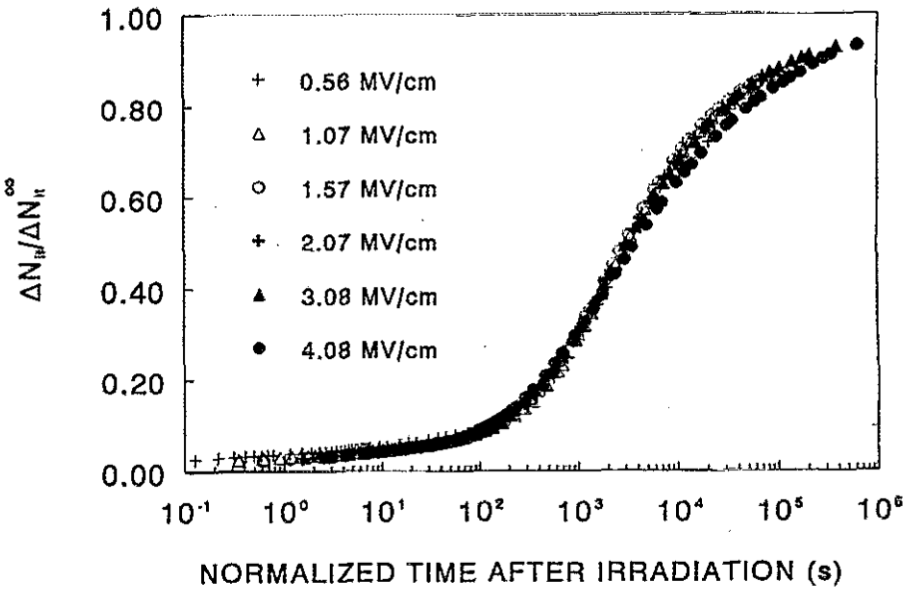

Figure 31. Universal behavior of proton transport, and CTRW model. Results obtained at different applied fields are scaled in a manner similar to that used in Figure 14. In this case, $\alpha = 0.38$.

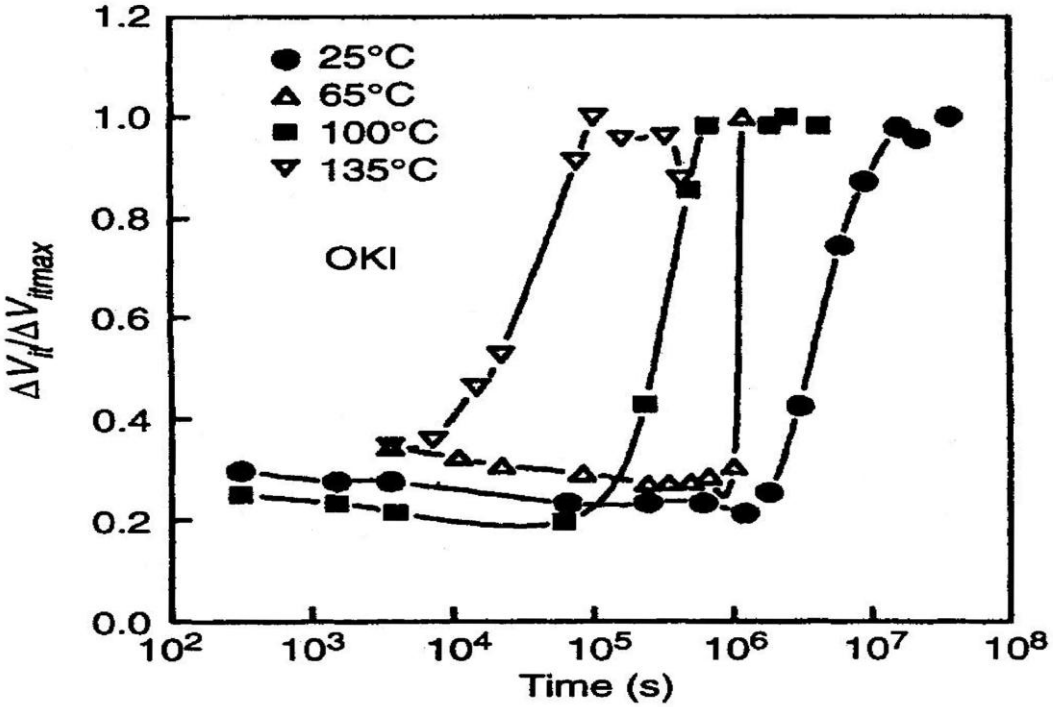

Figure 32. Latent interface trap formation for OKI p-channel transistors [130].

Finally, some samples exhibit what has been called a latent interface trap build-up, which is illustrated in Figure 32 [130]. This effect is thought to be due to hydrogen diffusing into the gate oxide region from another part of the structure, perhaps the field oxide or an encapsulating layer. The latency period arises because the hydrogen is diffusing from (relatively) far away.

From a testing point of view, this is a difficult effect to account for. There is no trace of it on the time scale of most laboratory tests, yet it can eventually be a large, even dominant, effect, on a time scale of months. Saks et al. [117] subsequently reported that the latent build-up is suppressed by a nitride encapsulating layer, which serves as a barrier to hydrogen diffusion. Unless one knows how the samples are encapsulated, it is not possible to predict ahead of time whether a latent build-up will occur or not.

2.2.6 Other Dielectrics.

We have finished our discussion of radiation effects mechanisms in SiO_2, which has been the workhorse dielectric for the semiconductor industry since the beginning. However, other dielectrics with higher dielectric constant (κ) are being used now, because of concerns that SiO_2 cannot be scaled further—that is, it cannot be made any thinner because of power consumption and reliability concerns. Even several years ago, gate oxide thicknesses in leading edge microprocessors were approaching 1 nm, which allowed leakage currents high enough that the processors produced as much heat per unit area as the burner of an electric stove. At one point, Intel presented a chart projecting that, if scaling continued at the same rate, microprocessors would soon produce as much heat per unit area as the surface of the sun [131]! Obviously, there would be problems with the technology before that point was reached. The idea is that with higher κ, the dielectric can be physically thicker, which would reduce leakage current, helping with power consumption and reliability, but still have the same or greater capacitance per unit area as SiO_2. At least three alternative oxides have some reports in the literature on their radiation response, although none have been studied nearly as much as SiO_2. These are silicon oxynitride, SiO_xN_y, hafnium oxide, HfO_2, and aluminum oxide, Al_2O_3. We will discuss each of these briefly. It is an important point, however, that, although these oxides are generally thicker than a pure SiO_2 film would be, they are still extremely thin, perhaps 5nm or less. According to Figure 2, a 5 nm oxide would have a radiation-induced ΔV_T of about 1 mV per Mrad. Therefore, these oxides will generally be very resistant to radiation damage, even if they trap 100% of the radiation-induced charge.

First, we consider oxynitride, since it has been in use longer, and also studied more [132-134]. Boesch and Dunn [132] studied SiO_2 and reoxidized nitride oxides at 77 K and 295 K, and found similar oxide charge generation in both dielectrics, and qualitatively similar charge transport. The main difference was that at cryogenic temperature, hole transport proceeded more quickly in the nitride oxide. Saks et al. [133] reported that the oxide control and all the nitrided oxides except the reoxidized sample had roughly similar hole trapping, but that interface traps were reduced in the nitrided oxides. The reoxidized sample had more of both hole traps and interface traps. Fleetwood and Saks [134] found that the nitride oxides had very favorable oxide and interface trap formation properties—as good as the best hardened oxides in the literature. But because of electrons compensating trapped holes near the interface, they had some trouble estimating the number of such holes for the pure oxides. This was less of a problem for the nitrided oxides.

There are two spectroscopic studies of the defects in oxynitrides [135, 136] which identify what they call the K_N center as an important defect in oxynitrides, in addition to the

known oxide defects. The K_N center is a trivalent Si atom with a dangling bond, back bonded to three nitrogen atoms.

Next, we discuss HfO_2, which is now being used in high volume production, and plays a critical role in virtually every laptop and PC in the world. There have been a few reports on the radiation response of HfO_2, although the reports in the literature are probably on samples far different from production parts. The first report on the radiation response of HfO_2 was by Kang et al. [137]. They reported that, unlike SiO_2, the response of HfO_2 was dominated by negative charge trapping. Other studies [138-140] identified three defect structures that contribute to the overall response. One of these, an O_2, appears to act as an electron trap. There is also an oxygen vacancy center similar to the SiO_2 E' center, which can act as either an electron or a hole trap. The third defect is analogous to the P_b center in SiO_2. There are several other studies of the radiation response of HfO_2 or Hf-silicate [141-143] and one other study which also includes the effects of BTS (bias temperature stress) [144]. Several of these studies indicate that Hf compounds are not especially radiation resistant—they trap charge with reasonably high efficiency. But recall that in Figure 2, ΔV_T ~ 1 mV per Mrad absorbed dose for an oxide about 5.3 nm thick. That measurement was done at 77 K, which means the charges were frozen in place, and the trapped fraction of the charge was 100%. In production technology, according to the ITRS roadmap, the effective oxide thickness (EOT) is about 1 nm. Therefore, the physical oxide thickness would be 1nm times the ratio of dielectric constants, or about 5-6 nm for HfO_2, or about the same as the oxide in Figure 2. For this reason, the maximum ΔV_T for a circuit using HfO_2 would also be in the range of 1 mV per Mrad. That is, the gate oxides should be extremely radiation resistant, just because they are thin. The response of a complex circuit, then, should be determined by the isolation structures, which are much thicker, but which do not contain Hf.

Finally, we discuss Al_2O_3, which was considered as an alternative to SiO_2 at the very beginning of CMOS technology [145]. Aluminum oxide was attractive from a radiation perspective because it trapped electrons, which tended to compensate radiation induced trapped holes. The problem was that it also trapped electrons in the absence of radiation, which meant that it was not very stable. There have been a few recent studies of the effect of radiation on Al_2O_3 where there is an interfacial layer of another material to prevent electron injection into the Al_2O_3 [144, 146,147]. There does not seem to be much industrial interest in following up on these studies, however.

2.2.7 Micro-Dose Effects.

Micro-dose is total ionizing dose damage which is due to a single ion. The possibility that micro-dose might cause a hard error in a microcircuit was first examined by Oldham et al. [17, 18]. In 1981, they concluded that such a failure was unlikely in the near future. However, in 1991, Koga et al. [148] reported that they had observed stuck bits in heavy ion testing of unhardened commercial memories. Koga et al. did not attribute the failures to single ion interactions, however. That the failures were due to single ions was demonstrated experimentally by Dufour et al. the following year [149]. Then Oldham et al. [150] and Poivey

et al. [151] presented additional analysis which agreed with, and helped to explain, the experimental results. The analysis is summarized in Figures 33 and 34. When an ion passes through the oxide, electron hole pairs are generated along the ion track, and, after recombination, some holes are left. In [150], the holes are distributed randomly in approximately the correct volume, and the field seen by each charge is determined by summing the coulomb repulsive force between each pair of charges, along with the external applied field. Then the charges are allowed to hop 1 nm, which is the average hopping distance determined in [37]. Then the field for each charge is recomputed, and they are allowed to hop again, and so on until all the charges reach the interface. Near the exit point for the ion, charges would be trapped very quickly, setting up a repulsive space charge field, which would keep other positive charges away. Charges farther from the interface had to diffuse radially before the applied field could push them to the interface. In Figure 34, it is assumed that all the charges reaching the interface are trapped there, which is almost certainly an overestimate. But the footprint they would present, if viewed from above, is shown. In [149], the transistors had 1 μm channel lengths, so the diameter of the charge footprint is about one-third of the channel length, which is enough to cause a measurable shift in V_T, depending on where it is in the channel.

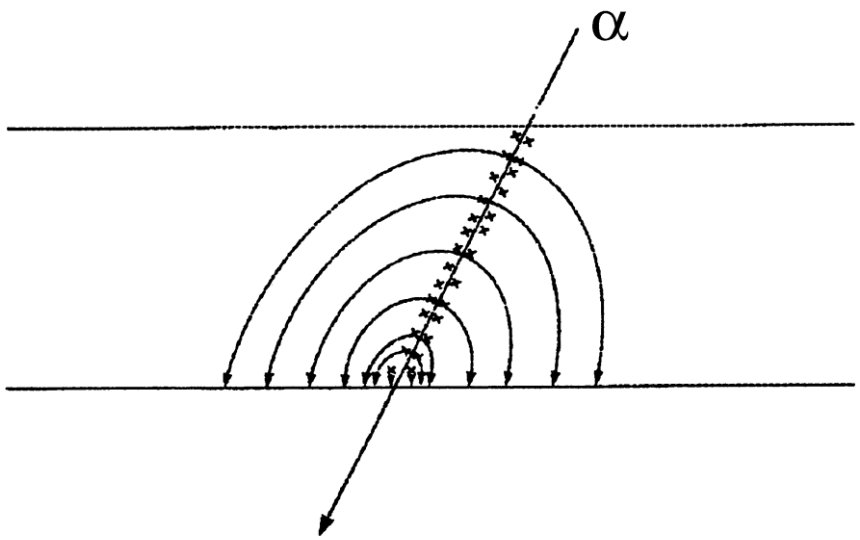

Figure 33. Schematic of paths followed by ion-induced charges transporting through gate oxide.

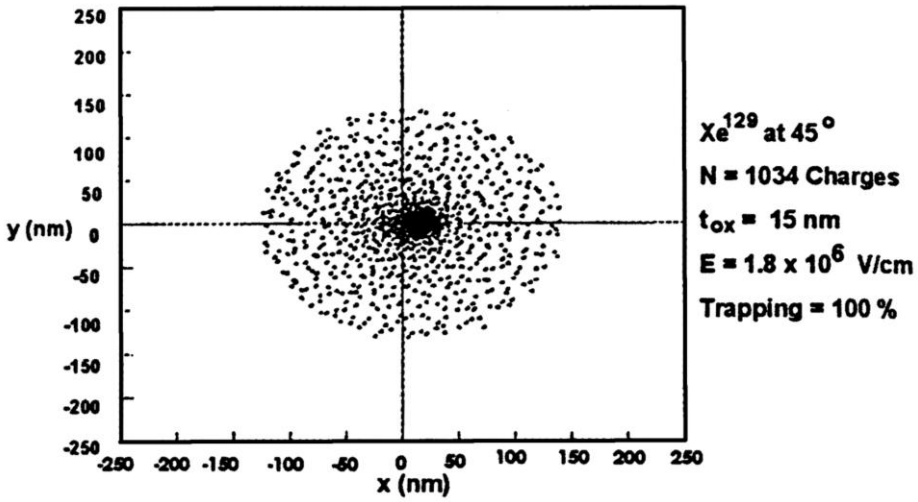

Figure 34. Calculated footprint of charges trapped at Si/SiO_2 interface, as seen from above. Number, N, is based on experimental results [151], but 100% trapping is unusual, even for unhardened, commercial oxides. Footprint would be smaller if trapping fraction were less.

The memory cell where stuck bits were being detected is illustrated in Figure 35. The two p-channel transistors in a standard 6T cell are replaced with large poly-Si resistors, which were on the order of $10^{12}\ \Omega$. These resistors limited the current through the cell, and the power consumption of the entire circuit. For 3.3 V technology, the maximum current that could flow to the drain of the n-channel device, on either side of the cell, was then on the order of 3 pA. Depending on the initial V_T of the transistors, charge deposition like that shown in Figure 34 could easily cause a shift in V_T that would result in leakage current greater than 3 pA. This would mean that charge would bleed off one of the drain junctions faster than it could be replaced. Then that junction could no longer be held high, and the bit would be stuck in the opposite state. Although this kind of micro-dose failure was the first one observed, there have since been others observed, or at least discussed. Loquet et al. [152] presented model results suggesting that stuck bits could also occur as a result of single ions hitting isolation oxides structures. And Swift et al. [153] presented results suggesting that stuck bits could also occur as a result of gate rupture. More recently, several authors have discussed micro-dose failures in power MOSFETs [154, 155], where the oxides are generally much thicker than advanced gate oxides, and which, therefore, trap much more charge.

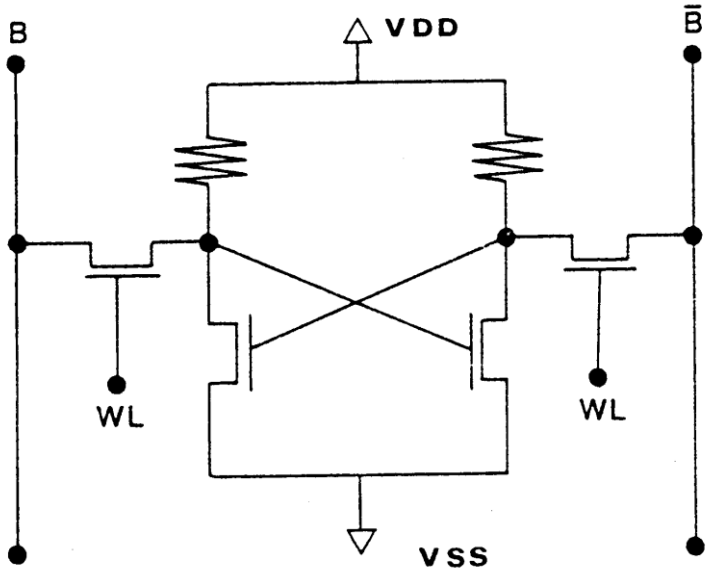

Figure 35. Four transistor SRAM cell. Transistors are all n-channel devices.

In addition, there is another micro-dose failure mechanism, which is not commonly recognized as such. Figure 36 shows a SEM picture of an insulator which had been exposed to 139 MeV S ions [156]. Along the ion track, there was a structural change in the target material, which resulted in a differential etch rate. Here, the tracks are revealed by the etch treatment. Although the insulator in this case is Lexan polycarbonate, similar results are observed in all insulators, including glasses, such as SiO_2 gate oxides. Similar results are not observed in metals or semiconductors. Fleischer et al. [157] discuss a total of nine possible models to explain these results, and they conclude that the results are a coulomb effect, due to free carrier interactions, and not due to atomic scattering. The physical processes are illustrated in Figure 37. First, an ion passes through the insulator and ionizes the atoms in the lattice. Second, if the LET of the ion is high enough, the atoms will be heavily ionized, and repulsive coulomb forces can be high enough to break chemical bonds. In this event, atoms will move apart, and create acute local stresses. The reason similar tracks are not observed in semiconductors and metals is that there is a higher density of mobile free carriers, which move quickly to neutralize the ionized atoms before the lattice can be disrupted. Third, there will then be an elastic relaxation which reduces the stresses by spreading the strain more widely. In this relaxation process, a bump or ridge will develop as more atoms move to relieve stress. An example was reported by Marinoni et al. [158], which is shown in Figure 38.

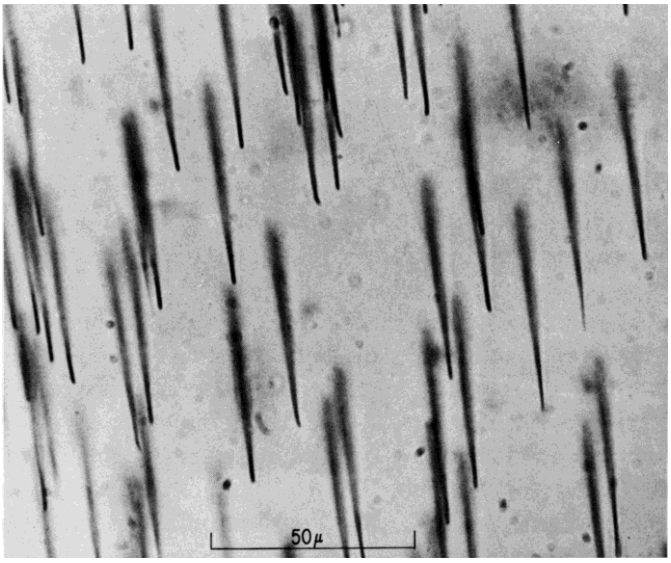

Figure 36. Sulfur ion tracks exposed by etching in Lexan polycarbonate [156]. (Copyright American Physical Society, reprinted by permission.)

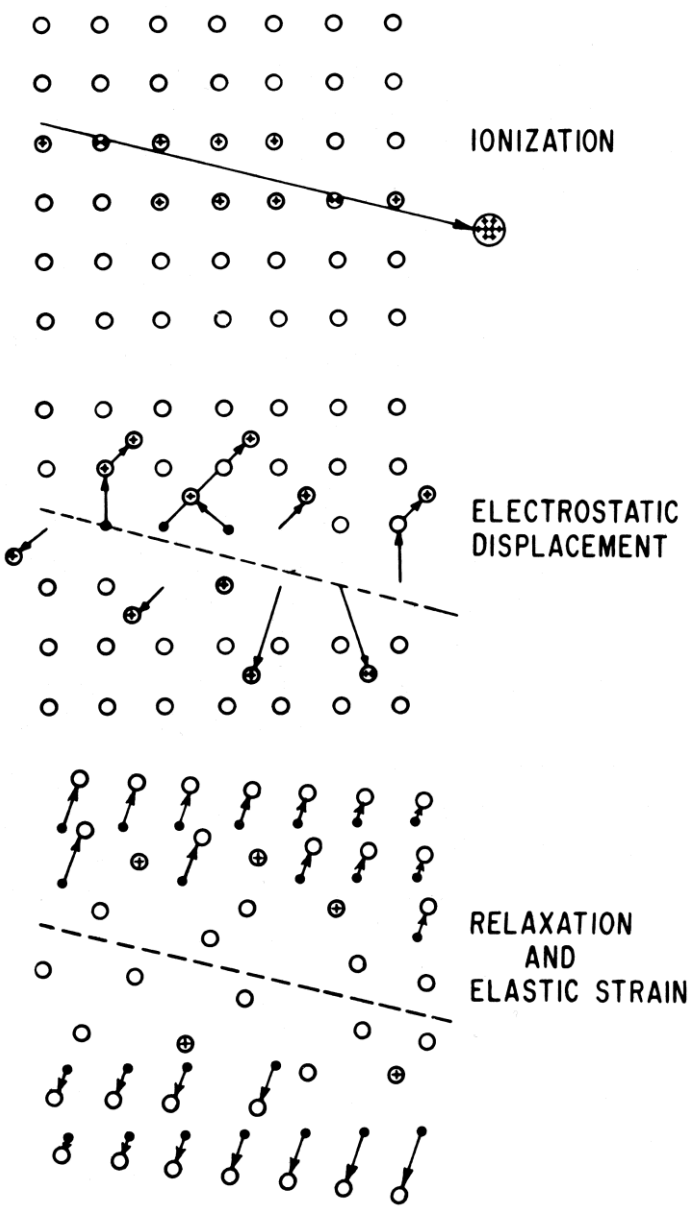

Figure 37. Mechanisms of track formation, after Fleischer et al. [157]: (1) ionization of atoms in the insulator lattice; (2) electrostatic displacement due to strong coulomb repulsion between heavily ionized atoms; and (3) elastic relaxation of the acute stresses caused by atoms moving apart. (Copyright University of California Press, reprinted by permission.)

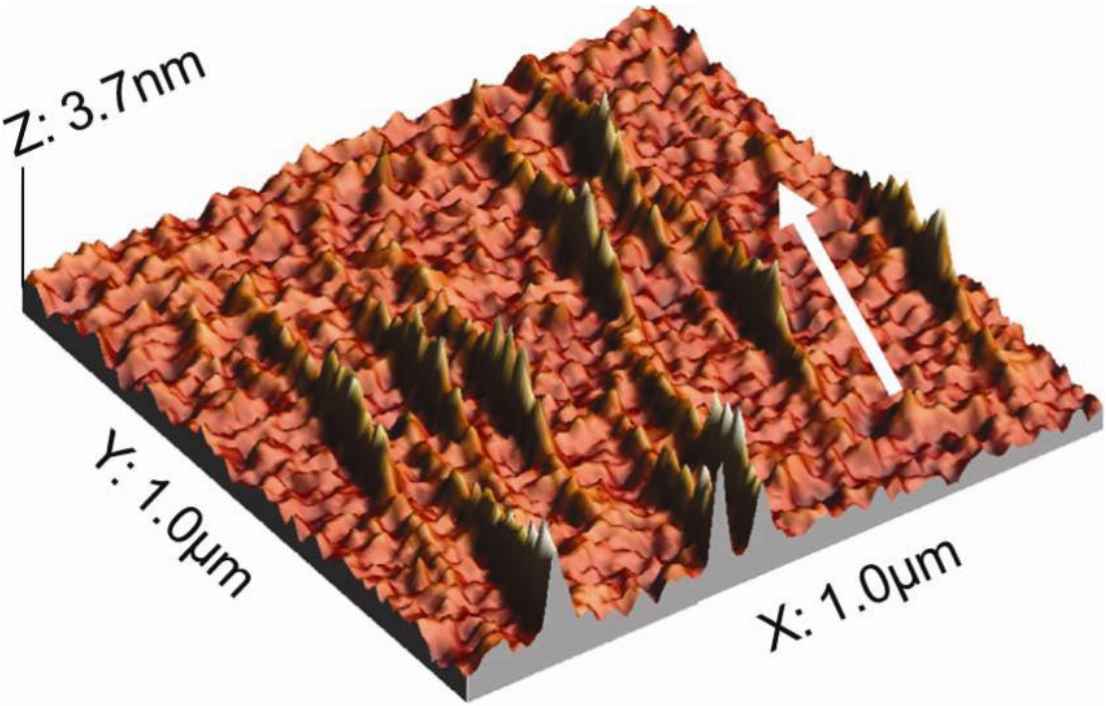

Figure 38. SiO_2 irradiated with heavy ions at grazing angles. Ridges form, a few nm high, along the tracks, detected with AFM (atomic force microscopy) [158].

Marinoni et al. [158] irradiated SiO_2 at grazing angles, and, using AFM, showed that ridges a few nm high had formed along the ion tracks. This result is exactly what one would predict from the processes illustrated in Figure 37. Here, the authors were trying to identify structural changes that could act as latent defects. Certainly, once the lattice structure of an insulator is disrupted, one would not expect it to be as good an insulator as it was before. Therefore, one might also expect to see low levels of leakage current, which have now come to be known as soft breakdown (SBD). SBD from heavy ions, starting even with almost the first ion, has been reported by Conley et al. [159] and Massengill [160]. While the leakage current from a soft breakdown event may not be enough to disrupt many circuits, Suehle et al. [161] performed standard life tests on samples exhibiting SBD. They found that they failed long before controls with no SBD. Although many circuits might be able to tolerate leakage currents at the SBD level, they still serve as a warning that other problems lie just ahead.

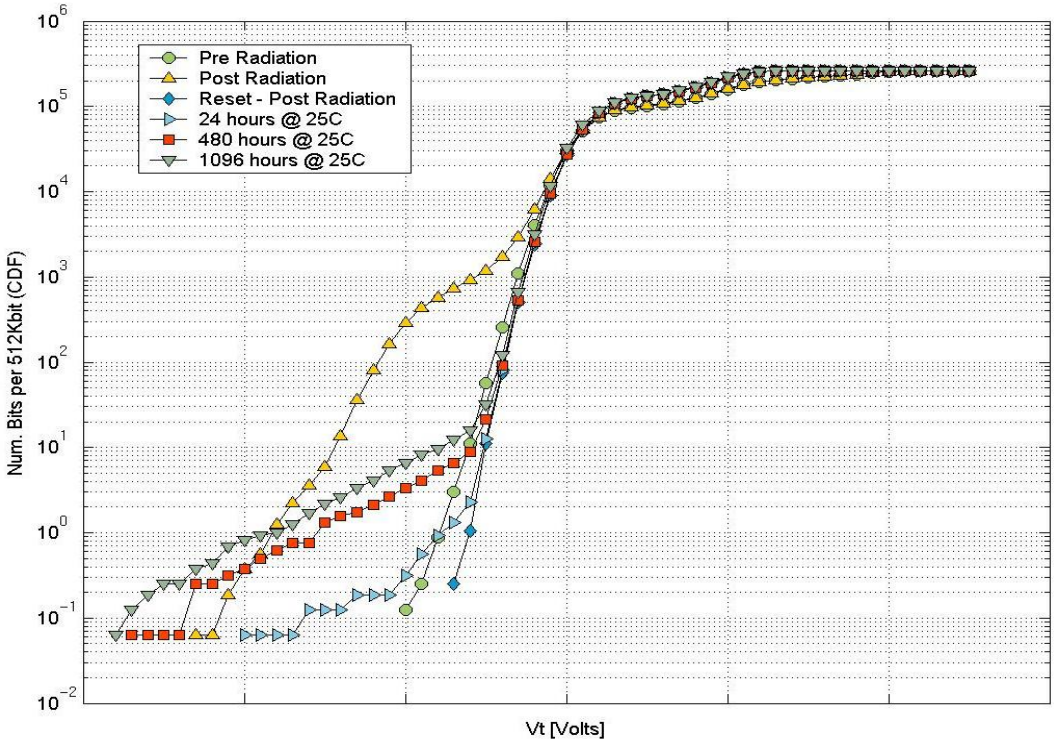

Figure 39. Retention results on floating gate flash memory, following irradiation with Xe ions (LET=54MeV/mg/cm2) [162]. Very similar results were also reported by Cellere et al. [163].

An example of one such problem is shown in Figure 39, which illustrates retention failures in floating gate NAND flash memory. The pre-radiation threshold voltage distribution is shown, along with a secondary peak after irradiation, with Xe ions, LET=54 MeV/mg/cm^2. The secondary peak occurs because the cells hit by heavy ions have a shift in V_T. When the memory is reset, the initial V_T distribution is restored. But the cells hit by ions have damage to the tunnel oxide, which forms a leakage path, allowing the stored charge to bleed off the floating gate in the days and weeks following the radiation exposure. Therefore, a tail forms on the V_T distribution of bits that have failed to retain their stored charge—retention failures. The threshold LET for this kind of retention failure seems to be around 30 MeV/mg/cm^2. Below that LET, the ions do not ionize the SiO_2 atoms heavily enough for the coulomb repulsive forces to disrupt the lattice. When these failures occur, they are due to micro-dose, a very high dose deposited by a single ion in a very small volume.

2.3 Implications for Radiation Testing, Hardness Assurance, and Prediction

We have now completed our review of the basic physical mechanisms underlying the radiation response of CMOS devices. Next we consider these mechanisms in the context of device and circuit testing, hardness assurance, and prediction.

2.3.1 Rebound or Super-Recovery

The rebound effect is illustrated in Figure 40, [77] which shows threshold voltage shift (ΔV_T) for a MOSFET, along with its components, oxide trapped charge (ΔV_{OT}) and interface trapped charge (ΔV_{IT}), during both irradiation and post-irradiation annealing. The annealing data is shown for two temperatures, 25 C and 125 C.

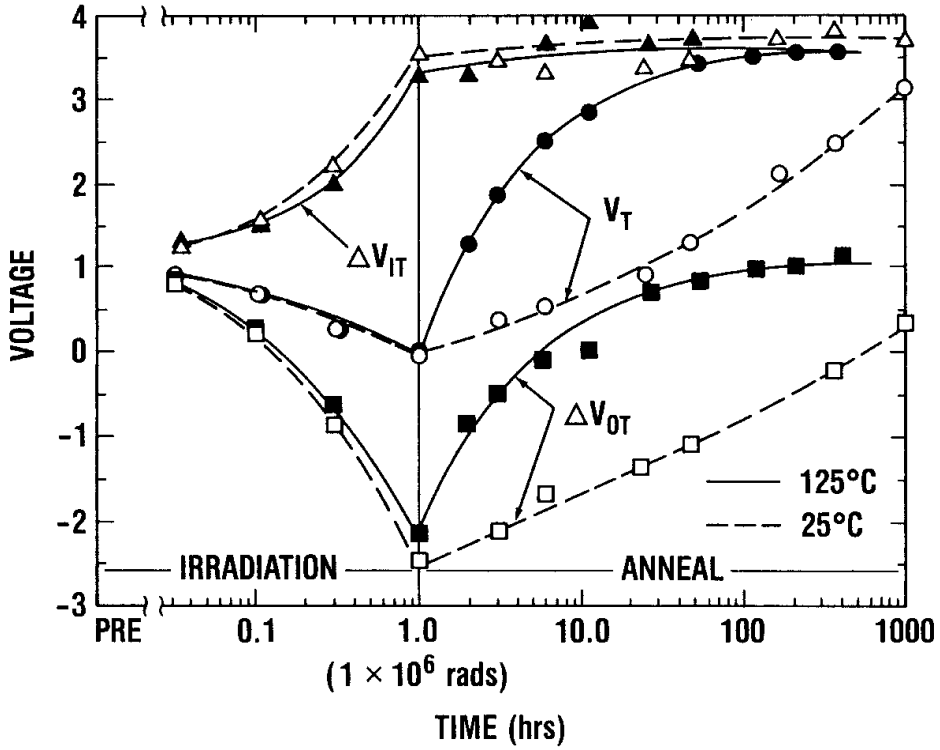

Figure 40. V_T, V_{OT}, and V_{IT} annealing; long term response illustrates rebound effect [77].

After irradiation, the threshold shift is less than 1V, but this relatively small shift is obtained by compensating positive oxide trapped charge with negatively charged interface traps (in this n-channel device). When the hole traps anneal, however, the final threshold shift is positive, about 3.5 V, which is more than enough to fail the device. The effect of raising the temperature is to anneal the hole traps faster, but the same final state is reached at room temperature. One could imagine a device that failed due to trapped positive charge immediately after irradiation, that would later work properly for a time as some of the holes annealed, that would then fail again later from trapped negative charge as more of the holes annealed. There is very little change in interface trap density during the annealing process at either temperature, so the late time failure would be due to interface traps that were there at the end of the irradiation.

To test for rebound, there is now a test method, which is standard in the US, TM-1019.7, which calls for a 50% overdose and a 100 C anneal for 168 hours, which will detect the effect in oxides similar to the one used in Figure 40 [164]. This method represents a compromise,

because 100 C is not a high enough temperature to accelerate the trapped hole annealing in all oxides, but if one goes much higher in temperature, the interface traps may anneal, too [100].

The rebound effect is of great practical concern for space environments, because components are typically exposed to relatively low dose rates for very long mission lifetimes. There is now strong emphasis on using unhardened commercial technology as much as possible, which is reasonable to consider in space because oxide traps may anneal as fast as they are created, or nearly so. A component that fails at a low dose in a laboratory test from oxide trapped charge, as many things do, may work quite well in space, because of the low dose rate and annealing. But this discussion only applies to the positive charge—negatively charged interface traps (in an n-channel device) will continue to build-up throughout the mission life. Therefore, it is necessary to check for rebound, too.

We note that rebound is only a problem on n-channel devices, because the hole traps and interface traps are both positive in p-channel devices. For this reason, their electrical effects add, instead of compensating. Of course, the hole traps do not change state with changes in applied bias in either n- or p-channel devices, while the interface trap state does depend on bias in general.

2.4 Apparent Dose Rate Effects

In CMOS devices the radiation response does not normally depend on the dose rate, except in the case of extremely short, intense nuclear-driven pulses. However, apparent dose rate effects are often observed if a given dose is delivered at two or more different rates in different tests, because the exposure times are different, and we have already discussed many different time dependent effects that will contribute to the overall response. Generally, if one allows the sample to anneal after the shorter exposure, so that the measurements are done at the same times, the response will be the same, within normal experimental error. The most definitive experiment showing the absence of a true rate dependence was reported by Fleetwood et al. [165] where identical samples were exposed to the same dose, with the dose rate varied over 11 orders of magnitude. The results for ΔV_T, ΔV_{OT}, and ΔV_{IT} are shown in Figure 41. In each case the sample with the highest rate exposure is allowed to anneal following irradiation. All the lower rate exposures fall almost perfectly on the annealing curve, indicating that if the dose and the time of the measurement are the same, the response will also be nearly the same.

An approach, which has been used with some success, to predict the response of a CMOS device at dose rates other than those available in the laboratory is the use of linear systems theory [58-60], [166]. If one determines, by testing, the impulse response function of a device to a short radiation pulse, then one can determine the response to an arbitrary exposure by doing a convolution integral, as long as the response is linear with dose (meaning that the response to the different dose increments simply add up). The impulse function used in [58-60] was linear-with-log(t), which is reasonable for many unhardened commercial oxides. In general, the impulse response function may be more complicated, but linear systems theory can still be used, in principle [20].

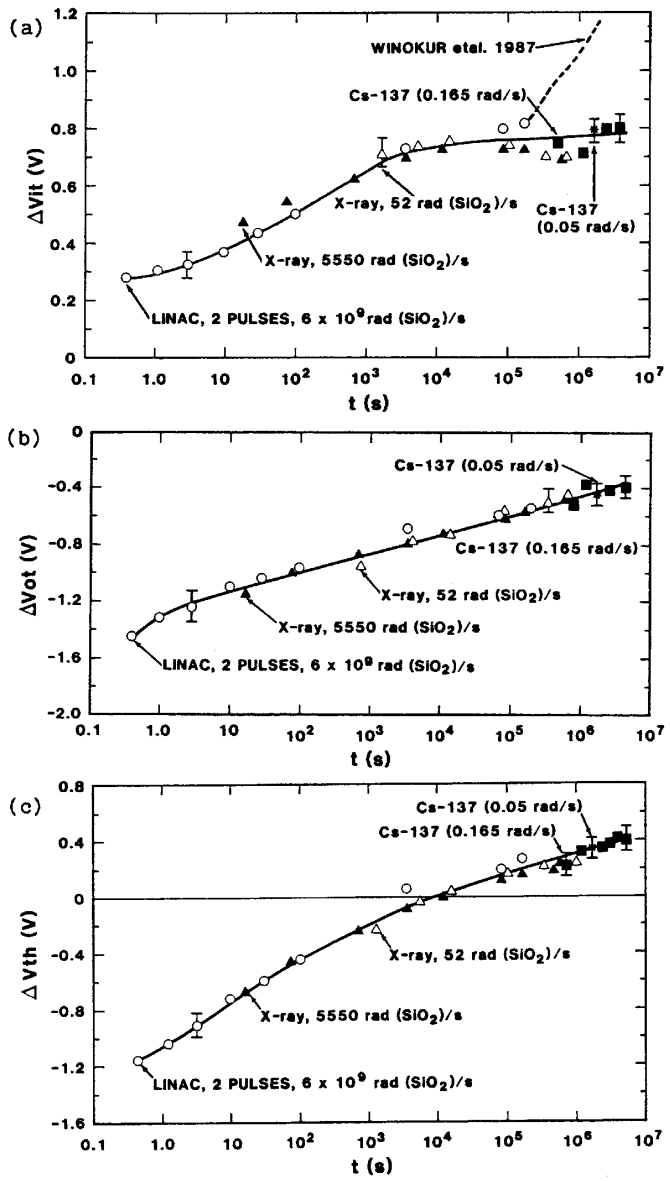

Figure 41. V_T, V_{OT}, V_{IT} annealing results showing absence of dose rate effect [165].

A spectacular example of the mischief that can be caused by testing at different dose rates is shown in Figure 42 [167]. In this case, a circuit was tested to failure at a wide range of dose rates. At high dose rates (the right hand side of the Figure), it failed at a dose of a few krad, because of the build-up of positive oxide trapped charge. At low dose rates (the left hand side), it failed at slightly higher doses due to negatively charged interface traps (rebound). But at one dose rate in the middle, where positive and negative charge generation rates were precisely balanced, it survived to very high doses. Obviously, testing at that unique dose rate would not be recommended, in general, although the manufacturer might want to do so.

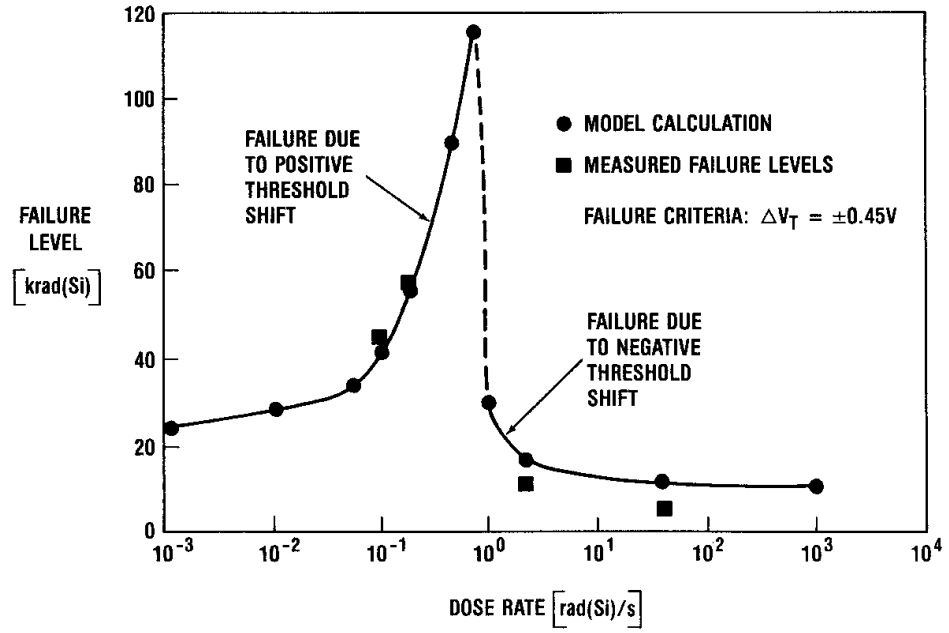

Figure 42. Dependence of circuit failure level on dose rate [167]

2.5 Charge Separation Techniques

In order to do sensible testing and analysis, one naturally wants to be able to separate the overall radiation response of a device or test structure into its components. Therefore, after the hole transport is complete, it is common practice to write $\Delta V_T = \Delta V_{OT} + \Delta V_{IT}$, where the right hand terms are the threshold voltage shifts due to oxide traps and interface traps, respectively. There are different methods for separating ΔV_T into its components, but they all use the assumption that interface traps are net neutral at midgap, so that ΔV_{MG} is a measure of oxide hole trapping (that is, $\Delta V_{MG} = \Delta V_{OT} = -q\Delta N_{OT}/C_{OX}$). Here, q is the electronic charge, C_{OX} is the oxide capacitance, and N_{OT} is the number of oxide traps. Then the shift due to interface traps is everything else, $\Delta V_{IT} = \Delta V_T - \Delta V_{MG}$. For a capacitor, one can use the stretch-out between midgap and inversion, or the stretch-out between threshold and midgap on the I-V characteristic of a transistor (which usually requires extrapolating the subthreshold current to midgap). Rather than discuss the details of these procedures, we simply give a few key references [77], [168-170]. We note that the assumption of midgap neutrality for interface traps was first used by Lenahan and Dressendorfer [56], and reexamined later by McWhorter [169], and still later by Lenahan [171] (again). McWhorter concluded that the point of neutrality for interface traps is close to midgap, perhaps 3kT below midgap. Lenahan concluded that neutrality for the P_{b0} center is at midgap, but he also detected a second center, called P_{b1}, which is present in smaller numbers, and which is net neutral a little below midgap (consistent with McWhorter). So the assumption that ΔV_{MG} is due entirely to oxide trapped charge is a useful approximation, which seems to introduce errors of only a few percent.

2.6 Dose Enhancement

Dose enhancement has been known and studied for many years, but it is a practical problem because of the widespread use of low energy (10 keV) X-ray sources. For a photon source (x-ray or gamma), most of the energy deposition is actually done by secondary electrons. The critical concept is called charged particle equilibrium (CPE). Normally, in a homogeneous slab of material, CPE is maintained because the number of secondary electrons scattering into any increment of volume is equal to the number of electrons scattering out. The problem in a MOS device is illustrated in Figure 43 [21], where there are several thin layers of different compositions, and therefore, different cross-sections. CPE is not maintained because more secondary electrons cross an interface from the high-Z side than from the low-Z side. In Figure 43, the solid lines indicate the deposition profile that would be predicted for 10 keV X-rays, using the mass absorption coefficients alone, without any secondary electron transport. Figure 43a indicates the situation when the oxide is thick compared to the range of the secondary electrons, where the broken line indicates the change in the depth-dose profile from the transport of secondary electrons into the oxide layer. The situation for a thin oxide is illustrated in Figure 43b, where the electrons go all the way through the oxide layer, and the dose-enhancement is indicated by the broken line. Dose enhancement as a function of oxide thickness is indicated in Figure 44 [21], [172-174]. For testing with an X-ray source, dose enhancement is an important effect, which means that the dose is different in different parts of the structure (e. g., gate oxides and field oxides). On the other hand, in a Co^{60} source, the mass absorption coefficient for all the materials shown in Figure 23 is essentially equal, and the dose is uniform because CPE is maintained [21-22], [174-176]. Generally, when one compares x-ray results with Co^{60} results, there will be a dose enhancement correction, which will be different for gate oxides than for isolation oxides. One needs to know the failure mechanism to apply the appropriate dose enhancement correction.

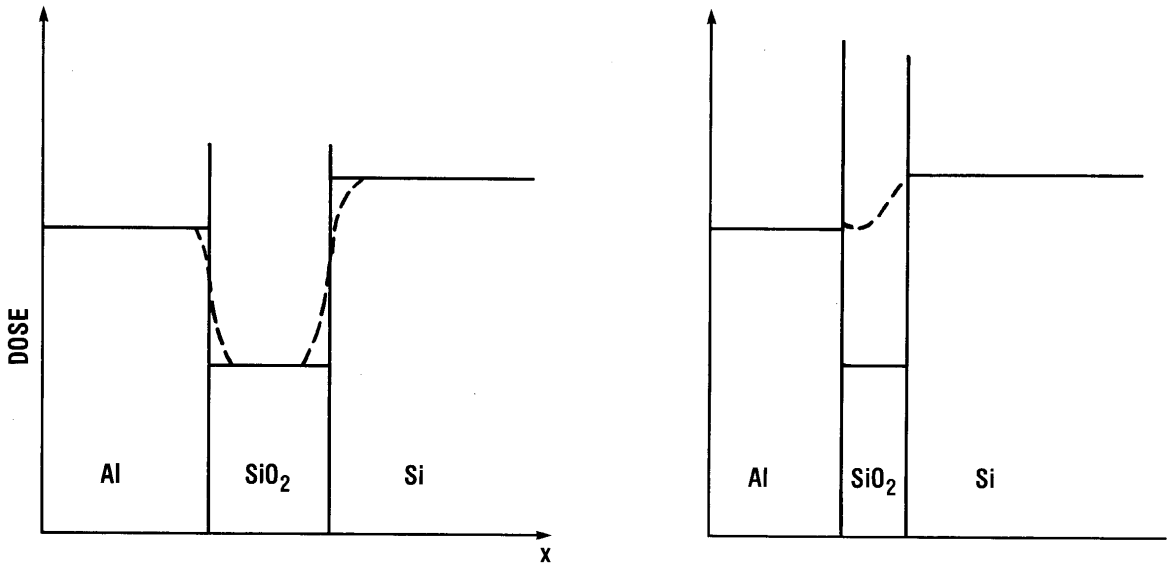

Figure 43. Schematic diagram illustrating dose enhancement in thick and thin oxide layers; solid lines are bulk equilibrium doses and dashed lines represent actual dose profiles.

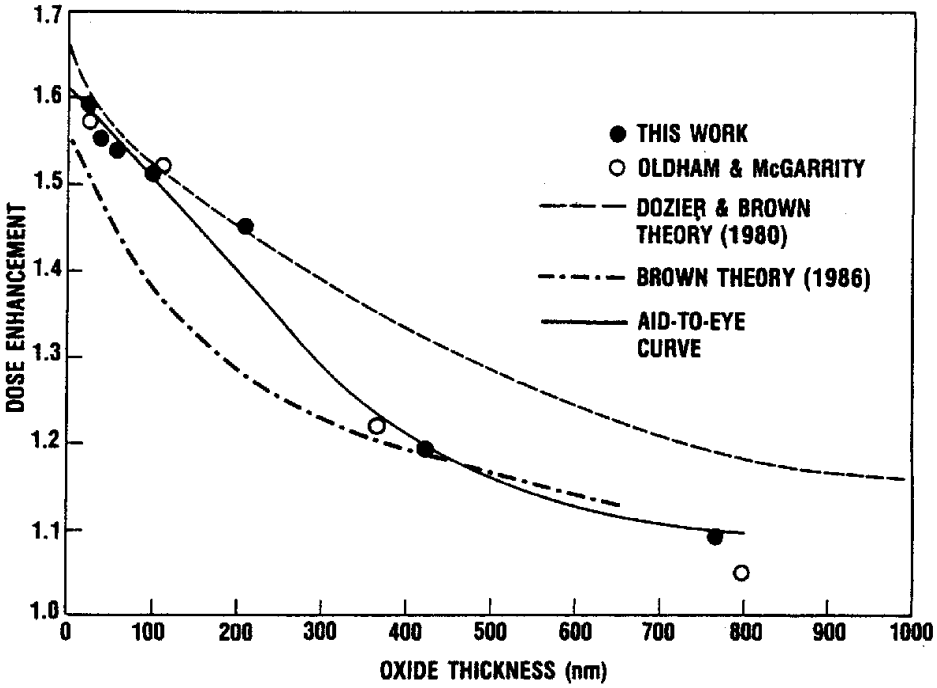

Figure 44. Measured and calculated dose enhancement as a function of oxide thickness for 10 keV x-rays [11].

2.7 Isolation Structures and Radiation-Induced Leakage Currents

For much of the recent history of the NSREC, the main total dose problem in MOS technology has been damage to field oxide isolation structures, which has meant shallow trench isolation (STI) structures. Charge buildup in the trench turns on a parasitic leakage path.

Current flows from source-to-drain, outside the active gate region. Experimentally, the effect of such a leakage path on the I-V characteristic of a device is illustrated in Figure 45.

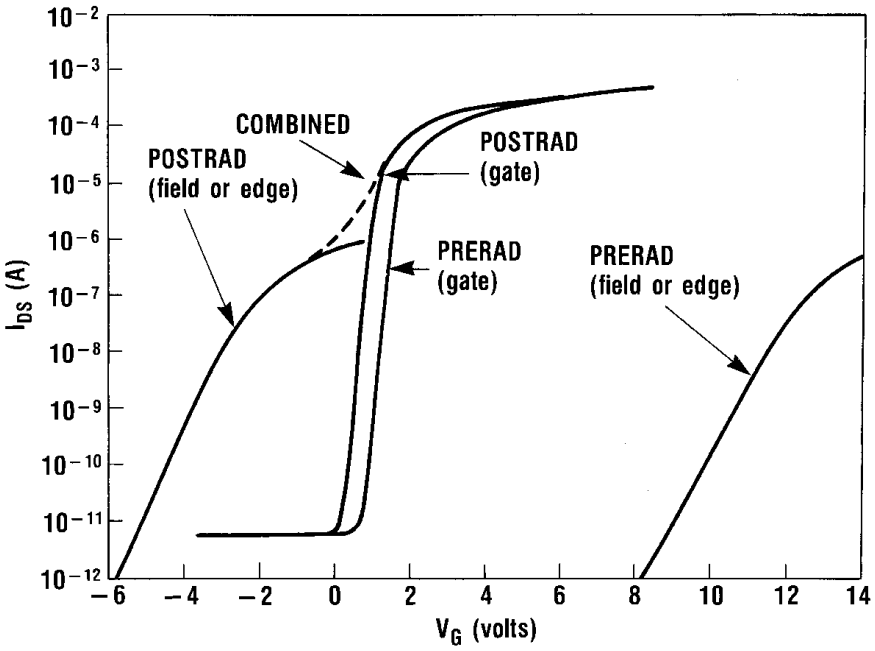

Figure 45. Schematic illustration of the I-V characteristic of an n-channel MOSFET and parasitic leakage transistor before and after irradiation. The parasitic device has much greater oxide thickness, and larger shift, so that it dominates the overall response after irradiation

The initial I-V characteristic of a transistor is shown, along with the small shift it undergoes when irradiated—the shift is small because the oxide is relatively thin. There is also a parasitic field oxide device curve, which is not visible experimentally, initially, because it is far to the right of the gate characteristic. But the trench oxide is much thicker than the gate oxide, so the shift per unit dose is much larger, and the curve eventually shifts past the gate characteristic. In the illustration, the post-radiation isolation oxide curve is on the left side of the Figure. The measured I-V curve, post-radiation, is indicated by the broken line, labeled "combined." The leakage current at 0 V increases from the pre-rad value by several orders of magnitude, which is often enough to cause functional failure of a circuit. Oldham et al. [177] and Terrell et al. [178] have reported on the radiation response, including annealing, of several older commercial field oxides, and there was wide variation in the results. It is basically impossible to predict the response of such an oxide, without studying the particular oxide in question. Some of them do anneal on a reasonable time-scale, which can be very useful in some applications (in space, for example). Trench oxides can be hardened [179], with sufficient investment, but the details are not generally discussed in the open literature. The companies consider these process details proprietary.

Although process details are closely held, there are some underlying mechanisms that can be discussed. For example, Turowski et al. [180] presented model results indicating that very

little charge is trapped near the top surface of an STI structure. Although applied fields in isolation structures are generally much less than in gate oxides, the field is still high enough to push most of the radiation-induced charge down some distance into the trench. The leakage current path that might form is affected by the non-uniform distribution of trapped charge.

STI structures are also three-dimensional objects, which can have complex shapes, which in turn can give rise to complex geometrical effects. Turowski [180] also discussed the implications of high electric fields in the vicinity of sharp corners at the top of the trench if the trench oxide is recessed, as opposed to planar or overfilled. The commercial industry has recognized the need to control the characteristics of the trench corner for manufacturability, even in the absence of radiation [181-182]. One technique used to increase V_T in the corner region, and make the corner less likely to turn-on as a parasitic leakage path is to increase the sidewall doping level [181,183]. Johnston et al. [184] reviewed earlier work on the radiation response of trench oxides, in addition to discussing process changes resulting from scaling. The earliest paper was by Shaneyfelt [179], which reported that unhardened commercial trench structures inverted at about 30 krads (SiO_2), and started to have measurable leakage currents in a 0.5 μm process. Later work, at smaller feature sizes reported higher failure doses [185-187], suggesting that trench oxide TID response was improving with scaling. One process change that he identified as a contributing factor was that sidewall p-type doping levels were higher, which increased the sidewall V_T, and reduced the need for special doping at the corners. Johnston et al. also presented modeling, where they calculated a non-uniform density of oxide trapped charge with depth, which they compared to other results which had all been obtained assuming a uniform sheet of charge. The most significant result from this modeling was that they identified the inversion region leakage path as being some distance below the corner, because the density of trapped charge is higher farther down in the trench than it is at the corner.

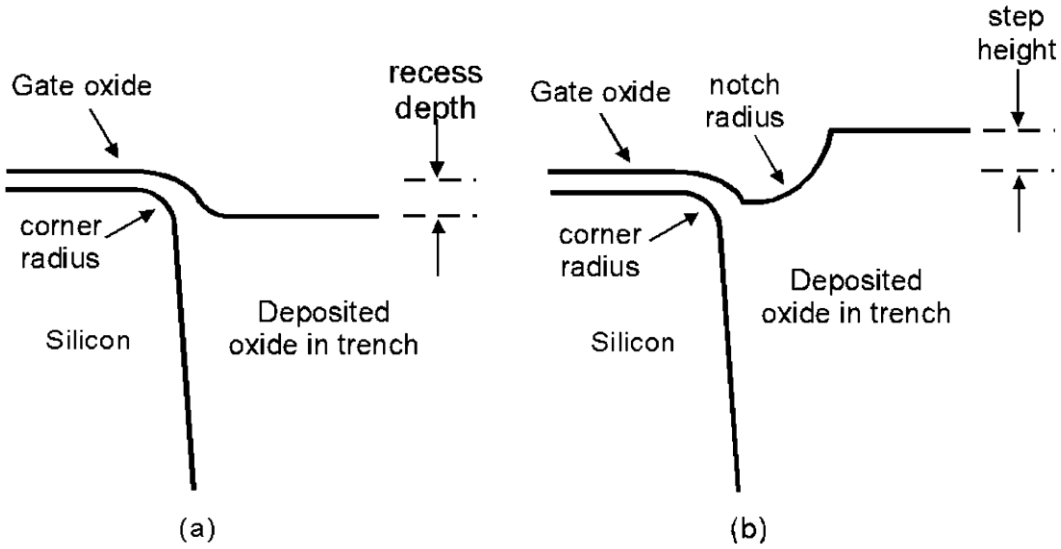

Figure 46. Trench oxide corner profiles; (a) recessed trench; (b) overfilled trench, with a notch at the corner [184].

Johnston et al. also discussed the trench structures shown in Fig 46. In both cases, it is necessary to round the corner. Generally, a sharp corner causes thinning of the oxide, which introduces stress into the oxide. It also causes higher electric fields because the equipotential lines are crowded together. These factors both contribute to reduced reliability. For the overfilled case, the notch and the step also contribute to unacceptable threshold voltage variation [188].

There are also radiation-induced isolation effects in the buried oxide (BOX) of SOI wafers, which we now discuss briefly. For a review, see Schwank et al. [189]. Radiation-induced charge can build up in buried oxides, by the same mechanisms we have already discussed. If there is enough charge at the back interface, an inversion region can form, which can contribute to radiation-induced leakage current. In a fully depleted structure, where the entire Si volume is supposed to be controlled by the front gate, a back channel, if it turns on, can alter the electrical characteristics of the entire device, and cause parametric failure. On the other hand, in a partially depleted device, the back channel is not necessarily in contact with the source or drain, nor is it necessarily coupled to the front channel. For this reason, partially depleted devices are generally less sensitive to radiation than fully depleted devices. But partially depleted devices exhibit the kink effect, which can be a problem even in the absence of radiation. It is due to the buildup of charge in the Si volume that is not directly controlled by the contacts. For this reason, partially depleted devices often have body ties, which impose an area penalty, compared to fully depleted devices.

2.8 Conclusions

We have reviewed the total ionizing dose radiation response of MOS materials, devices and circuits. Generally the response is very complex, with many different physical processes contributing. Each of these processes has a different time dependence, a different field dependence, and a different temperature dependence. Even though the overall, combined response is extremely complex, a high level of understanding has now been achieved, by isolating the different mechanisms, and by studying them one at a time. The study of these mechanisms has been a major theme of the NSREC throughout most of its 47 year history. The understanding that has been achieved stands as a major success for the conference and the conference community.

3 Total Dose Effects in Bipolar Technology (ELDRS)

3.1 Background.

At one time, bipolar devices were very resistant to TID-induced degradation, because they used junction isolation technology. However, the situation changed dramatically when the semiconductor industry started using oxide isolation structures. Figure 47 is from the Outstanding Conference Paper Award winner for the 1983 NSREC [190], which basically explained why parts expected to survive 1 Mrad or more had failed at just a few krads—an unexpected result, to say the least. As the Figure shows, radiation-induced trapped positive charge was building up in the oxide isolation structures, which had the effect of turning on

parasitic leakage paths that were not supposed to be on. From that point on, TID effects in bipolar technology received much more attention than previously.

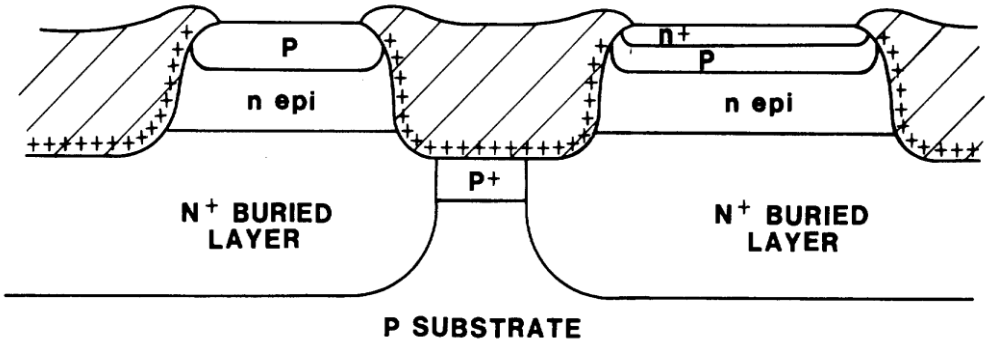

Figure 47. Radiation-induced charge buildup in bipolar oxide isolation oxides, after Pease et al. [190].

3.2 Discovery of ELDRS

A few years later, in 1991, Enlow et al. [191] reported increased degradation in bipolar devices irradiated at low dose rates, compared to standard high dose rate irradiations. This phenomenon came to known as ELDRS (Enhanced Low Dose Rate Sensitivity), and it has been much studied since then. For reviews, see [192,193]. The original data from Enlow et al. is shown in Figure 48. They compared data on parts from two vendors, irradiated at 300 rads (SiO_2)/sec and at 1.1 rads (SiO_2)/sec. The test structures are discrete transistors of different designs: a crystalline emitter in Figure 48a, and a poly-Si emitter in Figure 48b. In Figure 48, they plot $\Delta\ 1/\beta = 1/\beta - 1/\beta_i$, where β is the gain of the transistor. In both cases, the gain degradation is greater at the lower dose rate, in the initial irradiation. For Vendor A, in Figure 48a, the required space radiation level was 70 krads (SiO_2), compared to 200 krads (SiO_2) for Vendor B, in Figure 48b. Enlow et al. also wanted to test the hypothesis that the gain degradation was due to interface traps, and that annealing the high dose rate samples would reveal more interface traps and possibly bring the high dose rate and low dose rate responses together. Therefore, they performed the rebound test described above, giving each type of sample a 50% overdose, followed by a 168 hour anneal at 100° C. As the Figures show, the high temperature anneals increased the gain, and not the gain degradation, contrary to expectations. The impact of this paper was to show that low dose rate effects were important in bipolar devices, and that standard test methods, devised for CMOS, were not adequate to characterize these effects.

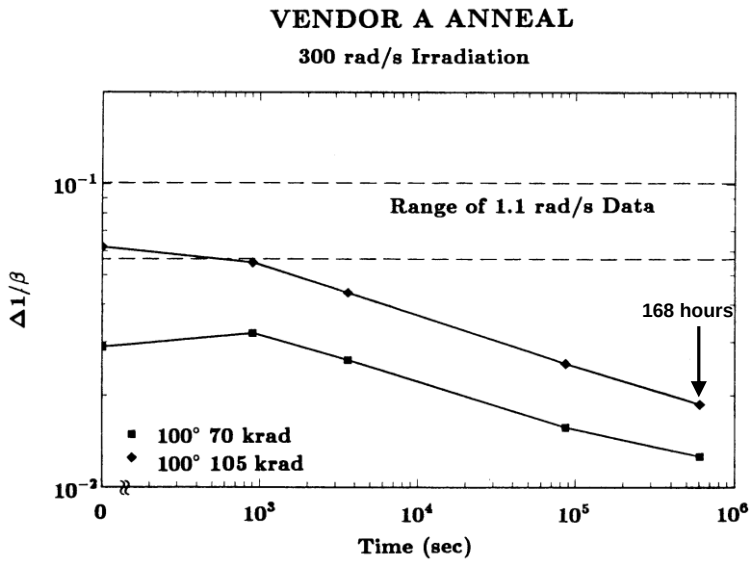

(a)

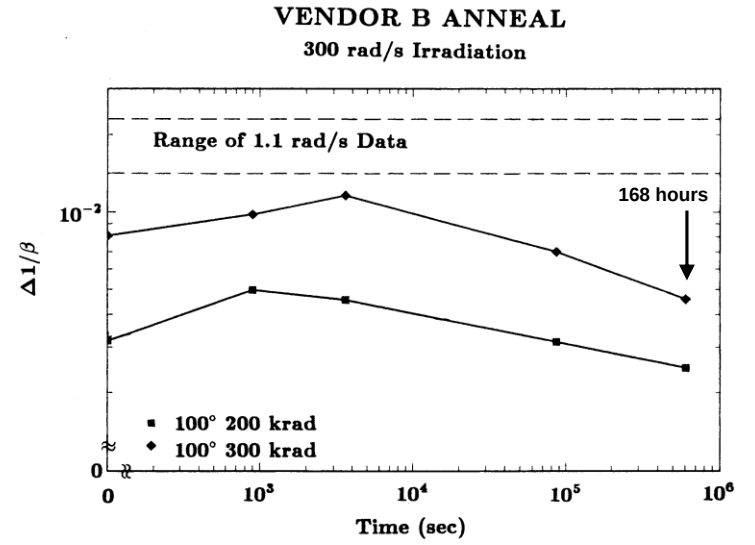

(b)

Figure 48. Enhanced damage at low dose rate, 1.1 rads (SiO_2), compared to 300 rads (SiO_2)/sec. High temperature annealing data is also shown: (a) Vendor A, crystalline emitter; and (b) Vendor B, poly-Si emitter.

Much of the original data was obtained on vertical NPN devices, illustrated in Figure 49. Charge trapped in the base oxide partially inverts the base, which leads to increased collector current, even when the base is biased off. Then when the base is turned on, the collector current increases less than might be expected, which means the gain is reduced. Although the effect was discovered on vertical NPN devices, it quickly became apparent that the worst case condition was actually the lateral PNP device, illustrated in Figure 50 [194].

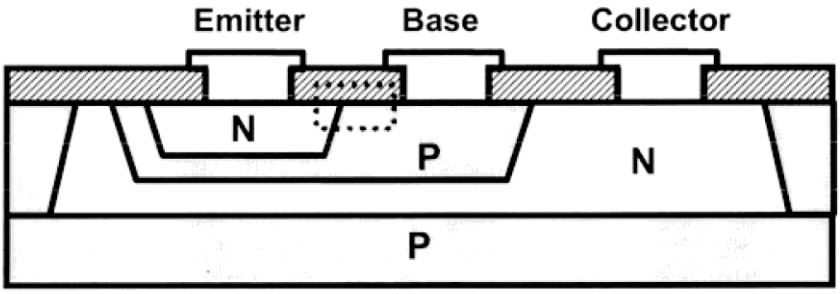

Figure 49. Vertical NPN transistor, where trapped charge in the base oxide causes reduced gain.

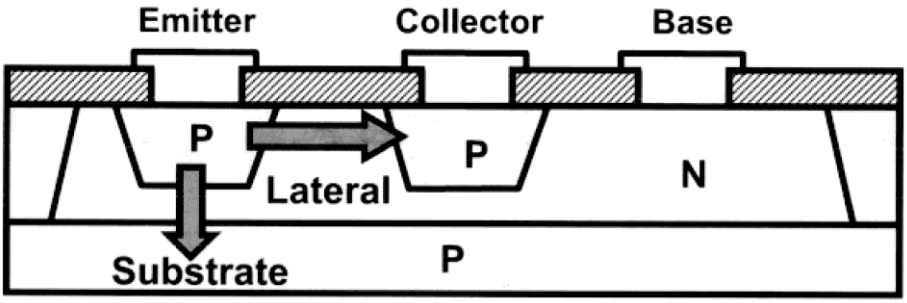

Figure 50. Lateral PNP transistor, where base conduction is along the surface, right under the base oxide.

In [194], the authors concluded that lateral PNP devices were the most sensitive because the current flow was along the Si surface, right below the base oxide. Defects in the oxide have the greatest effect because the current is closer to the oxide for longer than in any other device type they examined. The base doping level was also lower than in other types of devices. The lateral PNP was 20-50x more sensitive than in any other device type they tested. For this reason, many of the studies that followed focused on the lateral PNP devices.

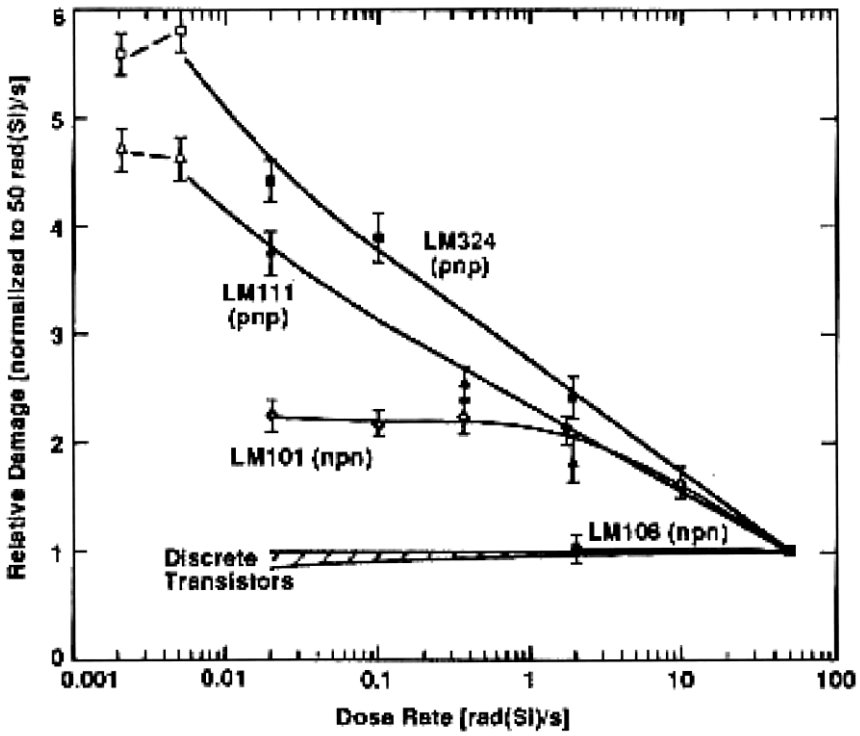

Figure 51. Low dose rate enhancement factors for selected linear bipolar circuits [195]. Input bias current was the parameter used to compare degradation.

In Figure 51, results by Johnston et al. [195] show enhanced damage at low dose rates, normalized to damage in irradiations performed at 50 rads (SiO_2)/sec. This came to be called the Low Dose Rate Enhancement Factor (LDREF). Here, the parameter used to compare degradation is the input bias current, and, as one might expect, circuits with PNP input transistors are more sensitive than those with NPN input transistors. The LDREF is up to a factor of 5-6 for the PNP circuits. This result was an early indication that simply over-testing at high dose rate would not be sufficient to characterize low dose rate effects.

One of the problems with many early ELDRS studies was highlighted by Kruckmeyer [196], who discussed the National Semiconductor LM 139, a quad comparator, which was a commonly used test vehicle. He pointed out that the part was available in several different grades, and that each grade was manufactured in a different fab facility. There were at least eight different fabs producing nominally the same part, at one time or another, each using different manufacturing processes and different layouts. For this reason, it was nearly impossible to make meaningful comparisons of different results in the literature—everybody had been working on something different.

This problem was recognized almost from the beginning, and eventually there was an effort to introduce standardized test samples. Specifically, an experiment was designed for the NSC LM124 quad op amp that used a specially designed test chip incorporating gated lateral pnp transistor structures, gated diodes, MOS capacitors and other special structures, as well as the LM124. The ELDRS test chip was designed and laid out by NAVSEA Crane and fabricated by NSC in the LM124 process in a 24-wafer lot. There were seven different process splits in this

lot. The first split was the normal process, which is shown in Figure 52. Over a lateral PNP transistor there is an oxide passivation layer, and a base electrode, which are covered with a layer of phospho-silicate glass (P-glass). Over the P-glass is also an encapsulating layer of silicon nitride (PG/NIT). The second split was similar, except that the nitride layer was left out (PG). The third split also left off the P-glass (NP—no passivation except oxide). Other splits were nitride over TEOS (TEOS/NIT), p-glass over TEOS (TEOS/PG), TEOS only and Silicon Carbide only (SiC). Test chips from these splits were distributed to most of the groups working on the ELDRS problem. We will discuss some of the results from these experiments later.

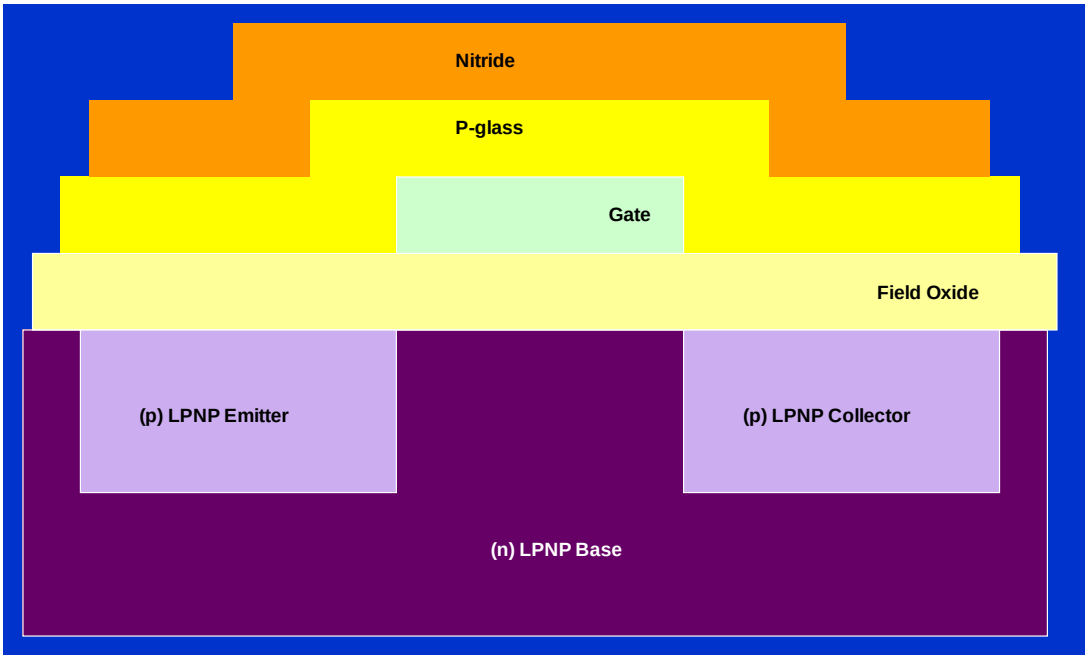

Figure 52. ELDRS test structure, LPNP transistor, from the standard process. Splits without nitride and without P-glass were also processed.

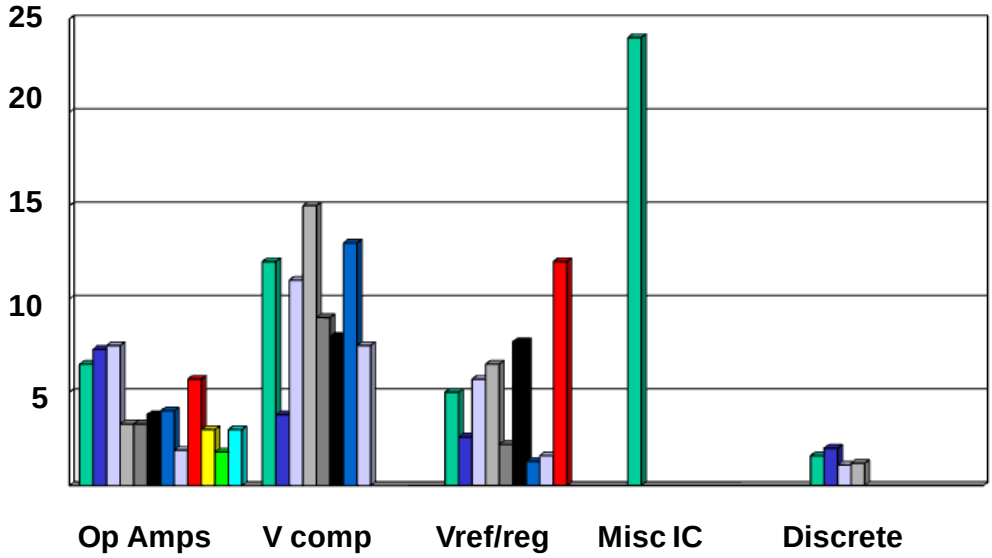

Figure 53. Low Dose Rate Enhancement Factor (LDREF) for selected bipolar circuits, after Pease, et al., REDW 2001.

We conclude this section by summarizing the low dose rate enhancement factors (LDREF) observed in many tests and reported by Pease et al. [197]. As one can see, values of five to ten or even higher are not uncommon for LDREF. The highest LDREF in Figure 53, more than 20, is given for a part called a "Misc. IC". This part is actually a temperature transducer, which we will discuss in more detail later.

3.3 Characteristics of ELDRS

ELDRS is a true dose rate effect, which distinguishes it from the time dependent effects commonly observed in CMOS. These sometimes give rise to *apparent* dose rate effects. This difference is illustrated in Figure 54 [198], where the change in input bias current for the LM111 comparator is shown for irradiation to 50 krads (SiO_2). After high dose rate irradiation, at 50 rads (SiO_2)/sec, the current is about 150 nA. The low dose rate irradiation, at 0.01 rads (SiO_2)/sec, required $5x10^6$ sec, and at the end of that time, the current was about 1300 nA. If the high dose rate sample is allowed to anneal for the same time required for the low dose rate irradiation, the current increases to about 350 nA. As the Figure indicates, this annealing effect is a time dependent effect (TDE). The difference between the high dose rate sample after annealing, and the low dose rate sample is the ELDRS effect, and it is indicated as a true dose rate effect (TDRE).

Often, ELDRS tests are performed only at one bias condition, either high or nominal bias, or with all leads grounded. An early mechanisms study [199] indicated that space charge effects at very low bias played a role in ELDRS, which suggested that zero bias might be the worst case condition. Other studies [200, 201] confirmed that zero bias was the worst case condition for several specific cases. One example is shown in Fig 55 [202] for the LT1185. For high dose rate, there is little difference between biased and unbiased irradiation. But at low dose rate, the

unbiased condition is clearly much worse, with functional failure at about 30 krads (SiO_2). However, for some other cases, notably offset parameters, the worst case test condition is with bias. Therefore, it is a characteristic of ELDRS that it is often not clear what the worst case bias is. For this reason, the standard test method, set out in MIL-STD-TM 1019.7, calls for doing all tests both with and without bias.

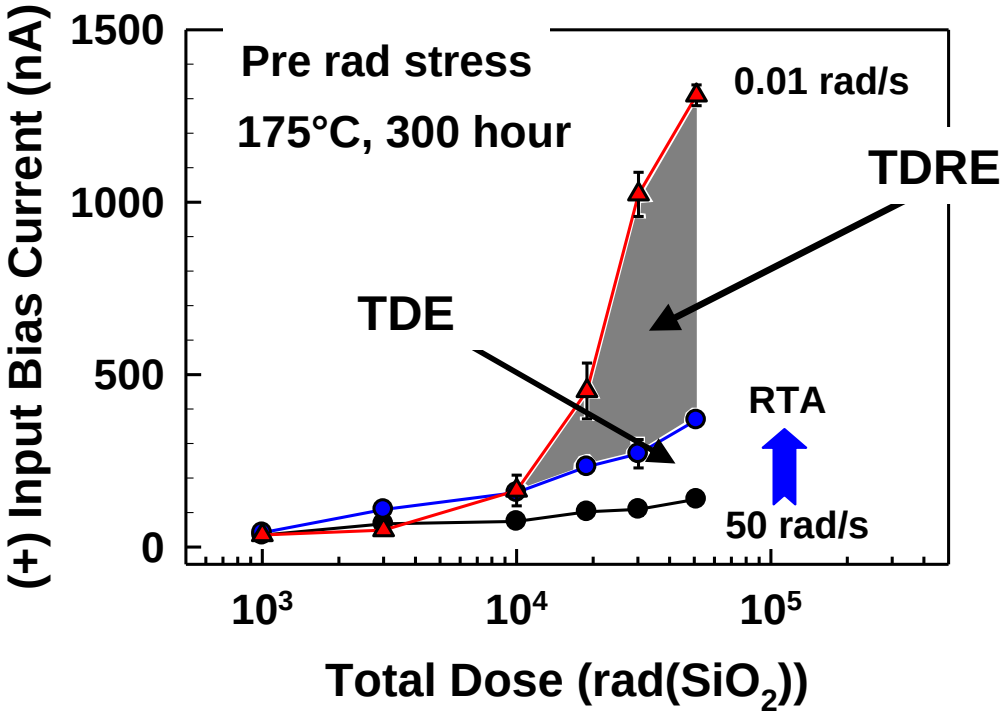

Figure 54. Time dependent effect and true dose rate effect for LM111. [198]

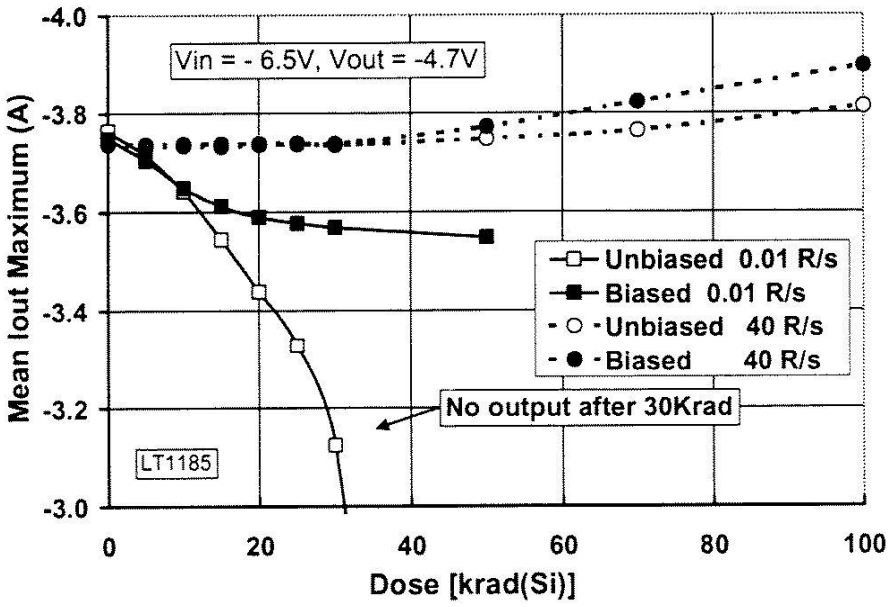

Figure 55. Biased and unbiased irradiation of the LT1185. At low dose rate, unbiased irradiation causes the biggest drop in output current. [202]

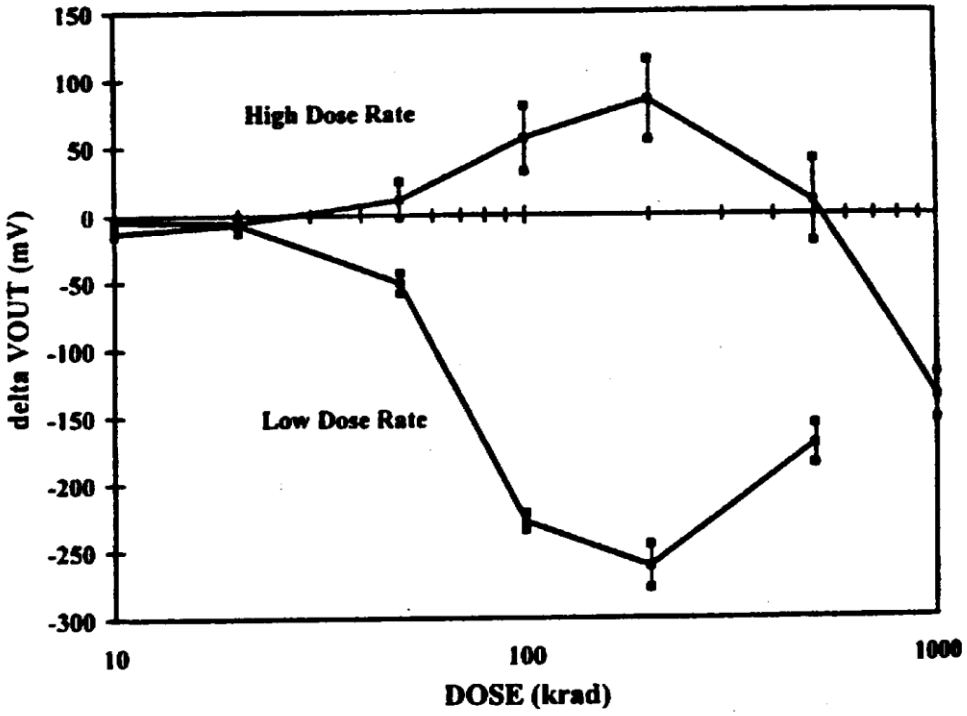

Figure 56. Complex circuit response of LM117 voltage regulator [203].

In Figure 56, we show an example of another ELDRS characteristic, which is that the response can be dominated by complex circuit behavior [203]. Here, the output voltage increases with dose initially, at high dose rates, but later shifts negative. At low dose rates, the opposite happens—the shift is negative initially, but positive at higher doses. The reason for this

is that the circuit includes both NPN and PNP transistors, which degrade at different rates, and by different mechanisms. The circuit response is the result of the complex interplay between these different transistors, which means the results can sometimes be very hard to explain.

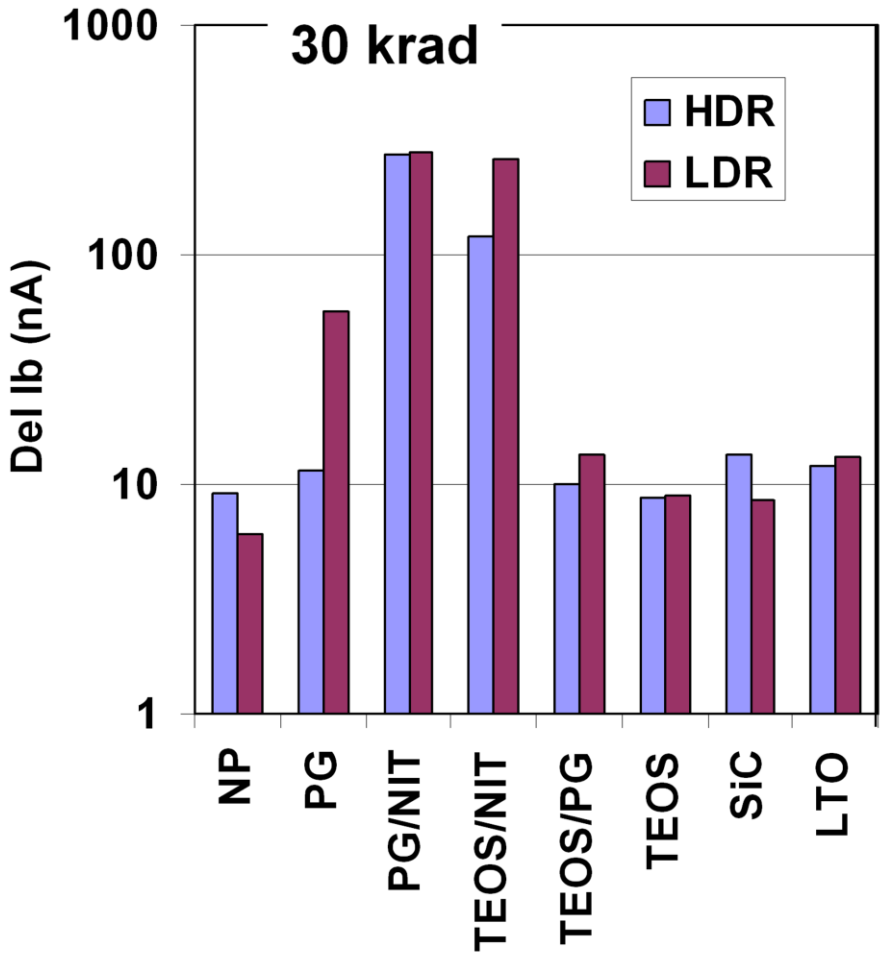

Figure 57. Effect of different passivation systems on radiation response of lateral PNP transistor at high and low dose rate. [204]

Another characteristic of ELDRS is that the radiation response depends strongly on the final passivation. In Figure 57, we show results obtained at high and low dose rates on the standard test chips described above, for several of the different passivation process splits [204]. For the split with no passivation (NP) except oxide, there is no ELDRS effect—high dose rate is the worst case condition. The strongest ELDRS effect is observed with P-glass (PG) final passivation, where the increase in I_b is about 5x greater at low dose rate, than at high dose rate. With nitride over the P-glass (PG/NIT), the nitride has the effect of softening the parts at both high and low dose rate. But there is no difference between the high and low dose rate responses. Nitride over TEOS (TEOS/NIT) is also relatively soft, but with some enhancement at low dose

rate. Then there are several other variations with no real difference between high and low dose rates.

The last characteristic of ELDRS that we will discuss here is that it has been observed in space. In Figure 58, we show results on two parts, the LM139 quad comparator, and the LM124 quad op amp, from the Microelectronics and Photonics Test Bed (MPTB) [205-208]. In both cases, the input bias current degradation matches very closely with ground test results from low dose rate Co-60 irradiation, 0.001 to 0.01 rads (SiO_2)/sec, but not with results at higher dose rates. The parts received a dose of about 45 krads (SiO_2) over the course of a seven year mission.

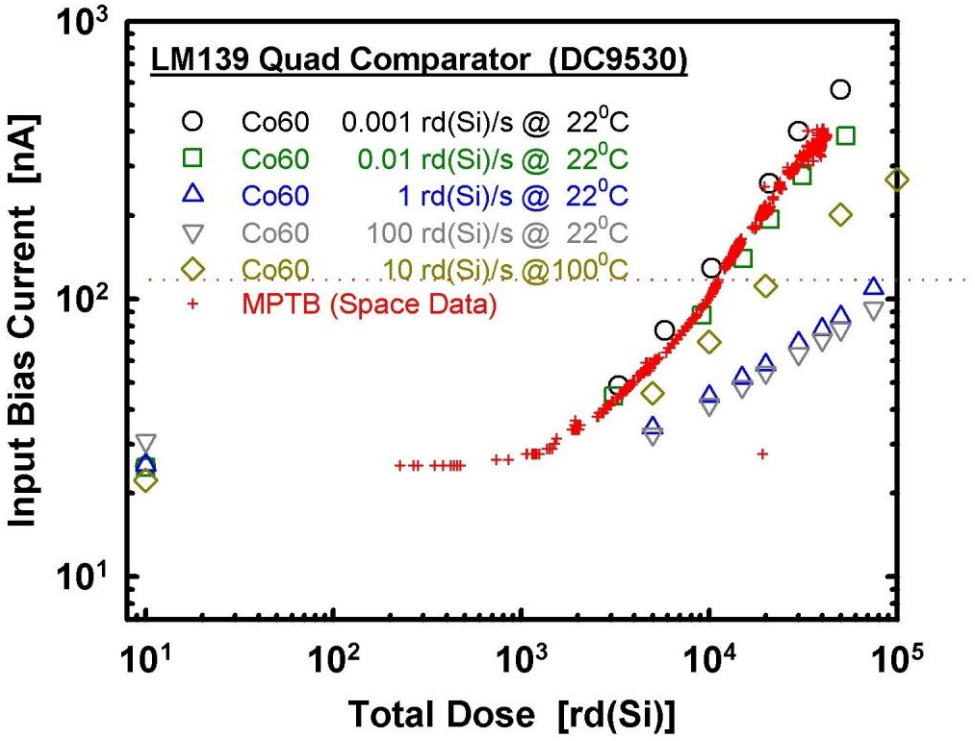

(a)

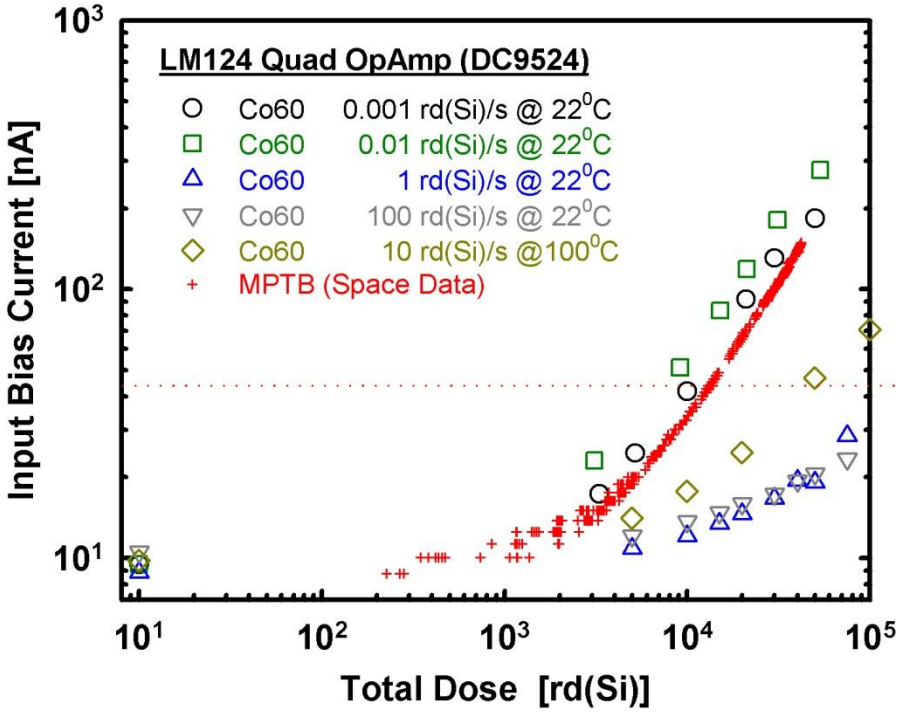

(b)

Figure 58. MPTB space radiation results, compared with ground test data: (a) LM139; and (b) LM124.

3.4 ELDRS Mechanisms and Models

Enlow et al., in their discussion, concluded that interface traps in the base oxide were the dominant mechanism in their experiments, causing an increase in base current by increasing surface recombination velocity. They also concluded [191] oxide trapped charge could also contribute by depleting the base region, but was not a large factor in his experiments because of relatively high base doping. They could not explain why a low dose rate irradiation produced more interface traps, however. Schmidt, [194] on the other hand, concludes oxide charge is the dominant effect in NPN devices, when the base surface actually is depleted. In PNP devices, oxide charge tends to bring the base region into accumulation, which reduces recombination, which is maximized when n and p carrier densities are equal. That is, oxide trapped charge tends to counter the effects of increased interface trap density, which act as recombination centers regardless of polarity.

Part of the explanation of why N_{IT} and N_{OT} are larger at low dose rates was provided by Fleetwood et al. [199], who showed that space charge effects played a role. They irradiated test capacitors from a bipolar process flow, and recorded N_{IT} and N_{OT} as a function of dose rate, finding about a factor of two increase in both at low dose rate, and somewhat less in reference [209]. These results were obtained with zero applied bias, and even small (e.g., fringing) fields were enough to change the results qualitatively. The N_{OT} results were explained in terms of the dipole model [79-81] for the oxide trapped hole. Fleetwood et al. found in TSC measurements that the number of trapped holes is actually about the same at high or low dose rate, but that more of them are compensated in the form of stable dipoles at high dose rate [199]. They suggest that the repulsive space charge field among the holes at high dose rate forces some of them closer to the interface, allowing more compensation by tunneling.

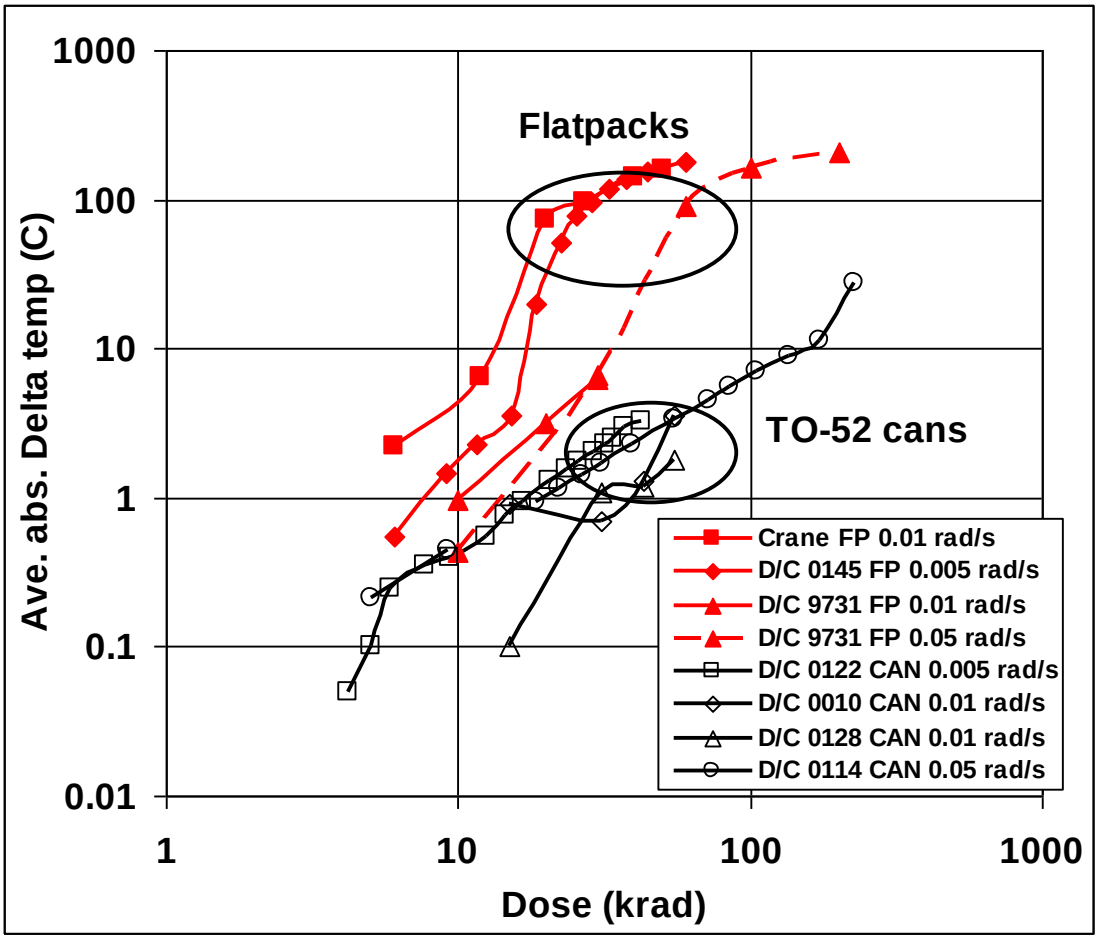

Figure 59. Response of the AD590 temperature transducer in flat-packs, as opposed to the response of the same parts in cans. The flat-packs have trace amounts of hydrogen in the package [210].

One factor that contributes to the buildup of interface traps in many ELDRS sensitive parts is that they have trace amounts of hydrogen in their packages. The impact that this hydrogen can have is demonstrated in Figure 59, for the AD 590 temperature transducer, which comes both in flat-pack packages and in metal cans [210]. The flat-packs have hydrogen in them and the cans do not. The difference in response, shown in Figure 59, can be as much as two orders of magnitude, depending on the dose. In Figure 59, all the irradiations are performed at relatively low dose rates, and the dose rates are the same for both packages. Recall that in Figure 53, the largest LDREF was for something identified only as a "Misc. IC". It was this same AD 590 temperature transducer. How this hydrogen in the package gives rise to an increase in the buildup of radiation-induced interface traps is an important part of the ELDRS mechanisms story.

There are at least three models in the literature that attempt to explain, or help to explain, how molecular hydrogen leads to a large interface trap buildup at low dose rates. All three, however, actually predict a *reduced* effect at high dose rates, rather than an increase at low dose rates. Basically, the higher density of free electrons in a high dose rate irradiation leads to a higher recombination rate with holes in the oxide—hence to fewer resulting holes at high dose

rate. One model, by Hjalmarson et al. [211,212], focuses on holes trapped in deep traps near the Si/SiO_2 interface, which act as cracking centers for H_2 molecules. The positively charged E' center is passivated by one hydrogen atom, to form a neutral defect, while the other hydrogen carries away the positive charge—that is, it becomes a proton. The proton then transports to the interface and reacts to form an interface trap, as we discussed previously for CMOS. A second model, by Fleetwood et al. [213], is very similar, except that the recombination and H_2 cracking involve holes hopping from one shallow trap to another in the bulk oxide, rather than in deep traps near the interface. A third model, by Boch et al. [214], focuses on the initial recombination process, where the higher density of electron/hole pairs leads to increased recombination at higher dose rates. This model does not specifically address interactions of the surviving holes with H_2 molecules, but it could obviously be extended to do so. It does predict a higher density of holes at low dose rates. Finally, we note that Tuttle et al. [215] use DFT (Density Functional Theory) calculations to examine H_2 interactions with E' centers. They conclude that their calculations for such interactions can explain many of the experimental results. All of these models seem to predict qualitatively similar results, which makes it difficult to choose among them.

3.5 ELDRS Hardness Assurance and Accelerated Test Methods

The purpose of this review is to discuss underlying mechanisms, rather than Hardness Assurance testing. However, there are mechanisms questions which have implications for test methods, which we will discuss briefly. There are approved standard test methods, which are widely used. In the US, there is MIL-STD-883/Test Method 1019, and the European Space Agency (ESA) has a standard test method ESCC 22900. Neither of these standards require testing at less than 0.01 rads (SiO_2)/sec, because, when they were adopted, the response of most tested parts seemed to have saturated at that level or higher. That is, testing at still lower dose rates seemed to produce no further low dose rate enhancement of the response of the part. Since then, however, exceptions have been observed [216]. Testing at 10-3 rads (SiO_2)/sec, it would take about one year to get to 30 krads (SiO_2), which is not practical in many cases. Therefore, there is a real need for an accelerated test method that would allow one to predict the results of an extremely low dose rate test, without taking one or more years to do one. Testing at elevated temperature (ETI, or elevated temperature irradiation) was proposed by Fleetwood [199], but work by several other authors showed that no single temperature worked for all parts [217-222].

A promising method is the switched dose rate method, suggested by Boch et al. [223]. Basically, parts are irradiated at high dose rate to several doses, and then the dose rate is switched low. The response curve then runs parallel to that of a low dose rate irradiation. Then the low dose rate segments can be used to construct a composite low dose rate curve. So far the main drawback of this technique is that it requires more parts than some other methods.

There are other techniques, which have been suggested, but we will not review them here because they all seem to have significant drawbacks.

3.6 ELDRS in CMOS?

Since ELDRS is so pervasive in bipolar devices, some have wondered if similar effects might be observed in CMOS, and have started to look for them. Consider the mechanisms we have discussed in connection with ELDRS: space charge effects, electron hole pair recombination, electron recombination with trapped holes, H_2 interactions with trapped holes, proton transport. These have all been observed in CMOS as well. Two experimental results have been reported, and offered as possible examples of ELDRS in CMOS. The first of these is shown in Figure 60 [224]. The reason ELDRS is suspected here is that the leakage current following low dose rate irradiation is higher at some times than after high dose rate irradiation. While this is clearly true at selected times, however, it is also true that the peak degradation after high dose rate irradiation is greater than after low dose rate irradiation. Therefore, the low dose rate enhancement factor, LDREF, is less than one. This situation is far different than the examples shown in Figure 51 or Figure 52, for example, which is why it would be easy to overlook.

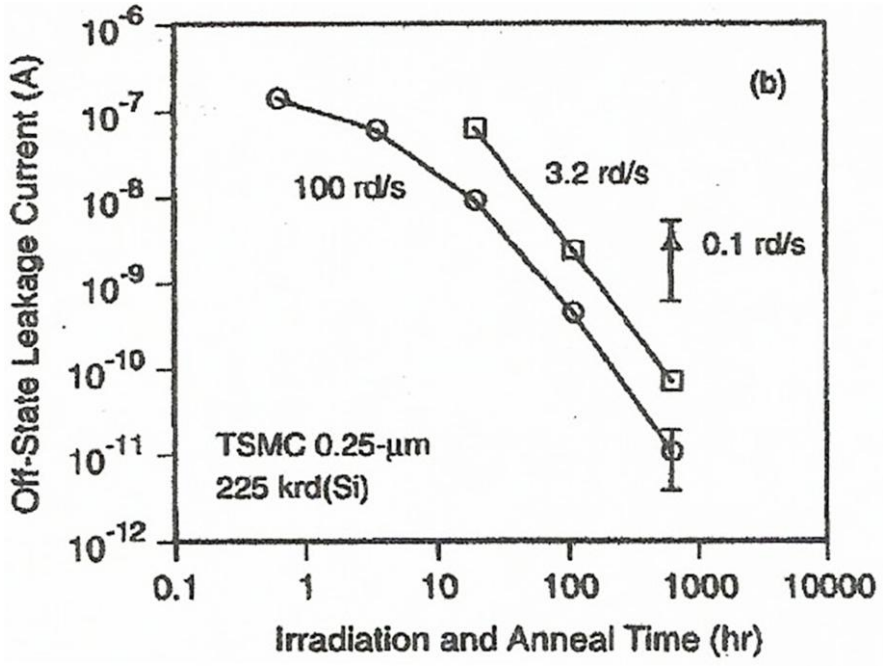

Figure 60. Example of possible ELDRS effect in CMOS. [224]

A second example is shown in Figure 61 [225], which shows the high and low dose rate leakage current responses of off-state individual transistors at two applied gate voltages. At the higher voltage, 1.8 V, the test transistor reaches 1 nA leakage at a lower dose at low dose rate, but the two curves come together by the time the leakage reaches 1 µA. At the lower voltage, 0.9 V, the leakage current starts to increase at a lower dose for the low dose rate irradiation, but the curves also appear to be coming together at the end of the exposure. Typically, one would expect the worst case test condition to be n-channel devices biased on, which probably draw currents of a few mA. One has to wonder if 1 nA of leakage would be significant in a circuit

drawing mA, especially if there is no dose rate dependence when the leakage reaches 1μA. This does appear to be an ELDRS effect, but it is a very small part of the overall response.

We note that Kruckmeyer et al. have tested recent CMOS products from their company, National Semiconductor, both at high dose rate and at low dose rate [226]. In all cases, they report greater parametric degradation at the higher dose rate. These results tend to confirm that ELDRS effects in CMOS are minimal, at least for the parts tested.

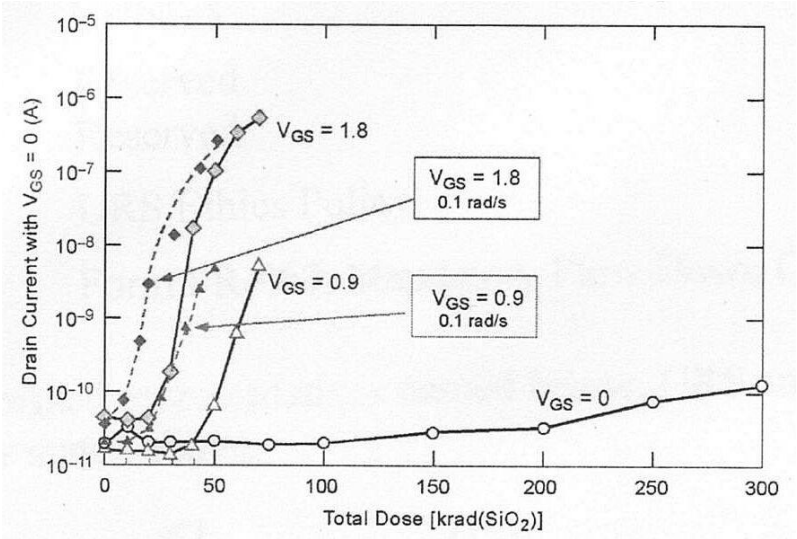

Figure 61. Off-state leakage current at high and low dose rates for CMOS transistors. [225]

There are two studies that seem to show an ELDRS effect in RADFETs, which are MOSFETs designed to be used as radiation dosimeters [227, 228]. Usually these have thick oxides, operate with no bias, except when being read, and they are made with special processing to maximize their sensitivity to radiation (that is, to maximize their hole trapping). A good dosimeter has to be sensitive. Because they have thick oxides, with high trapping efficiency, and no bias, one would expect them to have significant space charge effect, and it appears they do. The increase in sensitivity at low dose rate is in the range 1.5-2.0x, which is consistent with the space charge effects reported by Fleetwood [199, 209]. But RADFETs are very different than "standard" technology—they are specially processed to be as soft as possible, while everything else is intended to be as hard as can reasonably be achieved. An ELDRS effect in a RADFET does not mean the same thing will be observed anywhere else.

3.7 ELDRS Conclusions

Since the discovery of ELDRS 20 years ago, the effect has been studied extensively, and a degree of understanding has been achieved, although many more details remain to be worked out. The main experimental characteristics have been identified, and a standard test method is in place. There is a degree of understanding of the underlying mechanisms, although there is not

yet agreement on the details of the models that have been proposed. These are significant accomplishments, even though there is still additional work to be done.

4 Displacement Damage Effects

4.1 Introduction

In this section, we consider the effects of displacement damage, and displacement damage dose (DDD) in particular. In Figure 62, we show the LET for ionization energy loss and non-ionizing energy loss on the same scale for a Si ion incident on a Si target [229, 230]. Except at the very end of the track, the ionization energy loss is orders of magnitude greater than the non-ionizing (displacement producing) energy loss, which is one reason we usually discuss ionization effects first. But for compound semiconductors, which do not have oxides to trap charge, and for neutron irradiation, displacement damage is the main radiation effect. Therefore, we now turn our attention to displacement damage.

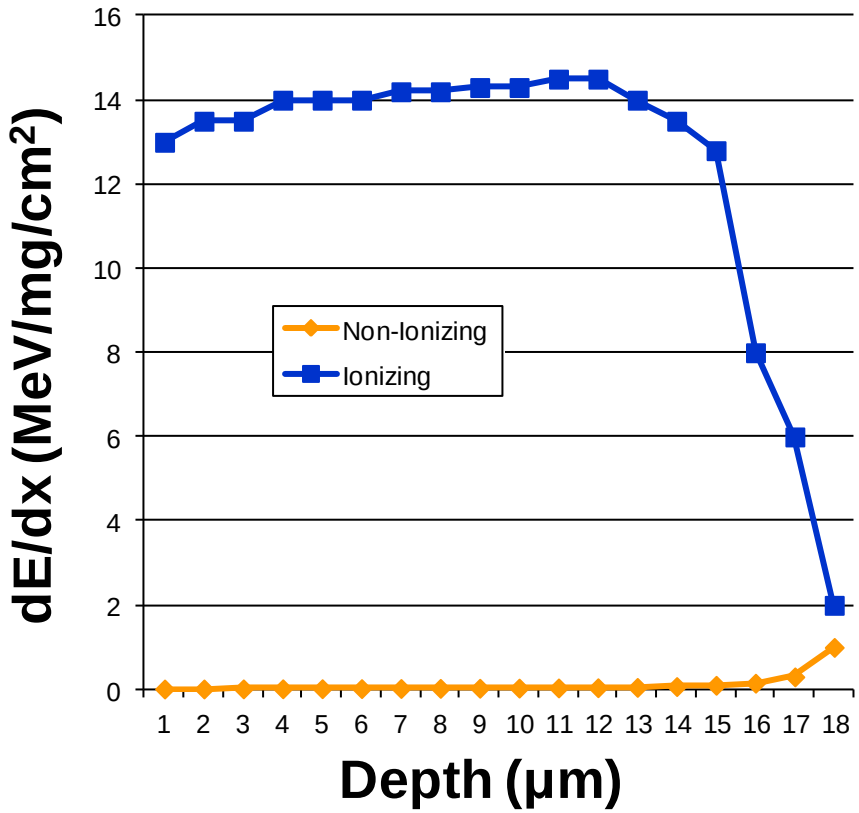

Figure 62. Ionizing and non-ionizing stopping power vs range for Si ions incident on Si [229, 230].

4.2 Formation of Displacement Damage Defects

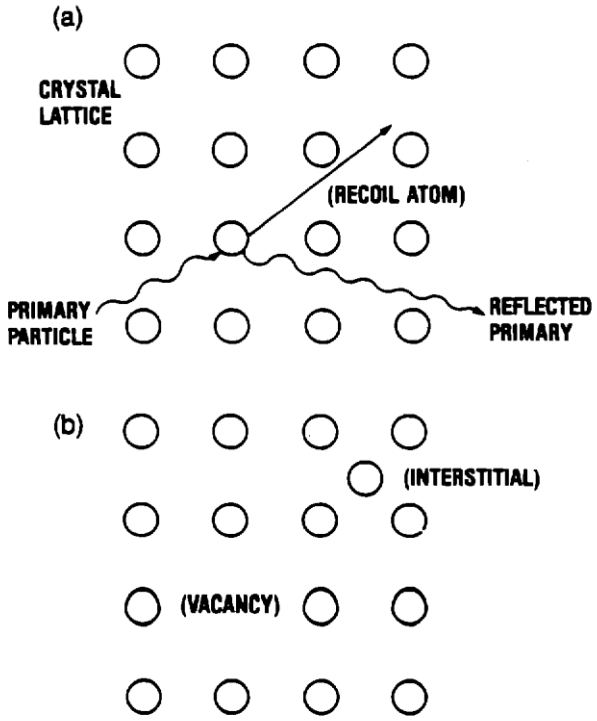

Figure 63. Displacement damage, formation of vacancy/interstitial (Frenkel) pair [231].

In Figure 63, we illustrate the formation of the simplest displacement damage defect. An energetic particle enters the target material, for example Si, and dislodges one of the Si atoms. This creates a vacancy where the atom had been, and the atom itself comes to rest some distance away, at an interstitial position. The vacancy and the interstitial atom together constitute a defect pair, which is also known as a Frenkel pair. The energy required to form a vacancy/interstitial defect pair for some materials of interest is given in Table I. A Frenkel pair is only the simplest kind of defect, however. Defects can move and form complexes—vacancies, in particular, are highly mobile. Two vacancies can come together and form a vacancy pair. Displacement damage defects, vacancies or interstitials or both can form complexes with impurity atoms—a phosphorous-vacancy pair, for example. Or they can form complexes of several defects (clusters).

Table 1. Threshold energy to produce atomic displacements [232].

Material	T_d (eV)
Diamond	35 +/ 5
Ge	27.5
Si	21
GaAs	7-11

4.3 Effects of Displacement Damage Defects

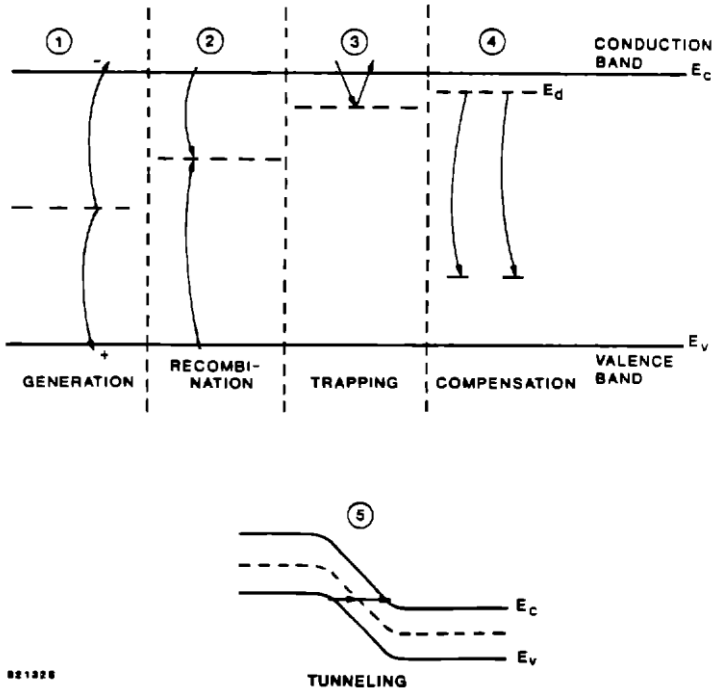

Figure 64. Electrical effects of displacement damage defects [233].

Figure 64 shows five effects that can occur because of displacement damage defects in the band-gap of Si or other semiconductors [233]. The first effect is the generation of electron/hole pairs. This process can be viewed as excitation of a valence band electron to the defect center, and subsequent excitation to the conduction band, or as hole emission from the center, followed by electron emission. Emission processes dominate over capture processes only when free carrier concentrations are significantly less than their thermal equilibrium values. Thus, these radiation induced generation centers are especially important in device depletion regions. Introduction of such centers is the mechanism for leakage current increases in Si devices.

The second process is the recombination of electron/hole pairs, where the defect captures a carrier of one polarity, followed by a second capture of a carrier of the opposite polarity. The mean time a minority carrier spends in its band before recombining is called the recombination lifetime. Radiation-induced recombination centers reduce this lifetime, which is the dominant mechanism for gain degradation in bipolar transistors.

The third process is the temporary trapping of carriers at (typically) shallow levels. The carriers are reemitted with no recombination event taking place.

The fourth process is the compensation of donors or acceptors by radiation-induced centers. In Figure 64, electrons from a donor level are compensated by deep level radiation-induced acceptors. This process is called carrier removal, because it reduces the majority carrier concentration.

The fifth process is tunneling of carriers through a barrier by means of defect levels. This defect assisted (or trap assisted) tunneling process can cause device current to increase.

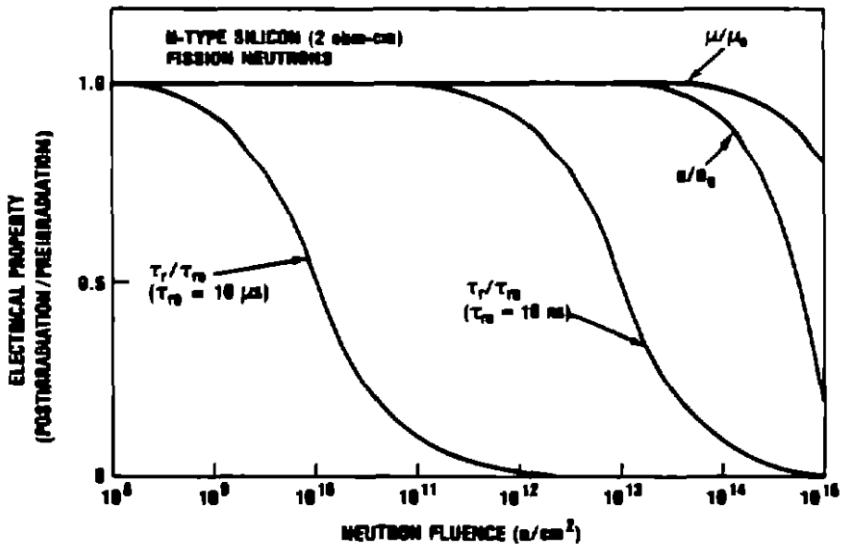

Figure 65. Device properties after neutron irradiation: minority carrier lifetime, carrier concentration, and mobility. Two values of pre-irradiation lifetime are shown [232].

In Figure 65, we show the effect on device electrical properties of neutron irradiation. The properties shown are minority carrier lifetime, carrier concentration, and mobility, all normalized to their pre-irradiation values. Two values of initial minority carrier lifetime are shown, 10 μs and 10 ns. The longer the initial lifetime is, the more sensitive the devices are. Even for a very short 10 ns initial lifetime, the lifetime starts to degrade by 10^{12} n/cm^2, although carrier concentration and mobility retain their values to somewhat higher neutron fluences.

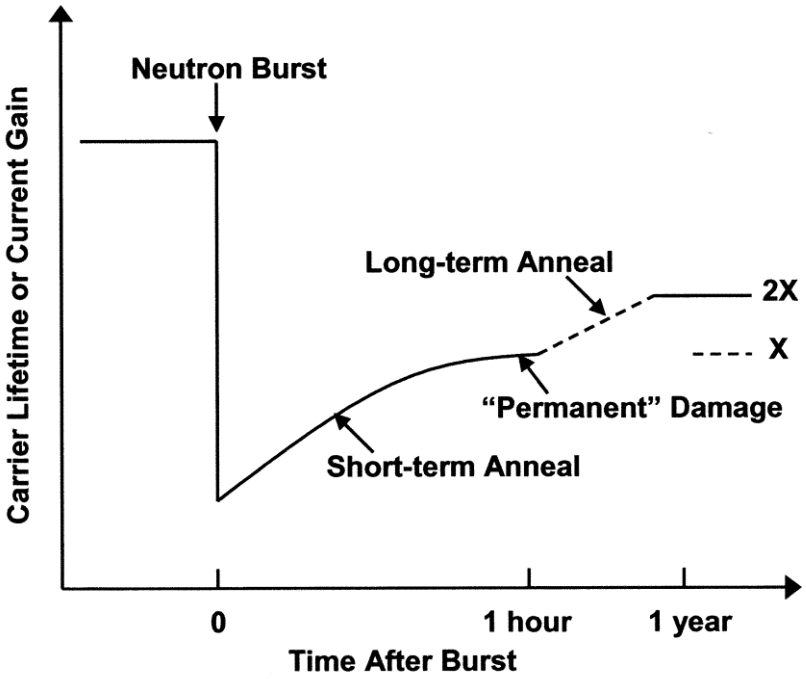

Figure 66. Short-term and long-term annealing of displacement damage [233].

In general, defects can reorder themselves to form more stable configurations. For example, vacancies can form complexes, or defects can recover. Damage recovering is called annealing (or forward annealing). Sometimes reverse annealing is also observed, where the effect of the damage increases with time. Usually annealing is divided into short term annealing (seconds to minutes) and long-term annealing (hours to years). These are illustrated in Figure 66. Generally, the annealing rate depends on the temperature and carrier injection rate.

4.4 Displacement Damage Models

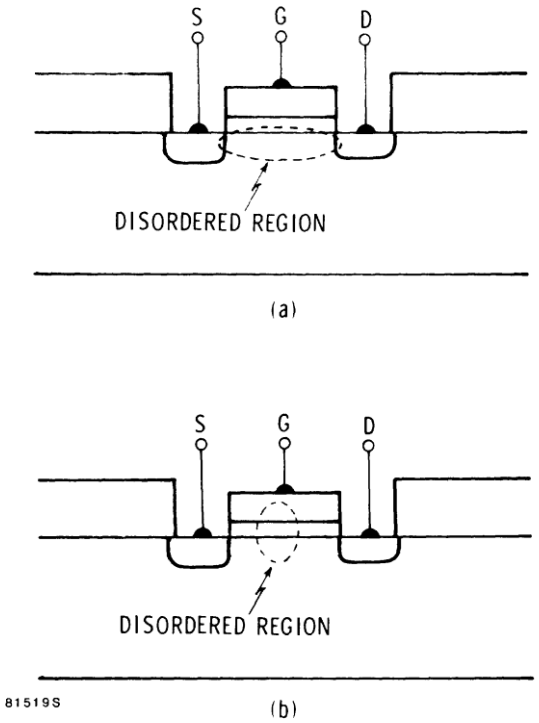

Figure 67. Hard errors in bipolar devices from single neutrons, after Srour et al. [235]

In Fig 67, which is from a paper presented in 1981 by Srour et al., the authors argued that single neutrons could be expected to cause hard errors in bipolar devices. At the time, technology in production had about 3 μm feature sizes, and the idea of 1 μm technology seemed revolutionary. The authors invoked the Gossick model [236], which predicts that all the displacement damage from a neutron will coalesce into one big damaged region, which can approach 1 μm in diameter. One can see in the Figure that the damage clusters are roughly the same size as the transistors. The paper was immediately controversial, primarily because of the use of the Gossick model. Other evidence which we will review shortly indicated that while small clusters do form, they are not close to the size predicted by the Gossick model.

Meanwhile, the other side of the argument came to be known as the NIEL (Non-Ionizing Energy Loss) model, which held that defect clusters were not important, and that what was important was the number of Frenkel pair defects, which was proportional to the NIEL, non-ionizing energy loss. To summarize the evidence supporting this position, we need to first introduce the Messenger-Spratt equation [237]:

$$1/h_{fe} = 1/h_{fe0} + K(E)\,\Phi \qquad (1)$$

where h_{fe} is the gain of a bipolar transistor, and the measure of radiation-induced degradation, h_{fe0} is gain before irradiation, K(E) is the damage factor, which depends on the

particle and its energy, and Φ is the particle fluence. There are different damage factors for other parameters, besides gain, as well.

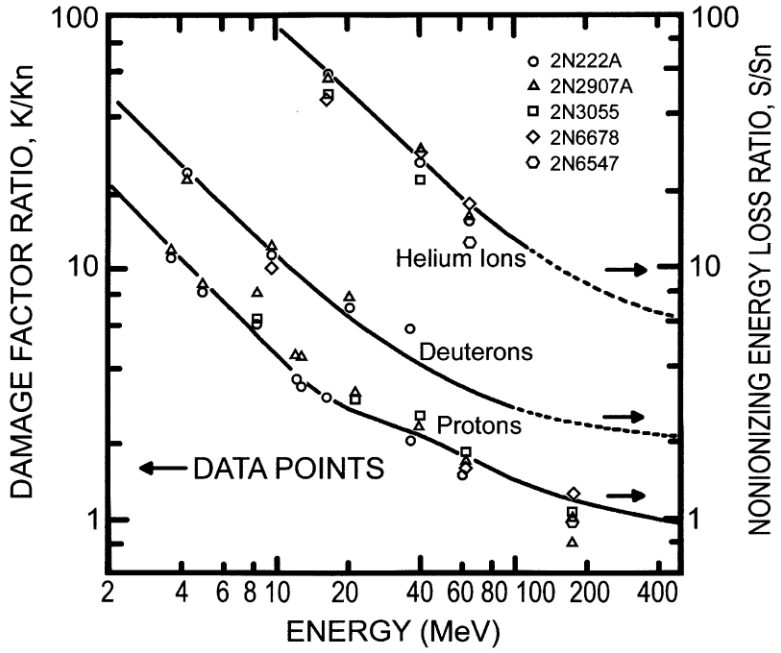

Figure 68. Damage factor ratios correlate with Non-Ionizing Energy Loss (NIEL).

One of the strongest pieces of evidence for the NIEL picture is shown in Figure 68 [238]. Measured damage factors for five parts are normalized (left axis), and plotted against normalized NIEL (right axis), for irradiations with protons, deuterons, and alpha particles at different energies. The damage factors correlate very nicely with NIEL, which helped establish the credibility of the NIEL picture.

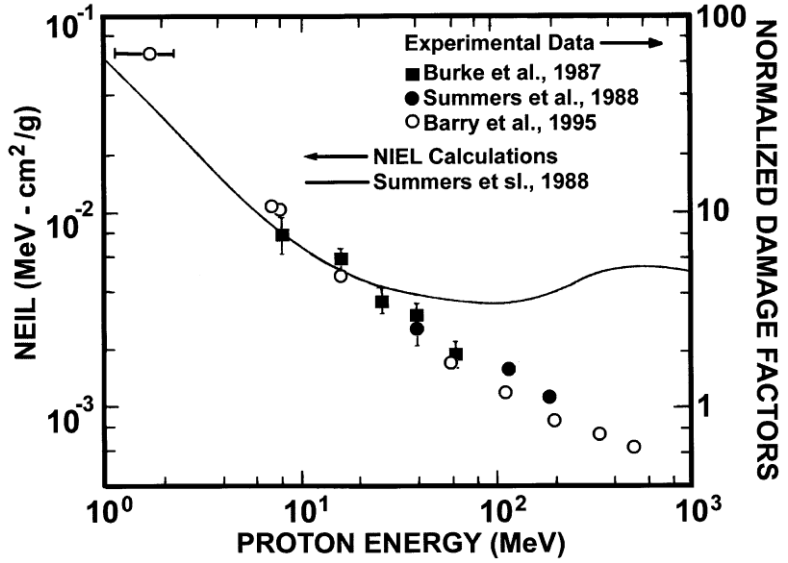

Figure 69. Measured damage factors deviating from the NIEL model [239].

However, it soon became clear that the NIEL model could not explain everything, as the results in Figure 69 show [239]. These results are for AlGaAs LEDs irradiated with protons, and the results deviate significantly from the NIEL prediction above about 20 or 30 MeV. Eventually, results like these led to further consideration of the role of damage clusters.

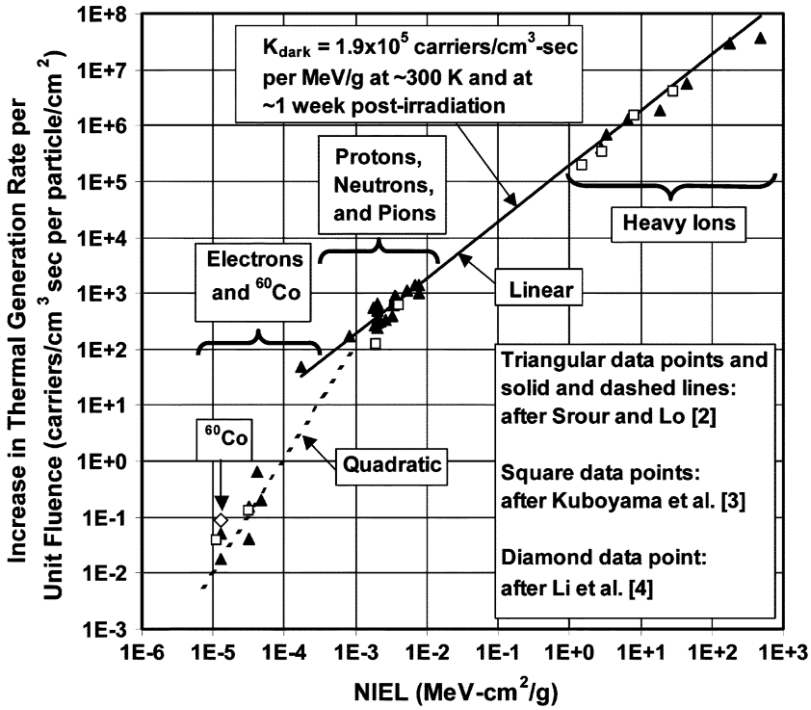

Figure 70. Damage factor for displacement damage: gammas and electrons produce isolated defect pairs, primarily; more massive particles tend to produce damage clusters.

Srour and Palko [240] analyzed data taken by themselves and others for the thermal generation of electron/hole pairs in Si. They defined the damage factor, K_{dark}, to be the thermal generation rate per unit volume in the depletion region, divided by the non-ionizing dose per unit fluence. In Figure 70, they plot K_{dark} times NIEL, as a function of NIEL, which gives the increase in the thermal generation rate per unit fluence, against NIEL per unit fluence. There is a universal response for most NIEL values, corresponding to protons, neutrons, pions, and heavy ions, but not to low NIEL particles such as electrons and gamma rays. They note that the high NIEL particles are more likely to cause cluster formation, because the defects will be relatively close together. The low NIEL particles, with a different response, will tend to form isolated defect pairs, and are unlikely to form clusters. They replot the data from Figure 70 in Figure 71, where the vertical axis now is just K_{dark}, and the horizontal axis is still NIEL per incident particle. They conclude that the high NIEL particles, above about $2x10^{-4}$ MeV-cm^2/g, all form small clusters, which dominate the dark current generation, and K_{dark} is a constant, about $2x10^5$ carriers/cm^3-sec-MeV/g. For particles that tend to form isolated defects, K_{dark} is much less, by perhaps a factor of 50.

Later, they performed another study [241] to examine the nature of these clusters. They conclude that the incident particle produces a primary knock-on atom (PKA), which may, depending on its energy, produce a cascade of secondary knock-on atoms. At the end of their range, these knock-on atoms have a high LET, and they basically melt a small volume of the Si target [242-249]. This melted Si is quenched before it can re-crystallize, leaving an amorphous inclusion. They say something similar happens in ion implantation, and has been extensively studied in the semiconductor industry for that reason. TEM studies indicate these amorphous regions are on the order of 5 nm. They also performed modeling which supports their conclusion. Ironically, the picture presented in [241], small clusters at the end of the tracks left by knock-on atoms, is very similar to much earlier simulation work presented by van Lint et al. [250], and illustrated in Figure 72. These results were part of the reason the Gossick model was controversial in 1981, and now the wheel appears to have come full circle.

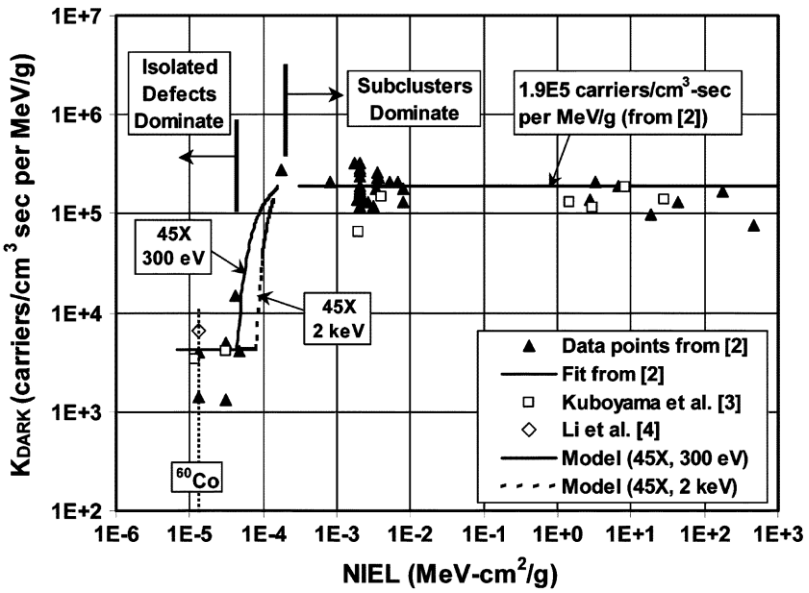

Figure 71. Damage factor data from Figure 70 renormalized to non-ionizing dose per particle.

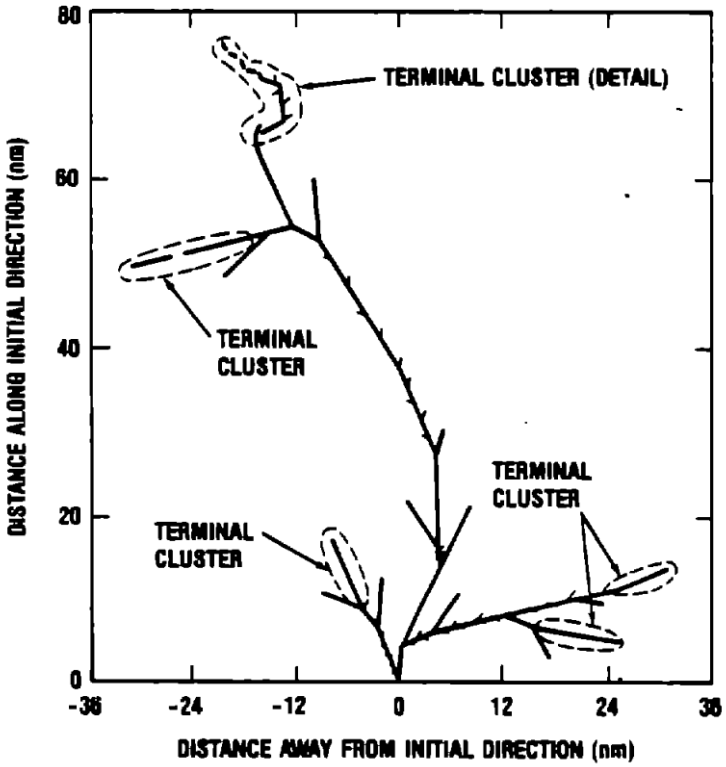

Figure 72. Small terminal clusters from displacement damage cascade, initiated by a neutron. [250]

4.5 Optoelectronic Devices.

Optoelectronic components are generally very sensitive to radiation damage, and primarily to displacement damage since they do not have oxides to trap ionization-induced charge. We have already discussed the underlying mechanisms. In this section, we will only give a few examples to illustrate the kinds of effects that might be observed. We note that Johnston devoted an entire Tutorial Short Course presentation to this topic, in 2004 [251], which covered this topic in far more detail than is possible here.

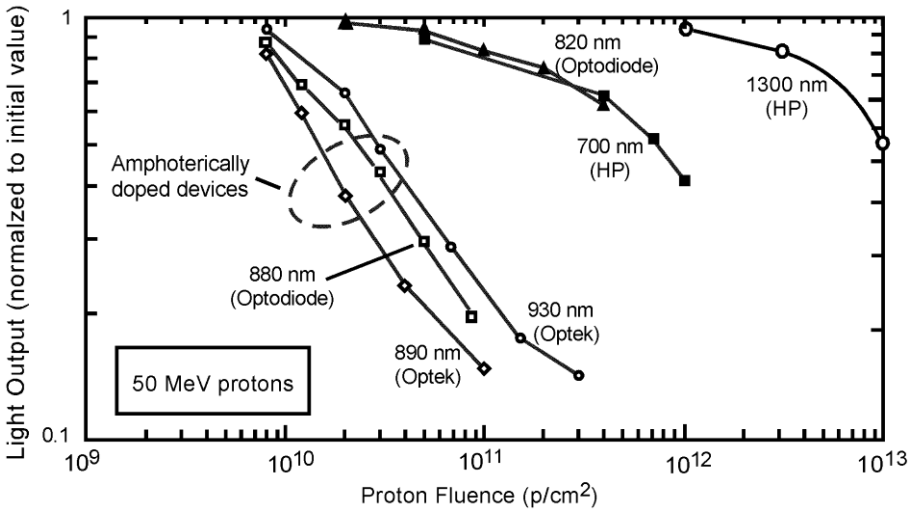

Figure 73. Reduction in light output for different LEDs, exposed to proton irradiation [252].

LEDs are perhaps the most sensitive of any common electronic component, because they have a broad transition region between the n- and p-type materials. The junction width is typically on the order of 50 μm, so they require long lifetimes to operate efficiently [253]. Recall from the discussion of Figure 65, that the longer the pre-irradiation lifetime is, the more sensitive the device will be to displacement damage. In Fig 73, we show the drop in light output for several commercially available LEDs, from proton irradiation. Measurable degradation starts as low as 10^{10} protons/cm^2, which does not represent a long flight in some orbits.

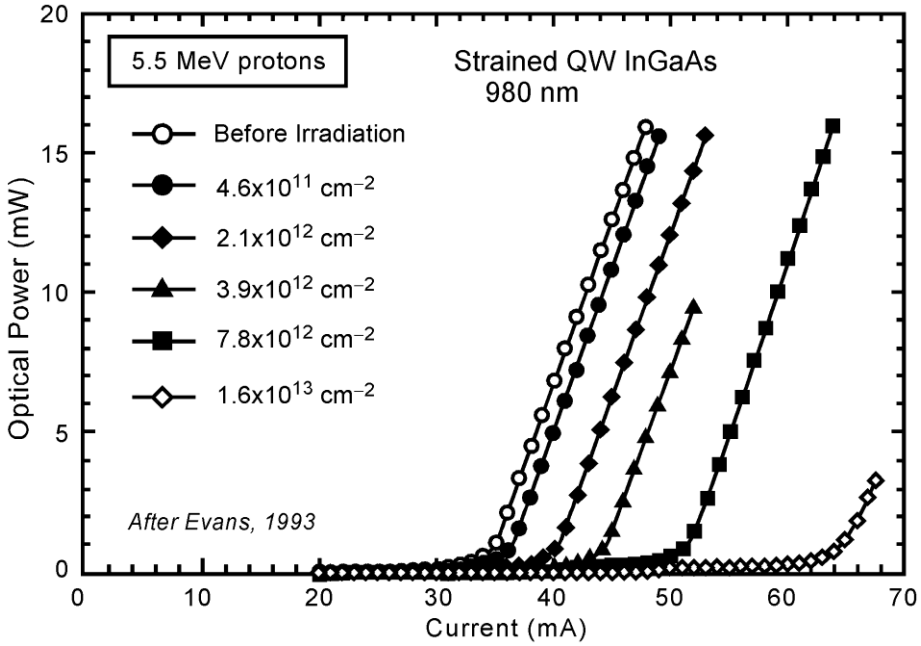

Figure 74. Increase in threshold current for laser diodes, following proton irradiation [252].

Laser diodes operate at higher electrical and optical power densities than LEDs, and they cannot function unless the photon density is high enough for stimulated emission. If radiation – induced recombination centers divert some of the current into non-radiative processes, then the threshold current for the laser will increase. Threshold current is a key parameter for laser diodes [252]. In the example in Figure 74, the threshold current more than doubles.

Optocouplers are used to convert optical signals to electrical signals. They typically have an LED to provide the optical signal, and a photo-transistor to sense it. CTF (current transfer ratio) is their most important parameter, and is defined as I_C/I_F, where I_F is the input current of the LED, and I_C is the output current of the photo-transistor. Radiation damage to two commercially available optocouplers is shown in Figure 75 [253], for three different kinds of particles. A key point here is that the damage is from displacement damage, because the gamma rays, which produce mostly ionization damage, produce only minimal degradation.

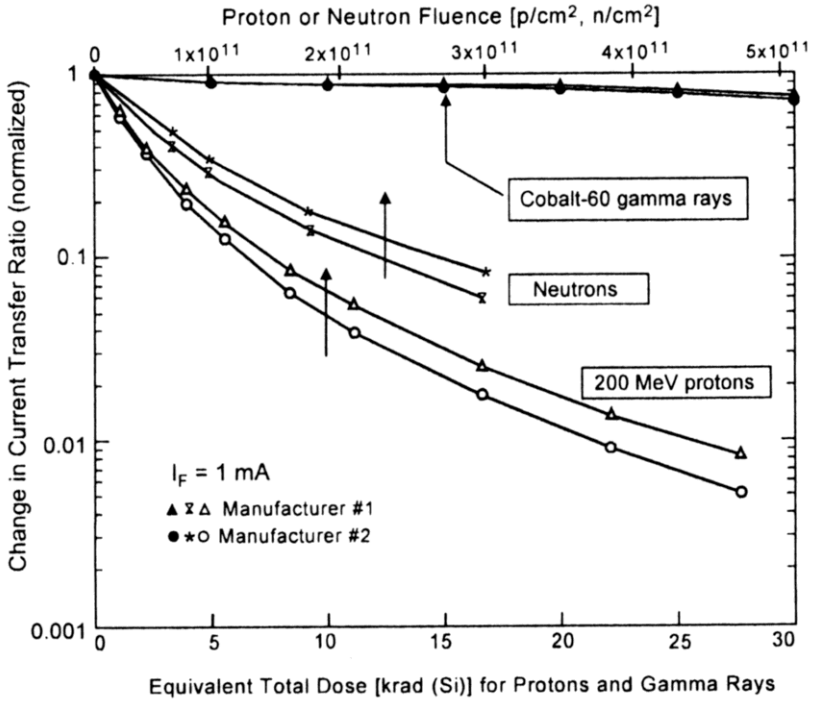

Figure 75. Damage to opto-couplers, following irradiation with different particles. Effects are from displacement damage, not ionization damage. [253] (Copyright World Scientific Publishing, reprinted by permission.)

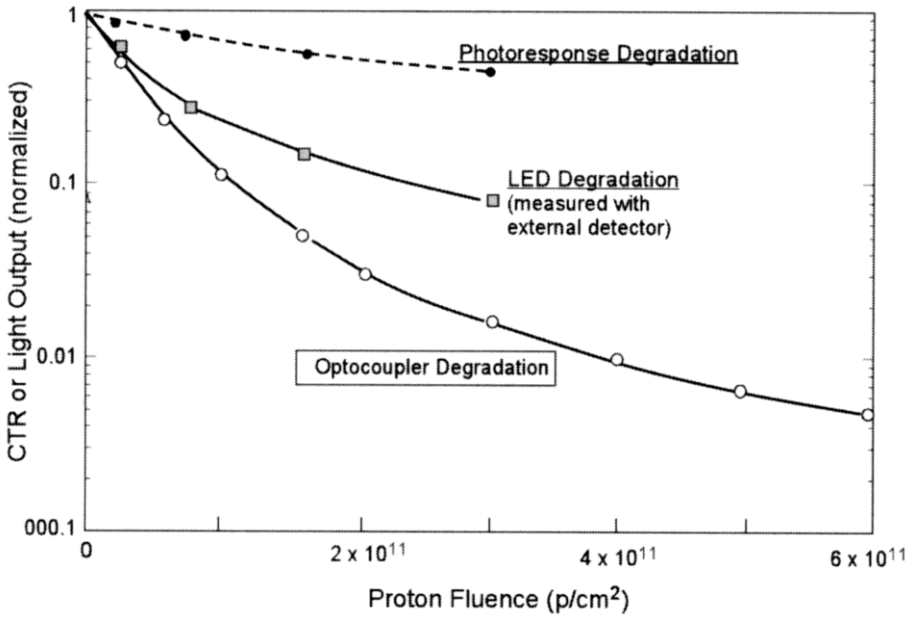

Figure 76. Opto-coupler degradation from proton irradiation, greater than expected from phototransistor response and LED response separately. [253] (Copyright World Scientific Publishing, reprinted by permission.)

In Figure 76 [253], proton-induced degradation for an optocoupler is shown, which makes the point that degradation for the whole unit is greater than for the sum of its parts. The

curve labeled “Photo-response Degradation” indicates the response of the photo-transistor to a constant light signal. The curve labeled “LED degradation” indicates the drop in the LED light output. But the optocoupler degradation is greater than the product of these two effects, because the photo-transistor does not operate efficiently at low light input levels.

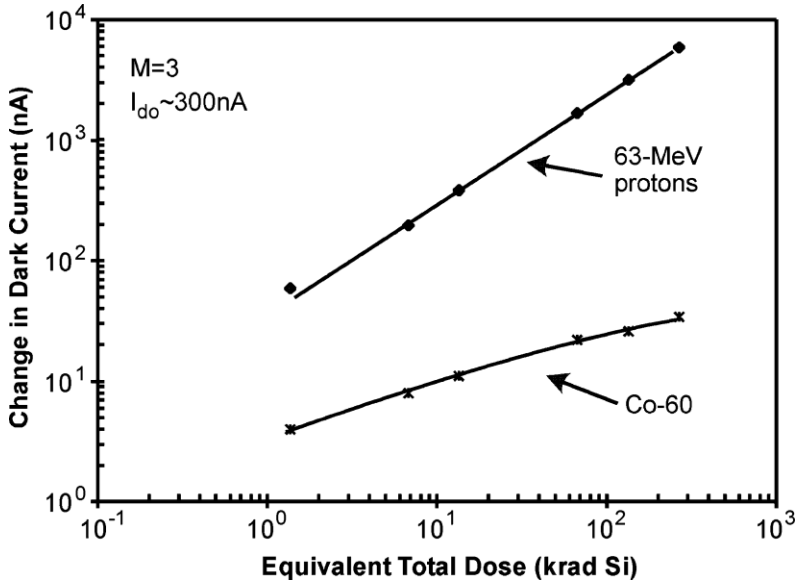

Figure 77. Avalanche Photodiode (APD) degradation, primarily from displacement damage. [254]

In Figure 77 [254], we show radiation degradation results for an avalanche photo-diode (APD) detector, exposed to two different kinds of radiation. The key point here is that degradation at the end of the irradiation is about two orders of magnitude greater for protons, which cause displacement damage, than for Co-60, which causes mostly ionization damage.

5 Conclusions

The physical mechanisms underlying the response of advanced CMOS microelectronics are now relatively well known in broad outline, but they may never be known in full detail. The models for interface trap production, and for the oxide hole trap, both date from the 1980s, although some of the confirming experiments were done in the 1990’s. But what the models tell us is that the overall response is extremely complicated. There are multiple processes involved, with complicated time dependences, and different field dependences, and different temperature dependences. How all the pieces fit together will always be a complicated story. Anytime the manufacturing processes change, trench oxides replacing planar isolation structures, or new dielectrics entering production, etc., many of the details of the response will have to be worked out again. Considering how often new manufacturing techniques are introduced, there is little chance the community will ever run out of things to do.

For bipolar devices, ELDRS was not even discovered until 1991, so the study of mechanisms has not had as long to make progress. For this reason, there is still work to be done,

but there has also been significant progress in recent years. For example, we discussed the different models trying to explain how hydrogen in the package gives rise to a large interface trap buildup. But it was not that long ago that the hydrogen in the package had not been identified, and there were no relevant models. The different models still need to be sorted out, but they still represent progress.

The biggest issue in the study of displacement damage has been the nature of the defect clusters, and also their impact. Now, a consensus seems to be developing that there are small damage clusters, and they do have an impact. NIEL is a useful parameter, but it does not explain everything by itself.

6 Acknowledgement

The author wishes to thank Ken LaBel and Bruce Wilson for their support, and Martha O'Bryan for technical assistance both with the presentation, and in preparing this manuscript.

References

[1] T. P. Ma and P. V. Dressendorfer, *Ionizing Radiation Effects in MOS Devices and Circuits*, Wiley-Interscience, New York, NY, 1989.

[2] T. R. Oldham, *Ionizing Radiation Effects in MOS Oxides*, Advances in Solid State Electronics and Technology (ASSET) Series, World Scientific Publishing, Singapore, 1999.

[3] J. M. Benedetto, H. E. Boesch, Jr., F. B. McLean, and J. P. Mize, *Hole removal in thin gate MOSFETs by tunneling*, IEEE Trans. Nucl. Sci., vol. 32, no. 6, p. 3916, 1985.

[4] N. S. Saks, M. G. Ancona, and J. A. Modolo, *Radiation effects in MOS capacitors with very thin oxides at 80K*, IEEE Trans. Nucl. Sci., vol. 31, no. 6, p. 1249, 1984.

[5] J. M. McGarrity, *Considerations for hardening MOS devices and circuits for low radiation doses*, IEEE Trans. Nucl. Sci., vol. 27, no. 6, p. 1739, 1980.

[6] R.C. Hughes, *Charge carrier transport phenomena in amorphous SiO_2: direct measurement of mobility and carrier lifetime*, Phys. Rev. Lett., vol. 30, pp. 1333, 1973.

[7] G. A. Ausman and F. B. McLean, *Electron-hole pair creation energy in SiO_2*, Appl. Phys. Lett., vol. 26, p. 173 (1975).

[8] O. L. Curtis, J. R. Srour, and K. Y. Chiu, *Hole and Electron Transport in SiO_2 Films*, J. Appl. Phys., 45, 406 (1974).

[9] H. H. Sander and B.L. Gregory, "*Unified Model of Damage Annealing in CMOS, From Freeze-In to Transient Annealing*," IEEE Trans. Nucl. Sci., NS-22, pp. 2157, 1975.

[10] H. E. Boesch and J. M. McGarrity, *Charge Yield and Dose Effects at 80K*, IEEE Trans. Nucl. Sci., NS-23,1520 (1976).

[11] J. M. Benedetto and H.E. Boesch, Jr., *The Relationship Between Co^{60} and 10 keV X-ray Damage in MOS Devices*, IEEE Trans. Nucl. Sci., NS-33, 1318 (1986).

[12] M. von Smoluchowski, *Uber Brownsche Molekularbewegung Unter Einwirkung Ausserer Krafte und Deren Zusammenhang mit der Verallgemeinerter Diffusionsgleichung*, Annalen der Physik, 44, 1103 (1915).

[13] L. Onsager, *Initial Recombination of Ions*, Phys. Rev., 54, 554 (1938).

[14] G. A. Ausman, *Field Dependence of Geminate Recombination in a Dielectric Medium*, Harry Diamond Lab Tech. Rept. HDL-TR-2097, Adelphi, MD (1987).

[15] G. Jaffe, *Zur Theorie der Ionisation in Kolonnen*, Annalen der Physik, 42, 303 (1913).

[16] P. Langevin, *L'Ionisation de Gaz*, Ann. Chim. Phys., 28, 289 (1903), and *Recombinaison et Mobilites des Ions dans le Gaz*, 28, 433 (1903).

[17] T. R. Oldham and J. M. McGarrity, *Ionization of SiO_2 by Heavy Charged Particles*, IEEE Trans. Nucl. Sci., NS-28, 3975 (1981).

[18] T. R. Oldham, *Charge Generation and Recombination in Silicon Dioxide from Heavy Charged Particles*, Harry Diamond Laboratories Technical Report HDL-TR-1985, Adelphi, MD 1982.

[19] T. R. Oldham, *Recombination Along the Tracks of Heavy Charged Particles in SiO_2 Films*, J. Appl. Phys., 57, 2695 (1985).

[20] T. R. Oldham, *Analysis of Damage in MOS Devices for Several Radiation Environments*, IEEE Trans. Nucl. Sci., NS-31, 1236 (1984).

[21] T. R. Oldham and J. M. McGarrity, *Comparison of Co^{60} and 10 keV X-ray Response in MOS Capacitors*, IEEE Trans. Nucl. Sci., NS-30, 4377 (1983).

[22] C.M. Dozier and D.B. Brown, *Effect of Photon Energy on the Response of MOS Devices*, IEEE Trans. Nucl. Sci., NS-28, 4137 (1981).

[23] M.R. Shaneyfelt, D.M. Fleetwood, J.R. Schwank, and K.L. Hughes, *Charge Yield for Co-60 and 10-keV X-Ray Irradiations of MOS Devices*, IEEE Trans. Nucl. Sci., NS-38, 1187 (1991).

[24] M. Murat, A. Akkerman, and J. Barak, *Charge yield and related phenomena induced by ionizing radiation in SiO_2 layers*, IEEE Trans. Nucl. Sci., vol. 53, no. 4, pp. 1973-1980, 2006.

[25] R.A. Weller, M.H. Mendenhall, R.A. Reed, R.D. Schrimpf, K.M. Warren, B.D. Seirawski, and L.W. Massengill, *Monte Carlo simulation of single event effects*, IEEE Trans. Nucl. Sci., vol. 57, no. 4, pp. 1726-1746, 2010.

[26] E.G. Stassinopoulos, G. J. Brucker, O. Van Gunten, A. R. Knudsen, and T. M. Jordan, *Radiation Effects on MOS Devices: Dosimetry, Annealing, Irradiation Sequence and Sources*, IEEE Trans. Nucl. Sci., NS-30, 1880 (1983).

[27] E. G. Stassinopoulos, O. Van Gunten, G. J. Brucker, A. R. Knudsen, and T. M. Jordan, *The Damage Equivalence of Electrons, Protons, Alphas, and Gamma Rays in Rad-Hard MOS Devices*, IEEE Trans. Nucl. Sci., NS-30, 4363 (1983).

[28] E. G. Stassinopoulos, G. J. Brucker, and O. Van Gunten, *Total Dose and Dose Rate Dependence of Proton Damage in MOS Devices During and After Irradiation*, IEEE Trans. Nucl. Sci., NS-31, 1444 (1984).

[29] G.J. Brucker, E.G. Stassinopoulos, O. Van Gunten, L. S. August, and T. M. Jordan, *The Damage Equivalence of Electrons, Protons, and Gamma Rays in MOS Devices*, IEEE Trans. Nucl. Sci., NS-29, 1966 (1982).

[30] G. J. Brucker, O. Van Gunten, E. G. Stassinopoulos, P. Shapiro, L. S. August, and T. M. Jordan, *Recovery of Damage in Rad-Hard MOS Devices During and After Irradiation by Electrons, Protons, Alphas, and Gamma Rays*, IEEE Trans. Nucl. Sci., NS-30, 4157 (1983).

[31] W. J. Stapor, L. S. August, D. H. Wilson, T. R. Oldham, and K. M. Murray, *Proton and Heavy Ion Damage Studies in MOS Transistors*, IEEE Trans. Nucl. Sci., NS-32, 4399 (1985).

[32] R. L. Pease, M. Simons, and P. Marshall, *Comparison of PMOSFET Response for Co^{60} Gammas and High Energy Protons*, J. Radiation Effects Research and Engineering, 18,126 (2000).

[33] P. Paillet, J. R. Schwank, M. Shaneyfelt, V. Ferlet-Cavrois, R. A. Loemker, and O. Flament, *Comparison of Charge Yield in MOS Devices for Different Radiation Sources*, IEEE Trans. Nucl. Sci., NS-49, 2656 (2002).

[34] H. E. Boesch, Jr., F. B. McLean, J. M. McGarrity, and G. A. Ausman, *Hole Transport and Charge Relaxation in Irradiated SiO_2 MOS Capacitors*, IEEE Trans. Nucl. Sci., NS-22, 2163 (1975).

[35] R. C. Hughes, *Hole Mobility and Transport in Thin SiO_2 Films*, Appl. Phys. Lett., 26, 436 (1975).

[36] R. C. Hughes, E. P. EerNisse, and H. J. Stein, *Hole Transport in MOS Oxides*, IEEE Trans. Nucl. Sci., NS-22, 2227 (1975).

[37] F. B. McLean, G. A. Ausman, H. E. Boesch, Jr., and J. M. McGarrity, *Application of Stochastic Hopping Transport to Hole Conduction in Amorphous SiO_2*, J. Appl. Phys., 47, 1529 (1976).

[38] F. B. McLean, H. E. Boesch, Jr., and J. M. McGarrity, *Hole Transport and Recovery Characteristics of SiO_2 Gate Insulators*, IEEE Trans. Nucl. Sci., NS-23, 1506 (1976).

[39] J. R. Srour, S. Othmer, O. L. Curtis. and K. Y. Chiu, *Radiation-Induced Charge Transport and Charge Build-Up in SiO_2 Films at Low Temperatures*, IEEE Trans. Nucl. Sci., NS-23, 1513 (1976).

[40] O. L. Curtis and J.R. Srour, *The Multiple Trapping Model and Hole Transport in SiO_2*, J. Appl. Phys., 48, 3819 (1977).

[41] R. C. Hughes, *Time-Resolved Hole Transport in a-SiO_2*, Phys. Rev., B15, 2012 (1977).

[42] F. B. McLean, H. E. Boesch, Jr., and J. M. McGarrity, *Field-Dependent Hole Transport in Amorphous SiO_2*, in The Physics of SiO_2 and Its Interfaces, S. T. Pantelides, ed., Pergamon Press, New York (1978), p 19.

[43] H. E. Boesch, Jr., J. M. McGarrity, and F. B. McLean, *Temperature and Field-Dependent Charge Relaxation in SiO_2 Gate Insulators*, IEEE Trans. Nucl. Sci., NS-25, 1012 (1978).

[44] H. E. Boesch, Jr., F. B. McLean, J. M. McGarrity, and P. S. Winokur, *Enhanced Flatband Voltage Recovery in Hardened Thin MOS Capacitors*, IEEE Trans. Nucl. Sci., NS-25, 1239 (1978).

[45] H. E. Boesch, Jr. and F. B. McLean, *Hole Transport and Trapping in Field Oxides*, IEEE Trans. Nucl. Sci., NS-32, 3940 (1985).

[46] E. W. Montroll and G. H. Weiss, *Random Walks on Lattices II*, J. Math. Phys., 6, 167 (1965).

[47] H. Scher and M. Lax, *Stochastic Transport in a Disordered Solid, I—Theory*, Phys. Rev., B7, 4491 (1973).

[48] H. Scher and M. Lax, *Stochastic Transport in a Disordered Solid, II—Impurity Conduction*, Phys. Rev., B7, 4502 (1973).

[49] G. Pfister and H. Scher, *Dispersive (Non-Gaussian) Transient Transport in Disordered Solids*, Adv. Phys., 27, 747 (1978).

[50] N. F. Mott and E. A. Davis, *Electronic Processes in Non-Crystalline Materials*, 2nd ed., Clarendon Press, Oxford (1979), pp. 65-97.

[51] I. G. Austin and N. F. Mott, *Polarons in Crystalline and Non-Crystalline Materials*, Adv. Phys., 18, 41 (1969).

[52] D. Emin, *Phonon-Assisted Transition Rates I—Optical-Phonon-Assisted Hopping in Solids*, Adv. Phys., 24, 305 (1975).

[53] B. E. Deal, M. Sklar, A. S. Grove, and E. H. Snow, *Characteristics of Surface-State Charge (Q_{SS}) of Thermally Oxidized Silicon*, J. Electrochem. Soc., 114, 266 (1967).

[54] F. J. Feigl, W. B. Fowler, and K. L. Yip, *Oxygen Vacancy Model for the E_1' Center in SiO_2*, Solid State Comm., 14, 225 (1974).

[55] R. A. Weeks, *Paramagnetic Resonance of Defects in Irradiated Quartz*, J. Appl. Phys., 27, 1376 (1956).

[56] P. M. Lenahan and P. V. Dressendorfer, *Hole Traps and Trivalent Silicon Centers in Metal/Oxide/Silicon Devices*, J. Appl. Phys., 55, 3495 (1984).

[57] F. B. McLean, *A Direct Tunneling Model of Charge Transfer at the Insulator Semiconductor Interface in MIS Devices*, Harry Diamond Laboratories, HDL-TR-1765, (1976).

[58] G. F. Derbenwick and H. H. Sander, *CMOS Hardness Prediction for Low-Dose-Rate Environments*, IEEE Trans. Nucl. Sci., NS-24, 2244 (1977).

[59] P. S. Winokur, *Limitations in the Use of Linear Systems Theory for the Prediction of Hardened-MOS Device Response in Space Satellite Environments*, IEEE Trans. Nucl. Sci., NS-29, 2102 (1982).

[60] P. S. Winokur, K. G. Kerris, and L. Harper, *Predicting CMOS Inverter Response in Nuclear and Space Environments*, IEEE Trans. Nucl. Sci., NS-30, 4326 (1983).

[61] S. Manzini and A. Modelli, *Tunneling Discharge of Trapped Holes in Silicon Dioxide*, Insulating Films in Semiconductors, J. F. Verweij and D. R. Wolters, ed., Elsevier Science Publishers B. V. (North Holland), p.112 (1983).

[62] T. R. Oldham, A. J. Lelis, and F. B. McLean, *Spatial Dependence of Trapped Holes Determined from Tunneling Analysis and Measured Annealing*, IEEE Trans. Nucl. Sci., NS-33, 1203 (1986).

[63] V. Lakshmanna and A. S. Vengurlekar, *Logarithmic Detrapping Response for Holes Injected into SiO_2 and the Influence of Thermal Activation and Electric Fields*, J. Appl. Phys., 63, 4548 (1988).

[64] M. Simons and H. L. Hughes, *Determining the Energy Distribution of Pulsed-Radiation-Induced Charge in MOS Structures from Rapid Annealing Measurements*, IEEE Trans. Nucl. Sci., NS-19 (No. 6), 282 (1972).

[65] M. Simons and H. L. Hughes, *Short-Term Charge Annealing in Electron-Irradiated Silicon Dioxide*, IEEE Trans. Nucl. Sci., NS-18 (No. 6), 106 (1971).

[66] J. G. Simmons and G. W. Taylor, *High-Field Isothermal Currents and Thermally Stimulated Currents in Insulators Having Discrete Trapping Levels*, Phys. Rev., B5, 1619 (1972).

[67] Z. Shanfield, *Thermally Stimulated Current Measurements on Irradiated MOS Capacitors*, IEEE Trans. Nucl. Sci., NS-30, 4377 (1983).

[68] Z. Shanfield and M. Moriwaki, *Radiation-Induced Hole Trapping and Interface State Characteristics of Al-Gate and Poly-Si Gate MOS Capacitors*, IEEE Trans. Nucl. Sci., NS-32, 3929 (1985).

[69] Z. Shanfield and M. Moriwaki, *Characteristics of Hole Traps in Dry and Pyrogenic Gate Oxides*, IEEE Trans. Nucl. Sci., NS-31, 1242 (1984).

[70] D. M. Fleetwood, R. A. Reber, and P. S. Winokur, *Effect of Bias on Thermally Stimulated Curent (TSC) in Irradiated MOS Devices*, IEEE Trans. Nucl. Sci., NS-38, 1066 (1991).

[71] D. M. Fleetwood, S. L. Miller, R. A. Reber, P. J. McWhorter, P. S. Winokur, M. R. Shaneyfelt, and J. R. Schwank, *New Insights into Radiation-Induced Oxide-Trapped Charge Through Thermally Stimulated Current Measurement and Analysis*, IEEE Trans. Nucl. Sci., NS-39, 2192 (1992).

[72] D. M. Fleetwood, M. R. Shaneyfelt, L. C. Riewe, P. S. Winokur, and R. A. Reber, *The Role of Border Traps in MOS High-Temperature Post-Irradiation Annealing Response*, IEEE Trans. Nucl. Sci., NS-40, 1323 (1993).

[73] D. M. Fleetwood, P. S. Winokur, R. A. Reber, T. L. Meisenheimer, J. R. Schwank, M. R. Shaneyfelt, and J. R. Schwank, *Effects of Oxide Traps, Interface Traps, and Border Traps on MOS Devices*, J. Appl. Phys., 73, 5058 (1993).

[74] D. M. Fleetwood, *Revised Model of Thermally Stimulated Current in MOS Capacitors*, IEEE Trans. Nucl. Sci., NS-44, 1826 (1997).

[75] P. J. McWhorter, S.L. Miller, and W. M. Miller, *Modeling the Anneal of Radiation-Induced Trapped Holes in a Varying Thermal Environment*, IEEE Trans. Nucl. Sci., NS-37, 1682 (1990).

[76] P. J. McWhorter, S. L. Miller and T. A. Dellin, *Modeling the Memory Retention Characteristics of SNOS Nonvolatile Transistors in a Varying Thermal Environment*, J. Appl. Phys., 68, 1902 (1990).

[77] J. R. Schwank, P. S. Winokur, P. J. McWhorter, F. W. Sexton, P. V. Dressendorfer, and D. C. Turpin, *Physical Mechanisms Contributing to Device "Rebound,"* IEEE Trans. Nucl. Sci., NS-31, 1434 (1984).

[78] C. M. Dozier, D. B. Brown, J. L. Throckmorton, and D. I. Ma, *Defect Production in SiO_2 by X-ray and Co-60 Radiations*, IEEE Trans. Nucl. Sci., NS-32, 4363 (1985).
[79] A. J. Lelis, H. E. Boesch, T. R. Oldham, and F. B. McLean, *Reversibility of Trapped Hole Annealing*, IEEE Trans. Nucl. Sci., NS-35, 1186 (1988).
[80] A. J. Lelis, T. R. Oldham, H. E. Boesch, Jr., and F. B. McLean, *The Nature of the Trapped Hole Annealing Process*, IEEE Trans. Nucl. Sci., NS-36, 1808 (1989).
[81] A. J. Lelis, and T. R. Oldham, *Time Dependence of Switching Oxide Traps*, IEEE Trans. Nucl. Sci., NS-41, 1835 (1994).
[82] R. K. Freitag, D. B. Brown, and C. M. Dozier, *Experimental Evidence for Two Species of Radiation-Induced Trapped Positive Charge*, IEEE Trans. Nucl. Sci., NS-40, 1316 (1993).
[83] R. K. Freitag, D. B. Brown, C. M. Dozier, *Evidence for Two Types of Radiation-Induced Trapped Positive Charge*, IEEE Trans. Nucl. Sci., NS-41, 1828 (1994).
[84] W. L. Warren, M. R. Shaneyfelt, D. M. Fleetwood, J. R. Schwank, P. S. Winokur, and R. A. B. Devine, *Microscopic Nature of Border Traps in MOS Oxides*, IEEE Trans. Nucl. Sci., NS-41, 1817 (1994).
[85] A. H. Edwards and W. B. Fowler, Final Report—ONR Contract N00014-92-J-2001, 1995.
[86] M. Walters and A. Reisman, *Radiation-Induced Neutral Electron Trap Generation in Electrically Biased Insulated Gate Field Effect Transistor Gate Insulators*, J. Electrochem. Soc., 138, 2756 (1991).
[87] J. F. Conley, P. M. Lenahan, A. J. Lelis, and T. R. Oldham, *Electron Spin Resonance Evidence for the Structure of a Switching Oxide Trap: Long Term Structural Change at Silicon Dangling Bond Sites in SiO_2*, Appl. Phys. Lett., 67, 2179 (1995).
[88] J. F. Conley, P. M. Lenahan, A. J. Lelis, and T. R. Oldham, *Electron Spin Resonance Evidence E_γ' Centers Can Behave as Switching Oxide Traps*, IEEE Trans. Nucl. Sci., NS-42, 1744 (1995).
[89] S. P. Karna, A. C. Pineda, R. D. Pugh, W. M. Shedd, and T. R. Oldham, *Electronic Structure Theory and Mechanisms of the Oxide trapped Hole Annealing Process*, IEEE Trans. Nucl. Sci., NS-47, 2316 (2000).
[90] C. J Nicklaw, Z. Y. Lu, D. M. Fleetwood, R. D Schrimpf, and S. T. Pantelides, *The Structure, Properties, and Dynamics of Oxygen Vacancies in Amorphous SiO_2*, IEEE Trans. Nucl. Sci., NS-49,2667 (2002).
[91] D. M. Fleetwood, H. D. Xiong, R. D. Schrimpf, Z. Y. Lu, S. T. Pantelides, and C. J. Nicklaw, *Unified Model of Hole Trapping, Charge Neutralization, and 1/f Noise in MOS Devices*, IEEE Trans. Nucl. Sci., NS-49, 2674 (2002).
[92] J.T. Ryan, P.M. Lenahan, T. Grasser, and H. Enichlmair, *Observations of negative bias temperature instability defect generation via on the fly electron spin resonance*, Appl. Phys. Lett., vol. 96, 223509 (2010).
[93] A. Scarpa, A. Paccagnella, F. Montera, G. Ghibaudo, G. Pananakakis, G. Ghidini, and P. G. Fuochi, *Ionizing Radiation Induced Leakage Current on Ultra-Thin Gate Oxides*, IEEE Trans. Nucl. Sci., NS-44, 1818 (1997).
[94] M. Ceschia, A. Paccagnella, A. Cester, A. Scarpa, and G. Ghidini, *Radiation Induced Leakage Current and Stress Induced Leakage Current in Ultra-Thin Gate Oxides*, IEEE Trans. Nucl. Sci., NS-45, 2375 (1998).
[95] L. Larcher, A. Paccagnella, M. Ceschia, and G. Ghidini, *A model of radiation induced leakage current (RILC) in ultra-thin gate oxides*, IEEE Trans. Nucl. Sci., vol. 46, no. 6, p. 1553, 1999.

[96] D. M. Fleetwood, *Border traps in MOS devices*, IEEE Trans. Nucl. Sci., vol. 39, no. 2, p. 269, 1992.

[97] D. M. Fleetwood, W. L. Warren, J. R. Schwank, P. S. Winokur, M. R. Shaneyfelt, and L. C. Riewe, *Effects of Interface Traps and Border Traps on MOS Post-Irradiation Annealing Response*, IEEE Trans. Nucl. Sci., NS-42, 1698 (1995).

[98] P. M. Lenahan and P. V. Dressendorfer, *An Electron Spin Resonance Study of Radiation-Induced Electrically Active Paramagnetic Centers at the Si/SiO_2 Interface*, J. Appl. Phys., 54, 1457 (1983).

[99] T. R. Oldham, F. B. McLean, H. E. Boesch, Jr., and J. M. McGarrity, *An Overview of Radiation-Induced Interface Traps in MOS Structures*, Semicond. Sci. and Technol., 4, 986 (1989).

[100] A. J. Lelis, T. R. Oldham, and W. M. Delancey, *Response of Interface Traps During High-Temperature Anneals*, IEEE Trans. Nucl. Sci., NS-38, 1590 (1991).

[101] F. B. McLean, *A Framework for Understanding Radiation-Induced Interface States in MOS SiO_2 Structures*, IEEE Trans. Nucl. Sci., NS-27, 1651 (1980).

[102] H. E. Boesch, Jr., F. B. McLean, J. M. McGarrity, and G. A. Ausman, *Hole Transport and Charge Relaxation in Irradiated SiO_2 MOS Capacitors*, IEEE Trans. Nucl. Sci., NS-22, 2163 (1975).

[103] P. S. Winokur and M. A. Sokoloski, *Comparison of Interface State Build-up in MOS Capacitors Subject to Penetrating and Non-Penetrating Radiation*, Appl. Phys. Lett., 28, 627 (1975).

[104] P. S. Winokur, J. M. McGarrity, and H. E. Boesch, Jr., *Dependence of Interface-State Buildup on Hole Generation and Transport in Irradiated MOS Capacitors*, IEEE Trans. Nucl. Sci., NS-23, 1580 (1976).

[105] P. S. Winokur, H. E. Boesch, Jr., J. M. McGarrity, and F. B. McLean, *Field- and Time-Dependent Radiation Effects at the Si/SiO_2 Interface of Hardened MOS Capacitors*, IEEE Trans. Nucl. Sci., NS-24, 2113 (1977).

[106] P. S. Winokur, H. E. Boesch, Jr., J. M. McGarrity, and F. B. McLean, *Two Stage Process for the Buildup of Radiation-Induced Interface Traps*, J. Appl. Phys., 50, 3492 (1979).

[107] P. S. Winokur and H. E. Boesch, Jr., *Interface State Generation in Radiation-Hard Oxides*, IEEE Trans. Nucl. Sci., NS-27, 1647 (1980).

[108] J. M. McGarrity, P. S. Winokur, H. E. Boesch, Jr., and F. B. McLean, *Interface States Resulting from a Hole Flux Incident on the Si/SiO_2 Interface*, Physics of SiO_2 and Its Interfaces, S. T. Pantelides, ed., Pergamon Press, New York, p. 428, 1978.

[109] H. E. Boesch, Jr. and F. B. McLean, *Interface State Generation Associated with Hole Transport in MOS Structures*, J. Appl. Phys. 60, 448 (1986).

[110] P. S. Winokur. F. B. McLean, and H. E. Boesch, Jr., *Physical Processes Associated with Radiation-Induced Interface States*, U. S. Army Harry Diamond Laboratories, HDL-TR-2081, Adelphi, MD 20783-1197 (1986).

[111] N.S. Saks and M.C. Ancona, *Time Dependence of Interface Trap Formation in MOSFETs Following Pulsed Irradiation*, IEEE Trans. Nucl. Sci., NS-34, 1348 (1987).

[112] N. S. Saks, C. M. Dozier, and D. B. Brown, *Time Dependence of Interface Trap Formation in MOSFETs Following Pulsed Irradiation*, IEEE Trans. Nuc. Sci., NS-35, 1168 (1988).

[113] N. S. Saks, R. B. Klein, and D. L. Griscom, *Formation of Interface Traps in MOSFETs During Annealing Following Low Temperature Radiation*, IEEE Trans. Nucl. Sci., NS-35, 1234 (1988).

[114] N. S. Saks and D. B. Brown, *Interface Trap Formation via the Two Stage H^+ Process*, IEEE Trans. Nucl. Sci., NS-36, 1848 (1989).
[115] N. S. Saks and D. B. Brown, *Observation of H^+ Motion During Interface Trap Formation*, IEEE Trans. Nucl. Sci., NS-37, 1624 (1990).
[116] N.S. Saks and R.W. Rendell, *Time dependence of post-irradiation interface trap build-up in deuterium annealed oxides*, IEEE Trans. Nucl. Sci., NS-39, 2220 (1992).
[117] N. S. Saks, R. B. Klein, R. E. Stahlbush, B. J. Mrstik, and R. W. Rendell, *Effect of Post-Stress Hydrogen Annealing on MOS Oxides after Co^{60} Irradiation or Fowler-Nordheim Injection*, IEEE Trans. Nucl. Sci., NS-40, 1341 (1993).
[118] S. R. Hofstein, *Proton and sodium transport in SiO_2 films*, IEEE Trans. Electron Dev., ED-14, 749 (1967).
[119] H. E. Boesch, Jr., *Time dependent interface trap effects in MOS devices*, IEEE Trans. Nucl. Sci., NS-35, 1160 (1988).
[120] D. L. Griscom, *Diffusion of radiolytic molecular hydrogen as a mechanism for the post-irradiation build-up of interface states in SiO_2-on-Si structures*, J. Appl. Phys., 58, 2524 (1985).
[121] D. B. Brown, *The time dependence of interface state production*, IEEE Trans. Nucl. Sci., NS-32, 3900 (1985).
[122] D. L. Griscom, D. B. Brown, and N. S. Saks, *Nature of radiation-induced point defects in amorphous SiO_2 and their role in SiO_2-on-Si structures*, The Physics and Chemistry of SiO_2 and the Si/SiO_2 Interface, C. R. Helms and B. E. Deal, eds., Plenum (1988).
[123] D.B. Brown and N.S. Saks, *Time dependence of radiation-induced interface trap formation in metal-oxide-semiconductor devices as a function of oxide thickness and field*, J. Appl. Phys., 70, 3734 (1990).
[124] F. J. Grunthaner, B. F. Lewis, N. Zamini, amd J. Maserjian, *XPS studies of structure-induced radiation defects at the Si/SiO_2 interface*, IEEE Trans. Nucl. Sci., vol. 27, no. 6, p. 1640, 1980.
[125] F. J. Grunthaner, P. J. Grunthaner, and J. Maserjian, *Radiation-induced defects in SiO_2 as determined with XPS*, IEEE Trans. Nucl. Sci., vol. 29, no. 6, p. 1462, 1982.
[126] F. J. Grunthaner and P. J. Grunthaner, *Chemical and electronic structure of the SiO_2/Si interface*, Materials Science Reports, North Holland, Amsterdam, 1, 65 (1986).
[127] S. K. Lai, *Interface trap generation in silicon dioxide when electrons are captured by trapped holes*, J. Appl. Phys., vol. 54, p. 2540 (1983).
[128] S. J. Wang, J. M. Sung, and S. A. Lyon, *Relation between hole trapping and interface state generation in metal-oxide-silicon structures*, Appl. Phys. Lett., vol. 52, p. 1431 (1988).
[129] D. M. Fleetwood, *Fast and slow border traps in MOS devices*, IEEE Trans. Nucl. Sci., vol. 43, no. 3, pp. 779-787, 1996.
[130] J. R. Schwank, D. M. Fleetwood, M. R. Shaneyfelt, P. S. Winokur, C. L. Axeness, and L. C. Riewe, *Latent interface trap build-up and its implications for hardness assurance*, IEEE Trans. Nucl. Sci., vol. 39, no. 6, p. 1953, 1992.
[131] A. Grove, *Changing vectors of Moore's law,* Int. Electron. Devices Meeting, San Francisco, CA, Dec. 2002.
[132] H.E. Boesch and G.J. Dunn, *Hole transport in $SiO_2$and reoxidized nitrided SiO_2 gate insulators at low temperature*, IEEE Trans. Nucl. Sci., vol. 38, no. 6, pp. 1083-1088, 1991.

[133] N.S. Saks, M. Simons, D.M. Fleetwood, J.T. Yount, P.M. Lenahan, and R.B. Klein, *Radiation effects in oxynitrides grown in N_2O,* IEEE Trans. Nucl. Sci., vol. 41, no. 6, pp. 1854-1863, 1994.

[134] D.M. Fleetwood and N.S. Saks, *Oxide, interface and border traps in thermal, N_2O and N_2O-nitrided oxides,* J. Appl. Phys., vol. 79, no. 3, pp. 1583-1594, 1996.

[135] J.P. Campbell, P.M. Lenahan, A.T. Krishnan, and S. Krishnan, *Identification of the atomic-scale defects involved in negative bias temperature instability in plasma nitride p-channel metal-oxide-silicon field-effect transistors,* J. Appl. Phys., vol. 103, 044505, 2008.

[136] J.T. Ryan, P.M. Lenahan, A.T. Krishnan, and S. Krishnan, *Spin dependent tunneling spectroscopy in 1.2 n dielectrics,* J. Appl. Phys., vol. 108, 064511, 2010.

[137] A.Y. Kang, P.M. Lenahan, and J.F. Conley, *The radiation response of the high dielectric constant hafnium oxide/silicon system,* IEEE Trans. Nucl. Sci., vol. 49, no. 6, pp. 2636-2642, 2002.

[138] J.T. Ryan, P.M. Lenahan, A.Y. Kang, J.F. Conley, G. Bersuker, and P. Lysaght, *Identification of the atomic scale defects involved in radiation damage in HfO_2based MOS devices,* IEEE Trans. Nucl. Sci., vol. 52, no. 6, pp. 2272-2275, 2005.

[139] P.M. Lenahan, and J.F. Conley, *Magnetic resonance studies of trapping center in high-κ dielectric films on silicon,* IEEE Trans. Dev. and Mat. Rel. vol 5, no. 1, pp90-102, 2005.

[140] J.T. Ryan, P.M. Lenahan, G. Bersuker, and P. Lysaght, *electron spin resonance observations of oxygen deficient silicon atoms in the interfacial layer of hafnium oxide based metal-oxide-silicon structures,* Appl. Phys. Let., vol 90, 173513, 2007.

[141] G. Lucovsky, D.M. Fleetwood, S. Lee, H. Seo, R.D.Schrimpf, J.A. Felix, J. Luning, L.B. Fleming, M. Ulrich, and D.E. Aspnes, *Differences between charge trapping states in irradiated nano-crystalline HfO_2 and non-crystalline Hf silicates,* IEEE Trans. Nucl. Sci., vol. 53, no. 6, pp. 3644-3648, 2006.

[142] X.J. Zhou, D.M. Fleetwood, L. Tsteris, R.D. Schrimpf, and S.T. Pantelides, *Effects of switched-bias annealing on charge trapping inHfO_2gate dielectrics,* IEEE Trans. Nucl. Sci., vol. 53, no. 6, pp. 3636-3643, 2006.

[143] J.A. Felix, D.M. Fleetwood, R.D. Schrimpf, J.G. Hong, G. Lucovsky, J.R. Schwank, and M.R. Shaneyfelt, *Total dose radiation response of hafnium silicate capacitors,* IEEE Trans. Nucl. Sci., vol. 49, no. 6, pp. 3191-3196, 2002.

[144] X.J. Zhou, D.M. Fleetwood, J.A. Felix, E.P. Gusev, and C. D'Emic, *Bias-temperature instabilities and radiation effects in MOS devices,* IEEE Trans. Nucl. Sci., vol. 52, no. 6, pp. 2231-2238, 2005.

[145] E. Harari and B.S.H. Royce, *The effect of electron and hole trapping on the radiation hardness of Al_2O_3MIS devices,* IEEE Trans. Nucl. Sci., vol. 20, no. 6, pp. 280-287, 1973.

[146] J.A. Felix, M.R. Shaneyfelt, D.M. Fleetwood, T.L. Meisenheimer, J.R. Schwank, R.D. Schrimpf, P.E. Dodd, E.P. Gusev, and C. D'Emic, *Radiation-induced charge trapping in thin $Al_2O_3/SiO_xN_y/Si(100)$ gate dielectric stacks,* IEEE Trans. Nucl. Sci., vol. 50, no. 6, pp. 1910-1918, 2003.

[147] J.A. Felix, M.R. Shaneyfelt, D.M. Fleetwood, J.R. Schwank, P.E. Dodd, E.P. Gusev, R.M. Fleming, and C. D'Emic, *Charge trapping and annealing in high-κ gate dielectrics,* IEEE Trans. Nucl. Sci., vol. 51, no. 6, pp. 3143-3149, 2004.

[148] R. Koga, W.R. Crain, K.B. Crawford, D.D. Lau, S.D. Pinkerton, B.K. Yi, and R. Chitty, *On the suitability of non-hardened high density SRAMs for space applications,* IEEE Trans. Nucl. Sci., vol. 38, no. 6, pp. 1507-1511, (1991).

[149] C. Dufour, P. Garnier, T. Carriere, J. Beaucour, R. Eccofet, and M. Labrunee, *Heavy Ion Induced Single Hard Errors in Submicronic Memories*, IEEE Trans. Nucl. Sci., NS-39, 1693 (1992).
[150] T. R. Oldham, K. W. Bennett, J. Beaucour, T. Carriere, C. Poivey, P. Garnier, *Total Dose Failures in Advanced Electronics from Single Ions*, IEEE Trans. Nucl. Sci., NS-40, 1820 (1993).
[151] C. Poivey, T. Carriere, J. Beaucour, and T. R. Oldham, *Characterization of Single Hard Errors (SHE) in 1M-bit SRAMs from Single Ions*, IEEE Trans. Nucl. Sci., NS-41, 2235 (1994).
[152] J.-G. Loquet, J.-P. David, S. Duzellier, D. Falguere, and T. Nuns, *Simulation of heavy ion-induced failure modes in nMOS cells of ICs*, IEEE Trans. Nucl. Sci., vol. 48, no. 6, p. 2278, 2001.
[153] G. M. Swift, D. J. Padgett, and A. H. Johnston, *A New Class of Single Hard Errors*, IEEE Trans. Nucl. Sci., NS-41, 2043 (1994).
[154] M.R. Shaneyfelt, J.A. Felix, P.E. Dodd, J.R. Schwank, S.M. Dalton, J. Baggio, V. Ferlet-Cavrois, P. Paillet, and E.W. Blackmore, *Enhanced proton and neutron induced degradation and its impact on hardness assurance testing*, IEEE Trans. Nucl. Sci., vol. 55, no. 6, pp. 3096-3105, 2008.
[155] S. Liu, C. DiCienzo, M. Bliss, M. Zafrani, M. Boden, and J.L. Titus, *Analysis of commercial trench power MOSFETs responses to Co-60 Irradiation*, IEEE Trans. Nucl. Sci., vol. 55, no. 6, pp. 3231-3236, 2008.
[156] R.L. Fleischer, P.B. Price, R.M. Walker, and E.L. Hubbard, *Track registration in various solid state nuclear track detectors*, Phys. Rev., vol. 133A, pp. 1443-1449, 1964.
[157] R.L. Fleischer, P.B. Price, and R.M. Walker, Nuclear Tracks in Solids, University of California Press, Berkeley, 1975.
[158] M. Marinoni, A.D. Touboul, D. Zander, C. Petit, F. Wrobel, A.M.J.F. Carvalho, R. Arinero, M. Ramonda, F. Saigne, C. Weulersse, N. Buard, T. Carriere, and E. Lorfevre, *High energy heavy ion irradiation-induced structural modifications: a potential physical understanding of latent defects*, IEEE Trans. Nucl. Sci., vol. 55, no. 6, pp. 2970-2974 (2008).
[159] J.F. Conley, J.S. Suehle, A.H. Johnston, B.Wang, T. Miyahara, E.M. Vogel, and J.B. Bernstein, *Heavy Ion Induced Soft Breakdown of Thin Gate Oxides*, IEEE Trans. Nucl. Sci., **NS-48**, 1913 (2001).
[160] L.W. Massengill, B.K. Choi, D.M. Fleetwood, R.D. Schrimpf, K.F. Galloway, M.R. Shaneyfelt, T.L. Meisenheimer, P.E. Dodd, J.R. Schwank, Y.M. Lee, R.S. Johnson, and G. Lucovsky, *Heavy-Ion-Induced Breakdown in Ultra-Thin Gate Oxides and High-K Dielectrics*, IEEE Trans. Nucl. Sci., **NS-48**, 1904 (2001).
[161] J.S. Suehle, E.M. Vogel, P. Roitman, J.F. Conley, A.H. Johnston, B. Wang, J.B. Bernstein, and C.E. Weintraub, *Observation of Latent Reliability Degradation in Ultra-Thin Oxides After heavy-Ion Irradiation*, Appl. Phys. Lett., **80**, 1282 (2002).
[162] T.R. Oldham, S. Mohammed, P. Kuhn, E. Prinz, H. Kim, and K.A. LaBel, *Effects of heavy ion exposure on nanocrystal nonvolatile memory*, IEEE Trans. Nucl. Sci., vol. 52, no. 6, pp. 2366-2372, (2005).
[163] G. Cellere, L. Larcher, A. Paccagnella, A. Visconti, and M. Bonanomi, *Radiation induced leakage current in floating gate memory cells*, IEEE Trans. Nucl. Sci., vol 52, no. 6, pp. 2144-2152, 2005.
[164] D.M. Fleetwood, P.S. Winokur, and T.L. Meisenheimer, *Hardness Assurance for Low-Dose Space Applications*, IEEE Trans. Nucl. Sci., NS-38, 1552 (1991).

[165] D. M. Fleetwood, P. S. Winokur, and J. R. Schwank, *Using Laboratory X-Ray and Cobalt-60 Irradiations to Predict CMOS Device Response in Strategic and Space Environments,* IEEE Trans. Nucl. Sci., NS-35, 1497 (1988).
[166] F.B. McLean, *Generic Impulse Response Function for MOS Systems and Its Application to Linear Response Analysis,* IEEE Trans. Nucl. Sci., NS-35, 1178 (1988).
[167] A. H. Johnston, *Super Recovery of Total Dose Damage in MOS Devices,* IEEE Trans. Nucl. Sci., NS-31, 1427 (1984).
[168] P. S. Winokur, J. R. Schwank, P. J. McWhorter, P. V. Dressendorfer, and D. C. Turpin, *Correlating the Radiation Response of MOS Capacitors and Transistors,* IEEE Trans. Nucl. Sci., NS-31, 1453 (1984).
[169] P. J. McWhorter and P. S. Winokur, *Simple Technique for Separating Effects of Interface Traps and Oxide Taps in Metal-Oxide-Semiconductor Transistors,* Appl. Phys. Lett., 48, 133 (1986).
[170] P. J. McWhorter, D. M. Fleetwood, R. A. Pastorek, and G. T. Zimmerman, *Comparison of MOS Capacitor and Transistor Post-Irradiation Response,* IEEE Trans. Nucl. Sci., NS-36, 1792 (1989).
[171] P. M. Lenahan, N. A. Bohna, and J. P. Campbell, *Radiation-Induced Interface Traps in MOS Devices: Capture Cross Sections and the Density of States of P_{b1} Silicon Dangling Bond Centers,* IEEE Trans. Nucl. Sci., NS-49, 2708 (2002).
[172] C. M. Dozier and D. B. Brown, *Photon Energy Dependence of Radiation Effects in MOS Structures,* IEEE Trans. Nucl. Sci., NS-27, 1694 (1980).
[173] D. B. Brown, *The Phenomenon of Electron Rollout for Energy Deposition and Defect Generation in Irradiated MOS Devices,* IEEE Trans. Nucl. Sci., NS-33, 1240 (1986).
[174] C.M. Dozier and D.B. Brown, *The Use of Low Energy X-Rays for Device Testing—A Comparison with Co-60 Radiation,* IEEE Trans. Nucl. Sci., NS-30, 4382 (1983).
[175] D.M. Fleetwood, D.E. Beutler, L.J. Lorence, D.B. Brown, B.L. Draper, L.C. Riewe, H.B. Rosenstock, and D.P. Knott, *Comparison of Enhanced Device Response and Predicted X-Ray Dose Enhancement Effects in MOS Oxides*, IEEE Trans. Nucl. Sci., NS-35, 1265 (1988).
[176] W. Beezhold, D.E. Beutler, J.C. Garth, and P.J. Griffin, *A review of the 40-year history of the NSREC's dosimetry and facilities session (1963-2003),* IEEE Trans. Nucl. Sci., vol. 50, no. 3, pp. 635-652, 2003.
[177] T. R. Oldham, A. J. Lelis, H. E. Boesch, J. M. Benedetto, F. B. McLean, and J. M. McGarrity, *Post-Irradiation Effects in Field-Oxide Isolation Structures,* IEEE Trans. Nucl. Sci., NS-34, 1184 (1987).
[178] J. M. Terrell, T. R. Oldham, A. J. Lelis, and J. M. Benedetto, *Time-Dependent Annealing of Radiation-Induced Leakage Currents in MOS Devices,* IEEE Trans. Nucl. Sci., NS-36, 1808 (1989).
[179] M.R. Shaneyfelt, P.E. Dodd, B.L. Draper, and R.S. Flores, *Challenges in Hardening Technologies Using Shallow-Trench Isolation,* IEEE Trans. Nucl. Sci., NS-45, 2584 (1998).
[180] M. Turowski, A. Raman, and R.D. Schrimpf, *Nonuniform total-dose-induced charge distribution in shallow trench isolation oxides,* IEEE Trans. Nucl. Sci., vol. 51, no. 6, pp. 3166-3171, 2004.
[181] A. Bryant, W. Haensch, S. Geissler, J. Mandelman, D. Poindexter, and M. Steger, *The current-carrying corner inherent to trench isolation,* IEEE Electron Dev. Lett., vol. 14, no. 8, pp. 412-414, 1993.

[182] P.C. Fazan and V.K. Mathews, *A highly manufacturable trench isolation process for deep submicron DRAMs*, Proceedings of the IEEE International Electron Devices Meeting, pp. 57-60, 1993.

[183] M. McLain, H.J. Barnaby, K.E. Holbert, R.D. Schrimpf, H. Shah, A. Amort, M. Baze, and J. Wert, *Enhanced TID susceptibility in sub-100 nm bulk CMOS I/O transistors and circuits,* IEEE Trans. Nucl. Sci., vol. 54, no. 6, pp. 2210-2217, 2007.

[184] A.H. Johnston, R.T. Swimm, G.R. Allen, and T.F. Miyahara, *Total dose effects in CMOS trench isolation regions,* IEEE Trans. Nucl. Sci., vol. 56, no. 4, pp. 1941-1949, 2009.

[185] R.C. Lacoe, *CMOS scaling design principles and hardening by design,* NSREC Tutorial Short Course, Monterey, CA, 2003.

[186] I.S. Esqueda, H.J. Barnaby, and M.L. Alles, *Two-dimensional methodology for modeling radiation-induced off-state leakage in CMOS technologies,* IEEE Trans. Nucl. Sci., vol. 52, no. 6, pp. 2259-2264, 2005.

[187] H.J. Barnaby, *Total-ionizing-dose effects in modern CMOS technologies*, IEEE Trans. Nucl. Sci., vol. 53, no. 6, pp. 3103-3121, 2006.

[188] T. Oishi, K. Shiozawa, A. Furukawa, and Y. Tokuda, *Isolation edge effect depending on gate length of MOSFETs with various isolation structures,* IEEE Trans. Electron Dev., vol. 47, no. 4, pp. 822-827, 2000.

[189] J. R. Schwank, V. Ferlet-Cavrois, M.R Shaneyfelt, P. Paillet, and P.E. Dodd, *Radiation effects in SOI technologies*, IEEE Trans. Nucl. Sci., vol. 50, no. 3, pp. 522-538, 2003.

[190] R.L. Pease, R.M. Turfler, D. Platteter, D. Emily, and R. Blice, *Total dose effects recessed oxide digital bipolar microcircuits*, IEEE Trans. Nucl. Sci., vol. 30, no. 6, pp. 4216-4223 (1983).

[191] E. W. Enlow, R. L. Pease, W. Coombs,R. D. Schrimpf, and R. N. Nowlin, *Response of Advanced Bipolar Processes to Ionizing Radiation,* IEEE Trans. Nucl. Sci., NS-38, 1342 (1991).

[192] R. L. Pease, *Total ionizing dose effects in bipolar devices and circuits,* IEEE Trans. Nucl. Sci., vol. 50, no. 3, pp. 539-551, 2003.

[193] R.L. Pease, *Enhanced low dose rate sensitivity (ELDRS)in linear bipolar circuits,* Proceedings of RASEDA Workshop, Takasaki, Japan, Oct 2010.

[194] D.M. Schmidt, D.M. Fleetwood, R.D. Schrimpf, R.L. Pease, R.J. Graves, G.H. Johnson, K.F. Galloway, and W.E. Combs, *Comparison of Ionizing-Radiation-Induced Gain Degradation in Lateral, Substrate, and Vertical PNP BJTs*, IEEE Trans. Nucl. Sci., **NS-42**, 1541 (1995).

[195] A.H. Johnston, G.M. Swift, and B.G. Rax, *Total dose effects in conventional bipolar transistors and linear integrated circuits*, IEEE Trans. Nucl. Sci., vol. 41, no. 6, pp. 2427-2436 (1994).

[196] K. Kruckmeyer, *Effect of TID hardening on SET response of National Semiconductor ELDRS-free LM139*, SEE Symposium, 2009.

[197] R.L. Pease, S.McClure, A.H. Johnston, J. Gorelick, T.L. Turflinger, M. Gehlhausen, J. Krieg, T. Carriere, and M.R. Shaneyfelt, *An updated data compendium of enhanced low dose rate sensitive (ELDRS) bipolar linear circuits,* IEEE Radiation Effects Data Workshop Record, p. 127, IEEE Catalog No. 01TH8588, 2001.

[198] M. R. Shaneyfelt, J. R. Witczak, J. R. Schwank, D. M. Fleetwood, R. L. Pease, P. S. Winokur, L. C. Riewe and G. L. Hash, *Thermal-stress effects on enhanced low dose rate sensitivity in linear bipolar ICs*, IEEE Trans. Nucl. Sci. NS-47, No.6, 2539-2545, December 2000.

[199] D. M. Fleetwood, S. L. Kosier, R. N. Nowlin, R. D. Schrimpf, R. A. Reber, Jr., M. DeLaus, P. S. Winokur, A. Wei, W. E. Combs and R. L. Pease, *Physical mechanisms conributing to enhanced bipolar gain degradation at low dose rates*, IEEE Trans. Nucl. Sci. vol. 41, No. 6, 1871-1883, December 1994.

[200] [18] R. L. Pease, S. McClure, J. Gorelick and S. C. Witczak, *Enhanced low-dose-rate sensitivity of a low-dropout voltage regulator*, IEEE Trans. Nuc. Sci. vol. 45, No. 6, 2571-2576, December 1998.

[201] [19] R. L. Pease, G. W. Dunham and J. E. Seiler, D. G. Platteter and S. S. McClure, *Total dose and dose rate response of an AD590 temperature transducer*, IEEE Trans. Nucl. Sci., NS 54, No. 4, pp. 1049-1054, August, 2007.

[202] S. S. McClure, A. H. Johnston, J. L. Gorelick and R. L. Pease, *Dose rate and bias dependency of total dose sensitivity of low dropout voltage regulators*, IEEE Radiation Effects Data Workshop Record, 100-105, 2000.

[203] H. Barnaby, H. J. Tausch, R. Turfler, P. Cole, P. Baker, and R. L. Pease, *Analysis of bipolar linear circuit response mechanisms for high and low dose rate total dose irradiations*, IEEE Trans. Nuc. Sci. NS-43, No.6, 3040-3048, December 1996.

[204] M. R. Shaneyfelt, R. L. Pease, M. C. Maher, J. R. Schwank, S. Gupta, P. E. Dodd, and L. C. Riewe, *Passivation layers for reduced total dose effects and ELDRS in linear bipolar devices*, IEEE Trans. Nucl. Sci. NS-50, No.6, 1784-1790, December 2003.

[205] J. L. Titus, W. E. Combs, T. L. Turflinger, J. F. Krieg, H. J. Tausch, D. B. Brown, R. L. Pease and A. B. Campbell, *First observations of enhanced low dose rate sensitivity (ELDRS) in space: one part of the MPTB experiment*, IEEE Trans. Nucl. Sci. NS-45, No.6, 2673-2680 (1998).

[206] J. L. Titus, D. Emily, J. F. Krieg, T. L. Turflinger, R. L. Pease and A. B. Campbell, *Enhanced low dose rate sensitivity (ELDRS) of linear circuits in a space environment*, IEEE Trans. Nucl. Sci. NS-46, No.6, 1608-1615 (1999).

[207] T. L. Turflinger, W. M. Schemichel, J. F. Krieg, J. L. Titus, A. B. Campbell, M. Reeves, R. J. Walters, P. W. Marshall, and R. L. Pease, *ELDRS in space: an updated and expanded analysis of the bipolar ELDRS experiment on MPTB*, IEEE Trans. Nucl. Sci. NS-50, No.6, 2328-2334, (2003).

[208] R. L. Pease, J. F. Krieg, T. L. Turflinger, A. B. Campbell, and R. J. Walters, *Recent data from the MPTB ELDRS experiment*, Journal of Radiation Effects: Research and Engineering, 2003.

[209] D.M. Fleetwood, L.C. Riewe, and J.R. Schwank, *Radiation effects at low electric fields in thermal, SIMOX, and bipolar-base oxides*, IEEE Trans. Nucl. Sci., vol. 43, no. 6, 2537-2346 (1996).

[210] R.L. Pease, G.W. Dunham, J.E. Seiler, D.G. Platteter, and S.S. McClure, *Total dose and dose rate response of an AD590 temperature transducer,* IEEE Trans. Nucl. Sci., vol. 54, no. 6, pp. 1049-1054 (2007).

[211] H. P. Hjalmarson, R. L. Pease, S. C. Witczak, M. R. Shaneyfelt, J. R. Schwank, A. H. Edwards, C. E. Hembree and T. R. Mattsson, *Mechanisms for radiation dose-rate sensitivity of bipolar transistors*, IEEE Trans. Nucl. Sci. vol. 50, No. 6, 1901-1909, December 2003.

[212] H. P. Hjalmarson, R. L. Pease and R. Devine, *Simulation of dose-rate sensitivity of bipolar transistors*, IEEE Trans. Nucl. Sci. NS-55, No.6, pp. 3009-3015, December 2008.

[213] D. M. Fleetwood, R. D. Schrimpf, S. T. Pantelides. R. L. Pease and G. W Dunham, *Electron capture, hydrogen release and ELDRS in bipolar linear devices*, IEEE Trans. Nucl. Sci. NS-55, No.6, pp. 2986-2991, December 2008.

[214] J. Boch, F. Saigne, R. D. Schrimpf, J-R. Vaille, L. Dusseau and E. Lorfevre, *Physical model for the low-dose-rate effect in bipolar devices*, IEEE Trans. Nucl. Sci. vol. 53, No. 6, 3655-3660, December 2006.

[215] B. R. Tuttle, D. R. Hughart, R. D. Schrimpf, D. M. Fleetwood and S. T. Pantelides, *Defect interactions in H2 in SiO2: Implications for ELDRS and latent interface trap buildup*, IEEE Trans. Nucl. Sci., vol. 57, no. 6, pp. 3046-3053 (2010).

[216] D. Chen, J.D. Forney, A.M. Phan, M.A.Carts, R.L.Pease, S.R. Cox, K.A. LaBel, K. Kruckmeyer, S. Burns, R.Albarian, B. Holcombe, B. Little, J. Salzman, G. Chaumont, H. Duperray, A. Ouellet, *The effects of ELDRS at ultra-low dose rates*, IEEE Radiation Effects Data Workshop Record, pp. 111-116, 2010.

[217] R. L. Pease, L. M. Cohn, D. M. Fleetwood, M. A. Gehlhausen, T. L. Turflinger, D. B. Brown and A. H. Johnston, *A proposed hardness assurance test methodology for bipolar linear circuits and devices in a space ionizing radiation environment*, IEEE Trans. Nucl. Sci. vol. 44, No.6, pp. 1981-1988, 1997.

[218] A. H. Johnston, B. G. Rax and C. I. Lee, *Enhanced damage in linear bipolar integrated circuits at low dose rate*, IEEE Trans. Nucl. Sci. vol. 42, No. 6, 1650-1659, December 1995.

[219]] R. L. Pease and M. Gehlhausen, *Elevated temperature irradiation of bipolar linear microcircuits*, IEEE Trans. Nucl. Sci. vol. 43, No. 6, 3161-3166, December 1996.

[220] T. Carriere, R. Ecoffet and P. Poirot, *Evaluation of accelerated total dose testing of linear bipolar circuits*, IEEE Trans. Nucl. Sci. vol. 47, No. 6, 2350-2357, December 2000.

[221] J. Boch, F. Saigne, R. D. Schrimpf, D. M. Fleetwood, R. Cizmarik, and D. Zander, *Elevated temperature irradiation at high dose rate of commercial linear bipolar ICs*, IEEE Trans. Nucl. Sci. NS-51, No.5, 2903-2907, October 2004.

[222] R. N. Nowlin, R. L. Pease D. G. Platteter and G. W. Dunham, *Evaluating TM1019.6 screening methods using gated lateral PNP transistors***,** IEEE Trans. Nucl. Sci. NS-52, No.6, 2609-2615, December 2005.

[223] J. Boch, F. Saigne, R. D. Schrimpf, J. R. Vaille, L. Dusseau, S. Ducret, M. Bernard, E. Lorfevre, and C. Chatry, *Estimation of low-dose-rate degradation on bipolar linear integrated circuits using switching experiments*, IEEE Trans. Nucl. Sci. NS-52, No.6, 2616-2621, December 2005.

[224] S. C. Witczak, R. C. Lacoe, J. V. Osborn, J. M. Hutson and S. C. Moss, *Dose rate sensitivity of modern nMOSFETs*, IEEE Trans. Nucl. Sci. NS-52, No.6, 2602-2608, December 2005.

[225] A.H. Johnston, R.T. Swimm, and T.F. Miyahara, *Low dose rate effects in shallow trench isolation regions*, IEEE Trans. Nucl. Sci., vol. 57, no. 6, pp.3279-3287, (2010).

[226] K. Kruckmeyer, J.S. Prater, B. Brown, and T. Trinh, *Analysis of low dose rate effects on parasitic bipolar structures in CMOS processes for mixed signal circuits*, presented at 2010 Radecs, and accepted for publication in IEEE Trans. Nucl. Sci.

[227] S. J. Kim, D. H. Ko, J. Seon, K. W. Min, Y. Shin and K. Ryu, *Enhanced low dose rate sensitivity in p-channel MOSFETs* Presented at the 2006 NSREC in Ponte Vedra Beach, FL, July, 2006.

[228] M. R. Shaneyfelt, T. A. Hill, T. M. Gurrieri, J. R. Schwank, R. S. Flores, P. E. Dodd, S. M. Dalton and A. Robinson, *An embeddable SOI radiation sensor*, IEEE Trans. Nucl. Sci. NS-56, No.6, 3372-3380, December 2009.

[229] J.F. Ziegler, *The Stopping Power and Ranges of Ions in Matter,*, vol 3,4, and 5, Pergamon Press, Inc., New York (1977).

[230] J. Lindhard, M. Scharff, and H. Schiott, Mat. Fys. Medd. Vid. Selsk., vol. 33, p. 1, (1963).
[231] F.B. McLean, *Basic Mechanisms of Radiation Effects in Electronic Materials and Devices*, NSREC Tutorial Short Course, 1987.
[232] Burgoin and Lanoo, *Point Defects I Solids*, Vol. 2, ed. by M. Cardona et al., Springer Verlag, 1983.
[233] J.R. Srour, *Displacement damage effects in electronic materials, devices, and integrated circuits,* IEEE NSREC Tutorial Short Course (1988).
[234] J.R. Srour, IEEE NSREC Tutorial Short Course, 1983.
[235] J.R. Srour, S. Othmer, A. Bahraman, and R.A. Hartman, *The search for neutron-induced hard errors in VLSI structures,* IEEE Trans. Nucl. Sci., vol. 28, no. 6, pp. 3968-3974 (1981).
[236] B.R. Gossick, *Disordered regions in semiconductors bombarded by fast neutrons,* J. Appl. Phys., vol. 39, no. 8, pp. 1214-1218, 1959.
[237] G.C. Messenger and J.P. Spratt, *The effects of neutron irradiation on silicon and germanium,* Proc. IRE, vol. 46, pp. 1038-1044, 1958.
[238] G.P. Summers, C.J. Dale, E.A. Burke, E.A. Wolicki, P.W. Marshall, and M.A. Gelhausen, *Correlation of particle-induced displacement damage in silicon,* IEEE Trans. Nucl. Sci., vol. 34, no. 6, pp. 1134-1139, 1987.
[239] A.L. Barry, A.J. Houdayer, P.F. Hinrichsen, W.T. Letourneau, and J. Vincent, *The energy dependence of lifetime damage constants in AlGaAs LEDs for 1-500 MeV protons,* IEEE Trans. Nucl. Sci., vol. 42, no. 6, pp. 2104-2107, 1995.
[240] J.R. Sour and j.W. Palko, *A framework for understanding displacement damage mechanisms in irradiated silicon devices,* IEEE Trans. Nucl. Sci., vol. 53, no. 6, pp. 3610-3620, 2006.
[241] J.W. Palko and J.R. Srour, *Amorphous inclusions in irradiated silicon and their effects on material and device properties,* IEEE Trans. Nucl. Sci., vol. 55, no. 6, pp. 2992-2999, 2008.
[242] M. Alurralde, F. Pachoud, M. Victoria, and D. Gavillet, *The displacement damage produced in Si by 590 MeV protons,* Nuclear Instruments and Mehtods in Physics Research, vol. B 80/81, pp. 523-527, 1993.
[243] S.U. Campisano, S. Coffa, V. Raineri, F. Priolo, and E. Rimini, *methods of amorphization in ion-implanted crystalline silicon,* Nuclear Instruments and Methods in Physics Research, vol. B 80/81, pp. 514-518, 1993.
[244] S.E. Donnelly, R.C. Birtcher, V.M. Vishnyakov, and G. Carter, *Annealing of isolated amorphous zones in silicon,* Appl. Phys. Lett., vol. 82, no. 12, pp. 1860-1862, 2003.
[245] O.W. Holland, C.W. White, M.K. El-Ghor, and J. D. Budai, *MeV self-ion implantation in Si at liquid nitrogen temperature: a study in damage morphology and its anomalous annealing behavior,* J. Appl. Phys., vol. 68, pp. 2081-2086, 1990.
[246] I. Jencic, M.W. Bench, and I.M. Robertson, *Electron-beam-induced crystallization of isolate amorphous regions in Si, Ge, GaP, and GaAs,* J. Appl.Phys., vol. 78, no. 2, pp. 974-982, 1995.
[247] M.O. Ruault, J. Chaumont, J.M. Pennisson, and A. Bouret, *High resolution and in-situ investigation of defects I Bi-irradiated Si,* Phil. Mag. Avol. 50, pp. 667-675, 1984.
[248] F. Pachoud, and M. Victoria, *microscopy of Semiconducting Materials, 1993,*A.G. Cullis, A.E. Staton-Bevan, and J.L. Hutchison, eds., Bristol UK; Philadelphia, PA, Inst. Of Physics, 1993, Inst Phys, Conf. Ser., no. 14, pp. 145-148.

[249] T.E. Gessner, M. Passemann, and B. Schmidt, *Calculation of neutron-induced defect clusters in silicon and comparison with TEM investigations,* Phys. Stat. Sol.(a), vol. 77, pp. 133-138, 1983.
[250] V.A.J. van Lint, R.E. Leadon, and J.F. Colwell, IEEE Trans. Nucl. Sci., vol. 19, no. 6, p. 181, 1972.
[251] A.H. Johnston, *Optical Sources, Fibers, and Photonic Subsystems,* IEEE NSREC Tutorial Short Course, 2004.
[252] A.H. Johnston, *Radiation effects in light emitting and laser diodes,* IEEE Tran. Nucl. Sci., vol. 50, no. 3, pp. 689-703, 2003.
[253] A.H. Johnston, *Reliability and Radiation Effects in Compound Semiconductors,* World Scientific Publishing, Inc., Singapore, 2010.
[254] H.N. Becker and A.H. Johnston, *Dark current degradation of near infrared avalanche photodiodes from proton irradiation,* IEEE Trans. Nucl. Sci., vol. 51, no. 6, pp. 3572-3578, 2004.